UNIVERSITY OF OKLAHOMA

GRADUATE COLLEGE

MATRIX HETEROGENEITY EFFECTS ON FLUID TRANSPORT IN POROUS MEDIUM: USING PERTURBATION THEORY

A DISSERTATION

SUBMITTED TO THE GRADUATE FACULTY

in partial fulfillment of the requirements for the

Degree of

DOCTOR OF PHILOSOPHY

By

EBRAHIM FATHI
Norman, Oklahoma
2010

MATRIX HETEROGENEITY EFFECTS ON FLUID TRANSPORT IN POROUS MEDIUM: USING PERTURBATION THEORY

A DISSERTATION APPROVED FOR THE
MEWBOURNE SCHOOL OF PETROLEUM AND GEOLOGICAL ENGINEERING

BY

Dr. I. Yucel Akkutlu, Committee Chair

Dr. Younane Abousleiman

Dr. Faruk Civan

Dr. Dean S. Oliver

Dr. Dimitrios V. Papavassiliou

ACKNOWLEDGEMENTS

I would like to express my sincere gratitude to Professor I. Yucel Akkutlu for all his supports and guidance through my PhD study at the University of Alberta and Oklahoma. I want to thank him for all the time and efforts he put to help me excel in my research. I really enjoyed all the research meetings and trips that we had. I would like to extend my appreciation to Pinar Akkutlu for her hospitality and kindness that made me feel at home.

I also want to thank Dr. Dean Oliver for all his helps, insightful suggestions and comments and for the opportunity to attend in his group research meetings. I appreciate that Dr. Younane Abousleiman, Dr. Faruk Civan, Dr. Dean Oliver, and Dr. Dimitrios V. Papavassiliou serving on my committee and for all their suggestions and comments during my studies.

My appreciation extends to all the staff in the MPGE, who have helped me during my studies at OU and when I was transferring from University of Alberta to Oklahoma.

My special thanks to all my dear friends both at the University of Alberta and Oklahoma. Special thanks to my dear friends Hamidreza Monzavi, Dr. Vahid Rezania, Sharareh Rezania, Dr. Mostafa Naghizadeh, Sara Nourazari and my siblings Hadi, Samira, and Alireza for all their help and wonderful time that we spend together.

This dissertation is dedicated to my mom and dad, Mahin and Ali, for all their supports, motivations, and their unconditional love.

TABLE OF CONTENTS

LIST OF TABLES

LIST OF FIGURES

ABSTRACT

In this dissertation the processes of transport and reaction in heterogeneous porous medium is upscaled from pore scale to the scale of interest (e.g., core sample or reservoir scale) and new governing equations describing gas transport and reaction including the effects of heterogeneity is introduced. New upscaled equations for the first time described observations have been made earlier in the laboratory regarding storage and transport of gas in tight formations, such as gas trapping mechanism in gas release experiments and gas threshold effect in gas uptake, gas loading effects, adsorbed phase transport and nonlinearity effects of gas sorption kinetics on diffusive transports. New upscaled governing equations provide basis for further experimental works to quantify and distinguish effects of local heterogeneities on transport and storage in tight formations.

Matrix heterogeneity effects on fluid transport in porous medium is investigated using an upscaling approach based on small perturbation theory. The approach allows us investigate the heterogeneity effects in spectral domain in the presence of non-equilibrium sorption with random partition coefficient. The work is motivated by the fact that (1) the porous medium is heterogeneous, i.e., it has a significant degree of spatial variability, and shows a complex structure at larger scales; (2) there always exists a lack of knowledge of the detailed local structure of these spatial variations; and (3) difficulties appear in obtaining sufficient data related to spatial and temporal distributions of mass and momentum variables, dictated by these large-scale variations. Here, the heterogeneity of the matrix is introduced using random porosity or permeability fields that holds the assumption of first and second orders of stationarity, i.e., constant mean and variance, and possess a well defined gaussian correlation

function. All transport and kinetics parameters and dependent variables (e.g., free and adsorbed gas concentration) are also affected by the matrix heterogeneity and represented by their average and perturbations around the mean (arithmetic average) values. First, fundamental investigation is performed on shale and coal samples with simplified gas transport and adsorption kinetics. The former is simplified by considering the free phase transport only in the micro-pores and the latter by assuming linear non-equilibrium sorption kinetics. Substituting the perturbed variables and coefficients into the basic governing equations leads to the set of stochastic partial differential equations including mean and perturbation equations. Mean equations are essentially upscaled new governing equations that includes the auto- and cross-correlations between different perturbed quantities. The auto- and cross-correlations could be found solving perturbation equations in the Laplace-Fourier domain and back-transforming them to the time-space domain.

It is found that upscaled deterministic gas mass balance includes new sink and source terms into the governing equations related to the local heterogeneity. Heterogeneity affects the gas transport and adsorption significantly through macro-transport and macro-kinetics terms. Macro-transport depends on P*é*clet number and interestingly persist at the diffusive limit, while micro-kinetics is related to the modified Thiele modulus. Heterogeneity retards gas release from the matrix and influences the ultimate gas recovery adversely. Both effects are directly related to the amount of initial gas adsorbed and the level of heterogeneity introduced to the system by the porosity variance. Next, the effects of heterogeneity on gas transport and adsorption in the presence of earlier ignored adsorbed phase transport and non-linear sorption kinetics investigated. The heterogenous porosity field leads to a significant improvement in adsorbed-phase transport when non-linear sorption kinetics is considered in very low permeability porous media. We theoretically observe new transport effects in the presence of adsorbed-phase. Furthermore, it is shown that the conventional

Langmuir isotherms are not representing the sorption behavior of the gas correctly in the heterogeneous formations where the nonlinearity in sorption kinetics acts as trapping mechanism for adsorbed phase and surface diffusion decreases the time needed to reach the saturation pressure. Finally we investigated the effects of heterogeneity introduced by random permeability field on advection- reaction problem, where one step nonlinear reaction takes place. The results show rich nonlinear interplay between the existing mechanisms. The effect of heterogeneity on steady planar reaction wave is also investigated. It is revealed that the planar reaction wave is intrinsically unstable. The later is anticipated to expand due to development of non–uniform velocity field along the reaction wave.

CHAPTER I

INTRODUCTION

In unconventional gas reservoirs like coalbed methane and shale gas reservoirs, gas well productivities are influenced primarily by low-permeable nature of the reservoir formation. Porosity and absolute permeability of the matrices are significantly less than those belong to the conventional gas reservoirs. In addition, due to large internal surface areas of the matrices, coalbed formations containing significant amounts of organic matters retain a large portion of natural gas at an adsorbed state. The later is a physical mechanism which plays an important role during the estimation of gas-in-place and the future reservoir predictions (King 1990; Ambrose*et al.,* 2010). Tight nature of the matrices and their ability to retain the gas at an adsorbed state also make these environments important gas trapping and storage locations. Coalbeds are considered to be one of the targeted subsurface environments for the greenhouse gas sequestration. Although no large-scale projects currently exist, field-tests are being performed for CO_2 injection and enhanced coalbed methane production, i.e., CO_2-ECBM. Gas shales are also likely to play an important role in sequestration similar in magnitude to coals in near future (Nuttall 2005; Kang *et al.,* 2010).

In order to have an accurate prediction of production rates and subsurface greenhouse gas sequestration, it is inevitable to first have a good understanding of coupled fluid phenomena involved with gas transport and storage in coalbed methane reservoirs, i.e., viscous flow, diffusive transport, adsorption and matrix-fracture interactions. Next, it is important to have a good estimate of rock and transport properties of the reservoir, and finally, sophisticated reservoir simulator is necessary to simulate and predict the behavior of the reservoir. In the case of coalbed methane, it can

be modeled using dual-porosity, dual-permeability or more accurately triple-porosity, dual-permeability models, later is used here to simulate coalbed methane reservoirs. Recent investigations based on X-ray computerized tomography (CT) and scanning electron microscope (SEM) of coal (Karacan 2003, 2007) have shown that coals are in fact complex composite materials consisting of a large group of minerals and organic matters exhibiting an intricate pore structure. Recently, Weida *et al.*,(2005) quantified such variability using cumulative gas production data of a set of wells drilled and completed in essentially the same way (open-hole) in a small area in a single coal seam. Experience with the conventional resources prescribes that the variability is due to reservoir permeability heterogeneity, also field data from the existing coal mines and drilled wells show that the absolute permeability values of the coal seams can change significantly from one location to another, even within the length of a meter. Further, under initial equilibrium conditions, since the natural gas is likely to be homogeneously distributed in the microstructure of the matrices, these variations in the production of the wells should be due to spatial changes in permeability. This point of view emphasizes only the existence of a network of fractures with a dynamic "effective" permeability field which is changing in time due to opening and closing of fractures as the places of the dominant transport for gas production. It may, however, overlook the influence of finer scale heterogeneities intrinsic to the matrices surrounded by those fractures and it may neglect their roles on the initial distribution of gas and on the production.

In order to investigate the effect of these fine scale heterogeneities, we consider local phenomena in a heterogeneous matrix using a theoretical approach. We therefore first develop the means to appropriately quantify the local matrix heterogeneities and then to up-scale (or homogenize) the gas flow, diffusive transport and adsorption processes over the matrix body. Hence, our work here builds on the premise that the local gas behavior in the matrix is simultaneously controlled by the gas sorption rates, viscous

and diffusive gas mass fluxes. Although the matrix exhibits local variations in the pore structure, we consider that these local variations are weak and that the porous medium still maintains a meaningful average porosity and a constant permeability values. We then investigate analytically and numerically the effects of porosity fluctuations, in particular, and the related material property variations on these physical mechanisms. For the investigation, initially, we locally describe mass conservation for a gas component (for which the matrix has a certain adsorption capacity, e.g., methane) in homogeneous media characterized by a time-independent porosity in space-time continuum. Next, the classical perturbation theory is employed to the governing equations where the structural and chemical variations are introduced in terms of fluctuating (random) porosity and partition coefficient, respectively. The analytical part of our work is concerned with description and analysis of the theoretical problem using the mean and perturbed governing equations in the Laplace-Fourier domain. The mean equations are, in fact, upscaled governing equations which include cross-correlations between porosity and dependent variables reflecting the mean influences of the introduced small-scale porosity fluctuations on the adsorbed and free gas concentrations and on the Fickian-type diffusivity. Obtaining explicit expressions for the later quantities are the most critical part of any work based on perturbations and noise analysis and, here, they are examined using the perturbed governing equations in the spectral domain.

This dissertation contains 7 chapters. In chapter 2, literature review of the previous works are presented and their strengths and weaknesses are discussed. This chapter includes two parts, first part reviews the physical, e.g., pore structure, chemical like mineral content and sorption behavior, and transport properties of the coal and shale samples and second part provides a background on using small perturbation theory to quantify the heterogeneity due to highly complex diagenesis processes of the sediments when dealing with subsurface processes, such as movement of ground water,

transport of contaminants in groundwater, in-situ recovery of oil and natural gas. In chapter 3, small perturbation theory basics and applications is discussed and we introduced new application of the method in petroleum engineering, where quantifying coal matrix heterogeneity effects on gas transport and storage is important. We approach this complex problem in a systematic manner, where we start with simple model with diffusive transport in matrix and linear sorption kinetics only and then we add viscose flow of gas in the matrix. Later In chapter 4, we introduced more complexity to the model including surface diffusion as an adsorbed phase transport mechanism and nonlinear sorption kinetics in the model. Finally, new upscaled deterministic governing equations for gas transport and storage in heterogeneous porous medium that includes most important transport and storage mechanisms are obtained. In chapter 5, we investigate the CO_2 enhanced coalbed methane recovery, where counter diffusion and competitive adsorption effects during CO_2 injection and coalbed methane production is investigated, assuming homogeneous rock properties. In chapter 6, the heterogeneity effects of porous medium introduced by random permeability field on reactive flow is investigated, where one step nonlinear dissolution reaction and ideal liquid solution, i.e., the fluid properties of which is not significantly influenced by the dissolution reaction, are assumed. In chapter 7, we are summarizing the main conclusions and contributions of this dissertation.

CHAPTER II

LITERATURE REVIEW

2.1 Physical, Chemical and Transport Properties of Coal and Shale

Coal and shale have slightly different definitions based on specific objective of the study. Generally shale is referred to a wide range of rocks, with vary fine grain size, capable of storing gas. It could be real shales like Antim shale in Michigan Basin or it could be tight sands such as Lewis shale in San Juan Basin. In our study shales are defined as sedimentary rocks with less than 50 % (wt/wt) of organic materials, whereas coals contain more than 50 % (wt/wt) of organic matters like inertinite, vitrinite, liptinite. They also contain some inorganic materials such as quartz, pyrite, and clay minerals (Jenkins *et al.*, 2008).

Coals have traditionally been considered as a porous material with a network of interconnected macropores, (Bond, 1956; Bhatia, 1987). According to this viewpoint, natural gas migration in and production from coalbeds have similarities to production from conventional naturally fractured reservoirs. This viewpoint, however, has been disputed by Larsen and Wernett (1988) suggesting that the macropores may not necessarily be connected; therefore, the gas molecules are anticipated to reach the macropores and fractures only by diffusive transport through the microporous solid material. Therefore, the surface diffusion may be the transport mechanism for the adsorbed molecules through the physically adsorbed layer on the micropore walls. Walker and Mahajan (1993) and Siemons *et al.*, (2007) provided further experimental evidence of diffusive gas transport in the coal micropores. In the macropores, however, there is well documented literature showing that the bulk and Knudsen diffusion of

the gas molecules are the main mechanisms for the free gas migration; Furthermore, having connectivity between the macropores, viscous flow of the gas also considered as gas transport mechanism in macropores having reasonably well matrix permeability. In the fractures, on the other hand, convective flow of free gas is the dominant transport mechanism that can be modeled as darcy flow of gas in the fractures, while macro dispersion transport of free gas could also be considered in the fractures too. Efforts also have been put forth to identify relationships between the matrix pore structure and its material content. Although these investigations have generally been qualitative, it is shown that the coal porosity is somewhat related to its material properties White *et al.*, (2005). Typically, porosity has a tendency to decrease as the coal rank, i.e., thermal maturity, increases from lignite to bituminous and anthracite. Gan *et al.*, (1972) observed that porosity is primarily dominated by the macropores in lower rank coals. The influence of maceral, i.e., organic, composition on porosity has also been considered by several groups. Harris and Yust (1976) found that liptinite portion of their coal sample is composed of macropores; inertinite is the highly porous maceral group consisting of mesopores and vitrinite portion is mainly meso- and micropores. Clarkson and Bustin (1996) supported the later argument showing that the coal micropore volume generally increases with the total vitrinite content. The mineral matter, on the other hand, occupies the space that would have otherwise been filled with the organic material; hence, it possibly reduces the internal surface area and sorption capacity of the coal. In addition to its influence on the pore structure, the material content appears to be important for the gas accessibility and storage by the coal. Chemical nature of the materials (composition and number of available sites for sorption, etc.) dictates coals affinity to the gas molecules. Lamberson and Bustin (1993) and Crosdale *et al.*,(1998) have shown that the gas storage capacity is generally higher for vitrinite-rich coals than for inertinite-rich coals. In addition, vitrinites have a tendency to release (desorb) gas at smaller rates, possibly due to

their microporous structure (Crosdale *et al.*, 1998). In coal and shale samples gas sorption capacity is a function of mineral composition, gas composition and thermal maturity of the sample (Jenkins *et al.*, 2008). Primarily ∼90% of the gas in coalbed methane reservoirs are stored as an adsorbed layer on internal surface area of the coal organic minerals, where it exhibits liquid like densities (Ambrose *et al.*, 2010.)

Shale gas reservoirs also have complex pore structure with the pore size varying in the range of nanometers. Based on the International Union of Applied and Pure Chemistry (IUAPC) they can be classified as micropores (< 2 nm), mesopores (2-50 nm), and macropores (> 50) in diameter (Bustin *et al.*, 2008). As pore size of shale decreases, for a given pore volume, the surface area of the solid matrix is increasing hence amount of gas as an adsorbed phase increases too. Gas storage in shale gas has been reported to be the same as coalbed reservoirs in which most of the gas stored as an adsorbed gas on the surface of solid materials by physical adsorption (Bustin, 2005). The solid material of the shale matrix includes organic (kerogen) and the inorganic constituents (clay, silica, feldspar, etc). Recent investigation on gas storage capacity of the organic rich shales predicted that most of the gas is associated with organic fraction of the matrix, i.e., kerogen network, (Loucks *et al.*, 2009; Wang and Reed 2009; Sondergeld *et al.*, 2010). Most recently using advanced imaging technologies Ambrose *et al.*, (2010) showed that the organic content of shale matrix includes the kerogen network with large inter-connected pockets, that includes most of the matrix porosity. The gas distribution and sorption capacity of different storage sites in shale depends on the pore system, organic content, maturity and temperature and pressure of the shale (Ramos 2004; Chalmers and Bustin 2006). However, there are some cases in high temperature and high pressure conditions with organic lean shales like Horn river basin and the Haynesville shale in Louisiana that the sorbed gas amount may be a very small portion of the total gas and macropores and fractures storing the majority of the gas in place (Bustin *et al.*, 2008).

Theses differences in pore structure of coal and shale reservoirs do not mean that gas production from shale gas reservoirs are faster than coalbed methane reservoirs. They both show short time fast decline curve and then very slow and steady depletion of the reservoir which could last several years. This process is apparent in colabed reservoirs due to very slow gas release from matrix (sorption kinetics and diffusion), but in shale gas reservoirs gradual reduction in decline curve happens due to very low matrix and fracture porosity and permeability, i.e., in the order of nano- to micro darcy range.

In the case of coalbed methane reservoirs, these investigations tends to consider the fracture network as the places of rapid convection and to stress the importance of sorptive-diffusive transport phenomena in a rather tight coal matrix as the controlling mechanisms. Hence, the ability of coal to store and release gas is dependent not only on the volume-averaged permeability (Darcian flow) but also on an intrinsic (coal dependent) transport reflecting the presence of additional gas/solid interactions in a composite matrix. Productivity of coalbed reservoirs are primarily controlled by coal absolute permeability and gas saturation state of the coal. Gas saturated coalbed reservoirs are producing as pressure gradient applied by producers. However, undersaturated reservoirs need to be dewatered first to reach a point that gas starts to desorb from coal matrix, this period in some cases takes several years. Fracture and macro pore permeability could vary from a few millidarcy to tens of millidarcy depending on the amount of pore pressure and effective stress applied due to overburden pressure. After starting the gas production from coalbed reservoir, coal matrix starts to shrink and this shrinkage effect due to gas release from coal increases the absolute permeability of the coal. On the other hand as coal pore pressure drops the effective stress on coal increases causing some reduction in absolute permeability which can modify the increasing permeability due to the shrinkage effect.

In the case of shale gas reservoirs, traditional methods for flow characterization applied by different authors using a hybrid mixture of methods used for coal and conventional reservoir rocks (Bustin *et al.*, 2008). However, these methods do not consider recent experimental observations of the shale gas pore structures, emphasizing the presence of network of kerogen pockets containing significant amount of gas in place in an adsorbed phase. Recently, new formulations supporting pressure pulse decay experiments and FIB/SEM image analysis introduced by Kang *et al.*,(2010) to characterize the flow and storage in shale gas reservoirs, where multi-continuum porous media in series is introduced including the organic matters mainely Kerogen pockets, inorganic matters and fractures. Transport mechanisms in different continua recognized as following: in Kerogen pockets the combination of slip flow and surface diffusion is the dominant mechanism, in inorganic matters viscose flow is the main transport mechanism and Darcian flow is recognized in fractures. Ertekin *et al.*, 1986 also described the deriving mechanism in tight formations as parallel transport of Darcy flow in larger pores and combination of diffusive transports in smaller pores.

2.2 Investigation of the Heterogeneity Effects on Fluid Transport and Reaction in Porous Medium

In our earlier discussions and most of the early developments on fluid flow in a porous medium the assumptions of homogeneous and isotropic rock and fluid properties held and analytical solutions for fluid flow in porous media developed (Theis, 1935; Polubarinova-Kochina, 1962). Analytical solution of fluid flow in porous media were successfully used in small scale problems. However, detailed experiments on hydraulic properties of porous media (Law, 1944) revealed the large degree of heterogeneity that affects analyzing flow and transport in porous media at large scale problems. Warren

and Price (1961) and Warren and Skiba (1964) made the earliest efforts on characterizing the flow and transport in porous media using random heterogenous fields. Same approach followed later in groundwater hydrology. In all of these studies they used numerical solutions of stochastic partial differential equations, However, Shvidler (1964) and Matheron (1967) used analytical methods to solve the problem.

The bottom line in all these studies was the fact that behavior of fluids flowing in a porous medium is influenced by the medium heterogeneities. While an attempt is being made to develop a quantitative description of flow in porous media in a scale much larger than an average pore size, dealing with the realm of heterogeneity becomes a fundamental and challenging problem. Finding appropriate average parameters, which can be applied to flow, transport and reaction in the scale of interest, and at the same time being able to incorporate the influence of intrinsic porous medium heterogeneity on the modeling and predictions, is desired during an investigation. Rapid developments in theoretical research of fluid flow in porous media in a probabilistic framework have been experienced during the last two decades. When dealing with subsurface processes, such as movement of ground water, transport of contaminants in groundwater, in-situ recovery of oil and natural gas, the heterogeneities are more pronounced due to highly complex diagenesis processes of the sediments (Gelhar 1993; Gelhar and Axness 1983, Wilhem *et al.*, 1997; Durlofsky *et al.*, 1997; Fathi *et al.*, 2007). Heterogeneity of a porous medium could be represented in terms of random quantities, which characterize its pore structure, e.g., its mineral concentration, internal specific surface area, permeability, porosity, etc. In practice, due to its importance on fluid flow, spatial variations in permeability or porosity are often used to describe the medium heterogeneity. The variations subsequently influence flow and transport variables and may affect others related to local phenomena such as adsorption or chemical reaction. Hence, the later variables are also random quantities, more precisely random fields, with spatial and temporal arguments. During

any theoretical modeling approach and analysis, these random fields should therefore appear in the stochastic partial differential equations describing the phenomenon of interest. The results obtained accordingly using a variety of tools are then represented in terms of their statistical moments. Gelhar and Axeness (1983) followed this approach to investigate the changes in macroscopic dispersion coefficient due to local spatial fluctuations in the permeability. For a statistically homogeneous system, they quantified the effect of large-scale non-uniformities on the flow and transport. Their approach has been generalized by many others to include various effects of medium heterogeneities, e.g., on contaminant plume degradation Durlofsky *et al.*, (1997) or on variable density and viscosity fluids Welty and Gelhar (1991) in aquifers. Similar approaches have been considered by several authors; see for example textbooks by D. Forster (1977) and L.W. Gelhar (1993), or publications by J.H. Cushman's group (e.g., Hu *et al.*, 1995) and recently, by L'Heureux (2004).

As mentioned earlier most of the gas in place in coalbed and shale gas reservoirs are stored as an adsorbed gas at the solid surface of the micropores with average pore radii of less than 10 nm and permeability in the order of micro darcy. Thus the porosity variations in these tight formations could have more significant effects on gas transport and storage than permeability. In next two chapters, we are investigating the effects of small fluctuations in porosity on gas transport and storage in coal and shale samples using small perturbation theory. Here the assumption of having single gas phase and single gas component is held, however, later in chapter 5 nature of the multi-component diffusive transport processes involved in CO_2 enhanced coalbed methane recovery, i.e., counter diffusion and competitive adsorption effects, in micro-porosities will be discussed.

CHAPTER III

MATRIX HETEROGENEITY EFFECTS ON GAS TRANSPORT AND ADSORPTION IN COALBED AND SHALE GAS RESERVOIRS

Production from coalbeds and shale gas reservoirs make up nearly 15% of the total annual natural gas supply in the United States. Many other countries currently investigate the potential of these unconventional resources. Australia, Canada, China and India have commercial projects on coal gas production, while others identify new shale gas resources as they consider the incremental shale gas production in the existing reservoir. These natural gas resources are estimated to exceed 25,000 Tscf globally and, under the projected energy portfolio, they are predicted to play an important role on energy supply (Jenkins and Boyer, 2008).

A vibrant and fast-growing literature exists related to various aspects of coals and gas shales, including operational (e.g., drilling, completion and production) and technological challenges. The later mainly involves difficulties in formation evaluation and characterization, in modeling gas-matrix-fracture phenomena and in developing reliable reservoir simulators. In times, these works directly point to an inability to accurately predict the ultimate gas recovery and to explain high variability in gas well productivity, which are common to nearly all coalbed and shale gas reservoirs.

In coalbeds and shales, gas transport and storage are important for accurate prediction of production rates and for the consideration of subsurface greenhouse gas sequestration. They involve coupled fluid phenomena in porous medium including

viscous flow, diffusive transport and adsorption. Standard approach to describe gas-matrix interactions is deterministic and neglects the effects of local spatial heterogeneities in porosity and material content of the matrix. The purpose of this work is to consider local phenomena in a heterogeneous matrix using a theoretical approach. Adopting weak-noise and mean-field approximations and using a statistical approach in spectral domain, matrix heterogeneity effects are investigated in the presence of non-equilibrium adsorption with random partition coefficient. We therefore first develop the means to appropriately quantify the local matrix heterogeneities and then to up-scale (or homogenize) the gas flow, diffusive transport and adsorption processes over the matrix body. Hence, our work here builds on the premise that the local gas behavior in the matrix is simultaneously controlled by the gas sorption rates, viscous and diffusive gas mass fluxes. Although the matrix exhibits local variations in the pore structure, we consider that these local variations are weak and that the porous medium still maintains a meaningful average porosity and a constant permeability values. We then investigate analytically and numerically the effects of porosity fluctuations, in particular, and the related material property variations on the mechanisms of transport and storage. For the investigation, initially, we locally describe mass conservation for a gas component (for which the matrix has a certain adsorption capacity, e.g., methane) in homogeneous media characterized by a time-independent porosity in space-time continuum. Next, the classical perturbation theory is employed to the governing equations where the structural and chemical variations are introduced in terms of fluctuating (random) porosity and partition coefficient, respectively. The analytical part of our work is concerned with description and analysis of the theoretical problem using the mean and perturbed governing equations in the Laplace-Fourier domain. The mean equations are, in fact, upscaled governing equations, which include cross-correlations between porosity and dependent variables, reflecting the influences

of the introduced small-scale porosity fluctuations on the adsorbed and free gas concentrations and on the Fickian-type diffusivity. Obtaining explicit expressions for the later quantities are the most critical part of any work based on perturbations and noise analysis and, here, they are examined using the perturbed governing equations in the spectral domain. Similar approaches have been considered by several authors; see for example textbooks by D. Forster (1977) and L. W. Gelhar (1993), or publications by J.H. Cushman's group (e.g., Hu *et al.*, 1995) and, recently, by L'Heureux (2004).

It is found that the local heterogeneities can generate non-trivial transport and kinetics effects which retard gas release from the matrix and influence the ultimate gas recovery adversely. Macro-transport shows $1/\left[1+N_{Pe}/(1+N_{Pe})\right]$ dependence on the P*é*clet number, and persists at the diffusive ultra-low permeability limit. Macro-kinetics is directly related to Thiele modulus by the following expression: $N_{Th}/(1+2N_{Pe})$. It leads to trapping of gas in the adsorbed phase during its release from the matrix, and to an adsorption threshold during gas uptake by the matrix. Both effects are proportional to the initially available adsorbed gas amount and becomes more pronounced with the increasing variance of the porosity field. Consequently, a new upscaled deterministic gas mass balance is proposed for practical purposes. Second part of the work involves numerical analysis of the upscaled governing equations describing gas adsorption and transport behavior in heterogeneous coal matrix. For the purpose, gas release from a matrix is considered and presented as a one-dimensional initial/boundary value problem. Numerical results are presented showing free and adsorbed gas distributions and fractional gas sorption curves for unipore coal matrix exhibiting Gaussian porosity distribution. Results showing the influence of heterogeneities on gas release rates are demonstrated using fractional gas recovery curves and comparing with the homogeneous case. The work is a unique

approach for our further understanding of the coalbeds and gas shales, and it is important for the development of sound numerical gas production and sequestration models.

3.1 Local Gas Behavior in the Matrix– Homogeneous Case

3.1.1 Kinetics of Gas Adsorption in Porous Media

Perhaps the earliest discussion on the existence of local conditions which require kinetics description of adsorption in coals and shales is in King (1990), who suggested that the assumption of equilibrium adsorption may be appropriate only in reservoirs undergoing rapid desorption, such as in the vicinity of producing wells. In the later case an explicit algebraic equation, i.e., an equilibrium adsorption isotherm, describing a relationship between the adsorbed and free gas amounts is introduced:

$$C_\mu = f(C, a, b...)$$

where a and b are model parameters. Among several models considered, Henry's law isotherm is the simplest one which linearly relates the adsorbed and free gas concentrations, i.e., $C_\mu = aC$. It is not commonly used for the gas-matrix systems due to its linearity, although, it has found some applications in theoretical description of complex systems (Ruckenstein *et al.*, 1971; Smith and Williams, 1984; Alvarado *et al.*, 1998) due to its simplicity. Instead, the Langmuir isotherm has been extensively considered: $C_\mu = abC/(1+aC)$. In this case, a is the Langmuir equilibrium constant and b represents complete monolayer coverage of the open surface by the gas molecules. The relationship is derived from both kinetic and statistical mechanical points of view under the assumptions of adsorption on a fixed number of sites that are energetically equivalent, and of absence of lateral interactions between the adsorbed molecules on neighboring sites. It represents a special form of the multi-layer BET adsorption equation, $C_\mu = abC/[(1-b)(1+b(C-1)]$. There have been several attempts to develop isotherms based on the so-called pore filling theory (Dubinin, 1966), a common form of which is the Dubinin-Astakhov equation $C_\mu = \phi \exp[-ab \ln(1/b)]/(1-\phi)$, where now b appears as a structural parameter for the surface heterogeneity.

Based on experimental observations using electron microscopy or from the analysis of the adsorption equilibrium data or the observation of the desorption behavior, Do and Wang (1998) argued that simple equilibrium isotherms may not represent the dynamics between the free and adsorbed phases in low-porosity heterogeneous materials such as activated carbon. They argued that the semi-liquid adsorption layer on the internal surfaces of the porous structure is in fact quite heterogeneous, leading to desorption time-scales that are longer than the characteristic adsorption time. Hence, the desorption curve often exhibits a long tail, indicating the presence of high energy sites releasing the adsorbed molecules at a much lower rate. Thus, although commonly used, the assumption of instantaneously available gas at the pore walls may not be suitable. Instead, ideally, using an adsorption kinetics model with finite time scales for both adsorption and desorption rates is desired.

When single-component sorption rates are considered, it is common to assume that sorption follows the so-called Langmuir kinetics with adsorption and desorption rates described as follow:

$$R_{ads} = k_{ads} C (C_{\mu s} - C_{\mu}) \tag{3.1}$$

$$R_{des} = k_{des} C_{\mu} \tag{3.2}$$

where the rates are in moles per unit volume of adsorbed gas per unit time with the adsorption and desorption rate coefficients k_{ads} and k_{des}, respectively. These coefficients are a measure of the rates of collision and desorption of gas molecule to the available adsorption sites and are commonly considered to be the functions of interaction energy E between the gas molecules and the solid sites. The difference between the adsorption and desorption rates gives the net rate:

$$R_{net} = k_{ads} (C_{\mu s} - C_{\mu}) C - k_{des} C_{\mu} \tag{3.3}$$

Consequently, in the absence of a transport mechanism of the adsorbed gas (e.g., surface diffusion), the rate of interchange between the adsorbed and free gas can be

described using the following mass balance:

$$\frac{\partial C_\mu}{\partial t} = k_{ads}(C_{\mu s} - C_\mu)C - k_{des}C_\mu \tag{3.4}$$

Note that, when equilibrium is reached, R_{net}=0 is observed. Hence, Langmuir equilibrium isotherm is obtained with $a = k_{ads}/k_{des}$, $b = C_{\mu s}$. Others used a linear approach for the adsorption kinetics of fluids in porous media, see for example Brusseau and Rao (1991), Hu *et al.*, (1995), and Alvarado *et al.*, (1998), assuming that the adsorption rate is independent of the adsorbed gas concentration. Hence, the following is suggested:

$$R_{ads} = k_{ads}(C_{\mu s} - C_\mu)C \cong k_{ads}C \tag{3.5}$$

$$R_{des} = k_{des}C_\mu \tag{3.6}$$

Rate of the interchange between the adsorbed and free gas phases then becomes:

$$\frac{\partial C_\mu}{\partial t} = k_{ads}C - k_{des}C_\mu \tag{3.7}$$

which can be written in the following form

$$\frac{\partial C_\mu}{\partial t} = k_{des}(KC - C_\mu) \tag{3.8}$$

Here, $K = k_{ads}/k_{des}$ is often referred to as the equilibrium partition (or, distribution) coefficient, and k_{ads} and k_{des} are the coefficients of forward and reverse adsorption kinetics, respectively. When equilibrium is reached, equation (3.8) reduces to Henry's law isotherm where a is defined as K.

Figure 1 compares numerical results of gas release from a matrix block using the linear kinetics and equilibrium adsorption models (there will be further discussion on the nature of partial differential equations solved later on). It shows the two linear isotherms constructed by periodically measuring the free and adsorbed gas concentrations in discreet time steps at the center of a matrix block. When the gas

desorption rate coefficient is large (left figure with k_{des}=1.0E-3), the kinetics model maintains the same straight line relationship between the adsorbed and free gas as in the equilibrium case. When the rate coefficient is not large enough (right figure with k_{des}=1.0E-5), however, the isotherm corresponding to the kinetics model deviates from the equilibrium and becomes rather steep. Consequently, the domain of free gas amount is decreased, whereas the range of adsorbed gas amount is the same. Both kinetics and equilibrium cases are passing through the origin; however, in this case, the kinetics model is not following a straight line relationship between the free and adsorbed gas amounts.

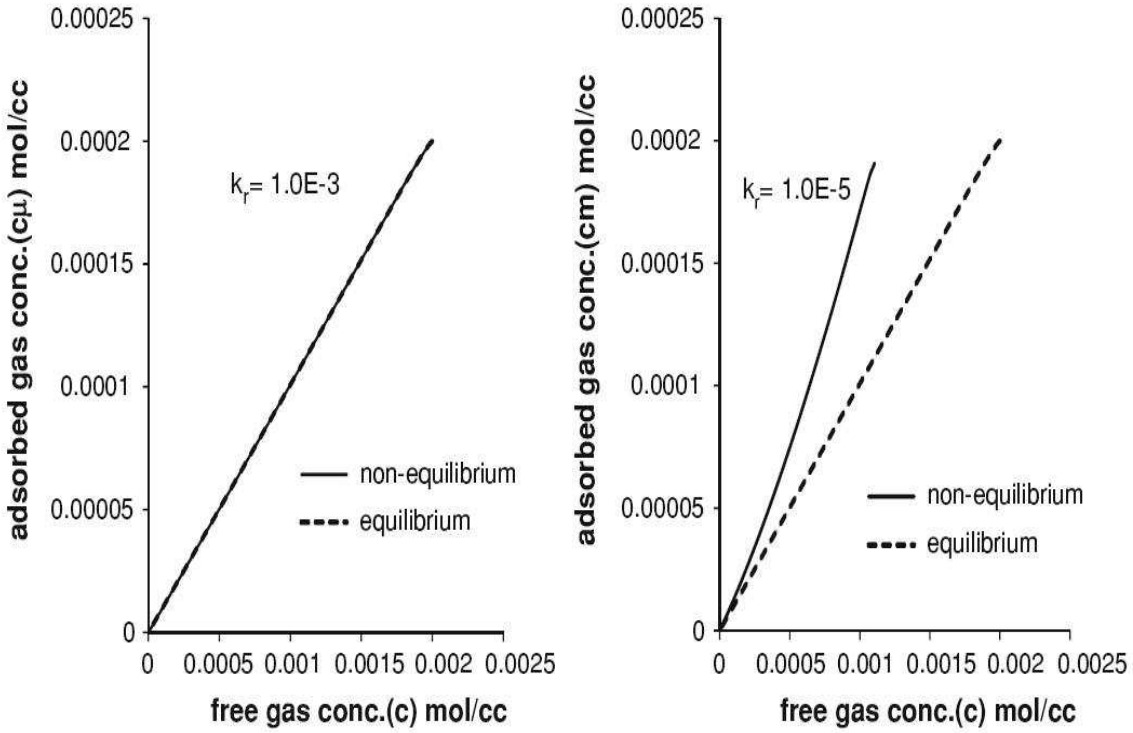

Figure 3.1: Effect of sorption kinetics on gas behavior in homogeneous porous medium. Free gas versus adsorbed gas concentrations during gas release at the center of a matrix block (1-D slab) with 10 cm half-length, $K = 0.1$, $D = 1.0\text{E-}3$ cm^2/s, $k = 4.934\text{E-}14$ cm^2, $\mu_g = 2.0\text{E-}7$ Kg/cm.s, $T = 293.15K$, $\partial C(x = 0, t)/\partial x = \partial C_\mu(x = 0, t)/\partial x = 0.0$ and $C(x = L, t) = C_\mu(x = L, t) = 0.0$

As mentioned, the sorption rate coefficients are functions of interaction energy E. Furthermore, in the case of adsorption in porous medium, the energy itself is a function of the characteristic pore size, i.e., $E(r)$ with the pore half-width r. Jagiello *et al.,*(1995) showed that the energy tends to be larger in smaller pores than in larger pores, i.e., $dE/dr < 0$. Hence, through the energy dependence of the partition coefficient, the adsorption kinetics is closely tied to the pore sizes of the matrix. This dependence is necessary in order to carry the kinetics information of the gas-solid system at the pore scale to a local continuum scale and could be explained as follows. Assume that the adsorption rate coefficient k_{ads} is independent of the interaction energy and hence its value is dictated only by the rate of collision of molecules to the surface. However, desorption rate coefficient k_{des} is allowed to follow an Arrhenius relation:

$$k_{des} = k_{r,\infty} \exp\left(\frac{-E}{R_g T}\right)$$

Then the partition coefficient is written in terms of the interaction energy as follows

$$K(E) = \frac{k_{ads}(E)}{k_{des}(E)} = \frac{k_{ads}}{k_{r,\infty}} \exp\left[\frac{E(r)}{R_g T}\right] \tag{3.9}$$

Now, using this definition, we take the derivative of the partition coefficient with respect to the pore size, r, and obtain

$$\frac{dK}{dr} = \frac{k_{ads}}{k_{r,\infty} R_g T} \exp\left[\frac{E(r)}{R_g T}\right] \frac{dE(r)}{dr} < 0 \tag{3.10}$$

Thus, we find that the changes in the partition coefficient is inversely proportional to the pore size of the matrix. This condition plays an important role in our investigation as we assume the presence of a direct coupling between the average pore size and the porosity values. Hence, we shall consider that the coefficient varies in a similar manner with the changes in porosity, i.e., $dK/d\phi$ <0.

3.1.2 Conservation of Gas Mass in Porous Media

The mass balance involves the following transient equations for the free and adsorbed gas amounts, where adsorption of free gas in the matrix and desorption is represented by a finite mass interchange between free and adsorbed gas.

$$\phi\frac{\partial C}{\partial t} + (1-\phi)\frac{\partial C_\mu}{\partial t} = \frac{\partial}{\partial x}\left(\phi\, D\frac{\partial C}{\partial x}\right) + \frac{\partial}{\partial x}\left(\phi C\frac{k}{\mu}\frac{\partial p}{\partial x}\right) \tag{3.11}$$

$$\frac{\partial C_\mu}{\partial t} = k_{des}(KC - C_\mu)$$

Here, x-t are the space-time coordinates, $C(x,t)$ the free gas concentration (mol/pore volume), $C_\mu(x,t)$ the adsorbed gas concentration (mol/solid volume), ϕ the interconnected porosity, $D(\phi)$ the tortuosity-corrected coefficient of molecular diffusion, k the absolute permeability of the porous medium, p the pore pressure, and μ the dynamic gas viscosity. Note that the formulation contains a diffusive transport term which is Fickian in nature. This roughly corresponds to bulk (pore) diffusion as the mechanism of transport. The existence of other mechanisms (e.g., Knudsen and surface diffusion) will not be considered in this work.

The formulation is different from the case where the solid material is considered to be in equilibrium with the gas in-place, i.e., the equilibrium adsorption dynamics. We introduce virial equation of state:

$$p = R_gTC + R_gTXC^2 + R_gTX_1C^3 + R_gTX_2C^4 + ... \tag{3.12}$$

with the parameters $X, X_1, X_2, ...$ representing the second, third, fourth,... virial coefficients, which are functions of temperature and composition. For practical purposes, it is common to use only the lower order terms of the equation:

$$p \cong R_gTC + R_gTXC^2 \tag{3.13}$$

Taking derivative of pressure with respect to the concentration and using the chain rule, equation (3.11) becomes:

$$\phi\frac{\partial C}{\partial t}+(1-\phi)\frac{\partial C_{\mu}}{\partial t}=\frac{\partial}{\partial x}\left[\phi\left(D+C\frac{kR_gT}{\mu}\left(2XC+1\right)\right)\frac{\partial C}{\partial x}\right] \tag{3.14}$$

$$\frac{\partial C_{\mu}}{\partial t}=k_{des}(KC-C_{\mu})$$

We performed sensitivity analysis using methane with a coal sample to determine the effect of ideal gas assumption (with XC=0) on the gas-matrix system Figure 3.2. The ideal gas assumption does not create significant effects and it has no impact on the concentration profiles and on the fractional gas recovery curve. The following governing equation for the ideal free gas mass will thus be adopted for simplicity in our analysis:

$$\phi\frac{\partial C}{\partial t}+(1-\phi)\frac{\partial C_{\mu}}{\partial t}=\frac{\partial}{\partial x}\left[\phi\left(D+C\frac{kR_gT}{\mu}\right)\frac{\partial C}{\partial x}\right] \tag{3.15}$$

$$\frac{\partial C_{\mu}}{\partial t}=k_{des}\left(KC-C_{\mu}\right)$$

Next, equation (3.15) is reorganized and written in the following form:

$$\frac{\partial C}{\partial t}=D\frac{\partial^2 C}{\partial x^2}+\alpha\frac{\partial C}{\partial x}+\beta\alpha'\frac{\partial C}{\partial x}+\beta C\frac{\partial^2 C}{\partial x^2}-\Phi k_{des}\left(KC-C_{\mu}\right) \tag{3.16}$$

$$\frac{\partial C_{\mu}}{\partial t}=k_{des}\left(KC-C_{\mu}\right)$$

Here, we introduce $\alpha=\partial(\phi D)/\phi\,\partial x$ as an effective drift velocity, reflecting changes in free gas concentration due to a non-constant diffusivity with a gradient. In addition, we have $\alpha'=\partial(\phi C)/\phi\,\partial x$ and we introduce ,$\Phi=(1-\phi)/\phi$ as the solid-to-bulk volume ratio, $\beta=kR_gT/\mu$ as the gas mobility.

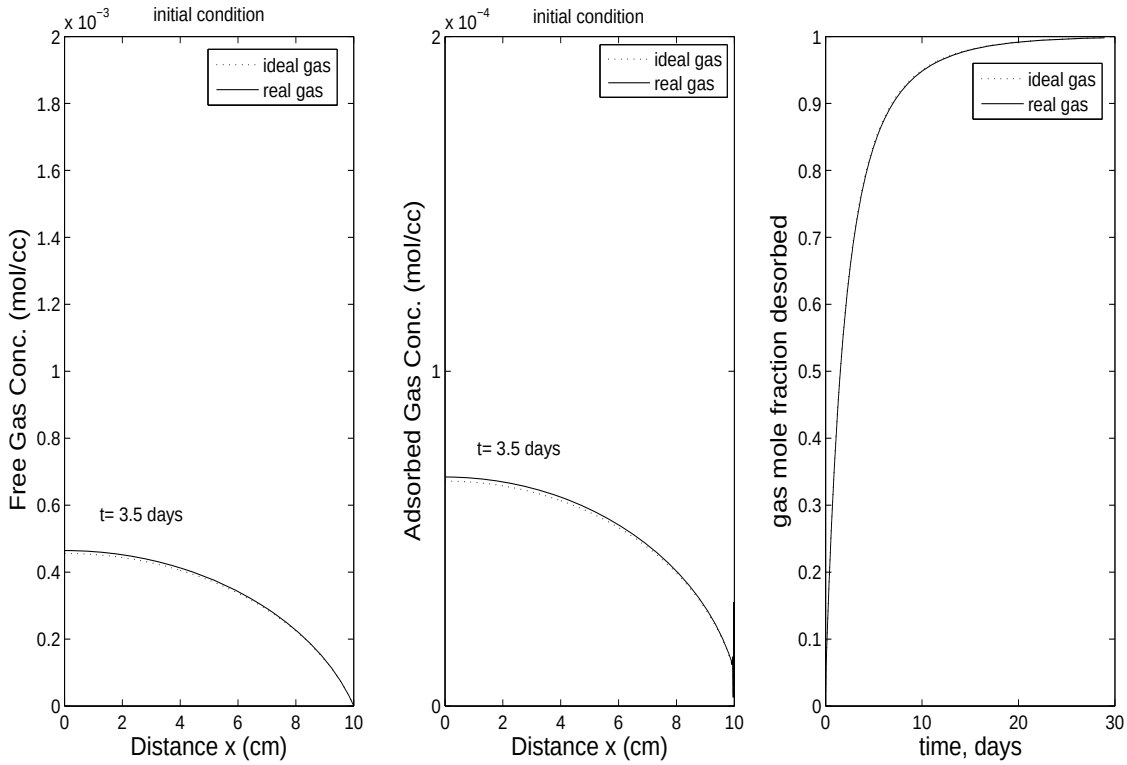

Figure 3.2: Comparison of ideal and real gas models. Left: free gas concentration profile versus distance from the center of coal matrix. Middle: adsorbed gas concentration profile versus distance from the center of coal matrix. Right: gas mole fraction desorbed versus time. Considered gas is methane and the half length of the matrix block (1-D slab) is 10 cm, k_{des} = 1.0E-5 s^{-1}, $K = 0.1$, D = 1.0E-3 $cm^2/s, k$ = 4.934E-14 cm^2, μ_g = 2.0E-7 Kg/cm.s, $T = 293.15K$, $\partial C(x = 0, t)/\partial x = \partial C_\mu(x = 0, t)/\partial x = 0.0$ and $C(x = L, t) = C_\mu(x = L, t) = 0.0$

Prior to the analysis of gas behavior in heterogeneous porous medium, it is worthwhile to briefly mention here the impact of outer boundary (i.e., the pressure condition in the surrounding fractures) on the ultimate gas recovery using equations (3.16). Figure 3.3 depicts the effect of outer boundary condition which will be used in our numerical simulation. The initially available free gas release takes place rapidly within a few days for all the cases considered. Following the completion of free gas release, the desorbed gas becomes the main source of production. During this latter period, the gas release is slow and a relatively long period of time is required for the ultimate gas recovery. In the case of zero partial pressure of methane at the outer boundary (i.e., ideal but unrealistic case of removing the released gas), complete recovery is achieved. However, when the partial pressure of methane at the boundary is increased to a finite value, which means less pressure drop across the coal matrix, the results show that the gas release rate is lower and the ultimate gas recovery is less than unity. Here, we assumed fixed outer boundary conditions which are equal to 15% and 25% of the initially distributed free gas in the matrix. In the following analysis, the outer boundary of the matrices will be fixed to a constant value.

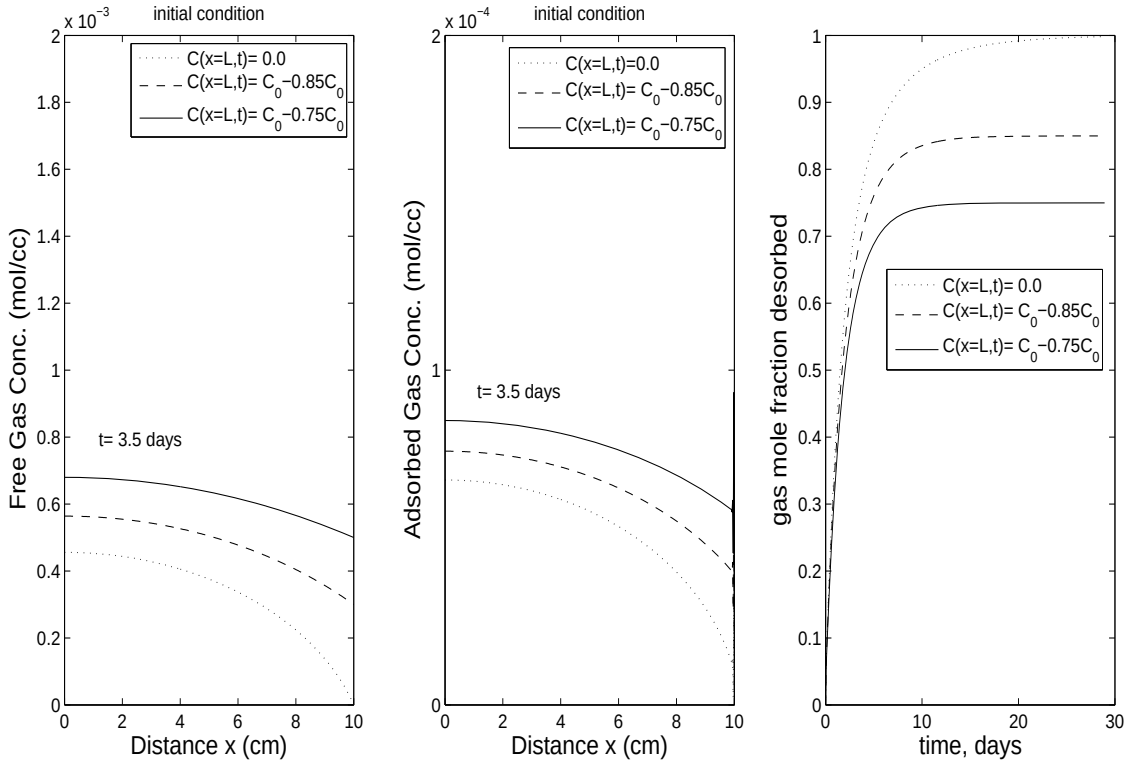

Figure 3.3: Influence of outer boundary condition on ultimate gas recovery from a matrix block surrounded by fractures. Left: free gas concentration profile versus distance from the center of matrix. Middle: adsorbed gas concentration profile versus distance from the center of matrix. Right: gas mole fraction desorbed versus time. Initial pore pressure is 4874.6 Kpa

3.2 Gas Behavior in Heterogeneous Matrix

In our naturally occurring porous medium heterogeneity is represented by a time-independent, spatially variable random porosity field $\phi = \bar{\phi} + \tilde{\phi}$ in terms of its mean $\bar{\phi}$ and small fluctuation $\tilde{\phi}$. Further, it is considered that the matrix porosity obeys stationarity of moments of order one and two (mean and the variance of porosity kept constant) with a well-defined spatial covariance function. All the dependent variables, transport and rate coefficients are affected by the medium heterogeneity presented by the porosity random field; therefore, they are also considered to be random variables. Consider that an over-bar and a tilde over a quantity denote its average value and its fluctuations about the mean, respectively. We then have:

$$\alpha = \bar{\alpha} + \tilde{\alpha}$$

$$\alpha' = \bar{\alpha}' + \tilde{\alpha}'$$

$$C = \bar{C} + \tilde{C}$$

$$C_\mu = \bar{C}_\mu + \tilde{C}_\mu$$

$$D = \bar{D} + \tilde{D}$$

$$\Phi = \bar{\Phi} + \tilde{\Phi}$$

$$K = \bar{K} + \tilde{K}$$

Note here that the partition coefficient K is also considered as a random variable so that the porosity fluctuations have the potential to create variations in gas adsorption and desorption rates. This is a reasonable and important approach since coals and shales are mixtures of various minerals and organic material exhibiting an intricate pore network. Variations in the material properties (e.g., rank and maceral content) add to structurally complex nature of coals and shales, influencing gas retention (adsorption) capacity. Substituting these expressions into the governing gas mass equations (3.16), and taking the expectation, the mass balance equation for mean

free and adsorbed gas concentrations are obtained.

$$\frac{\partial \bar{C}}{\partial t} + \bar{\Phi}\frac{\partial \bar{C}_\mu}{\partial t} - \bar{D}\frac{\partial^2 \bar{C}}{\partial x^2} = \bar{R} \tag{3.17}$$

$$\frac{\partial \bar{C}_\mu}{\partial t} = k_{des}\left(\bar{K}\bar{C} + \overline{\tilde{K}\tilde{C}} - \bar{C}_\mu\right)$$

Subtracting the obtained mean equations from the original ones (i.e., equations 3.16), the mean removed equations are derived as following:

$$\frac{\partial \tilde{C}}{\partial t} + \bar{\Phi}\frac{\partial \tilde{C}_\mu}{\partial t} - \bar{\alpha}\frac{\partial \tilde{C}}{\partial x} - \bar{D}\frac{\partial^2 \tilde{C}}{\partial x^2} - \beta\bar{\alpha}'\frac{\partial \tilde{C}}{\partial x} - \beta\bar{C}\frac{\partial^2 \tilde{C}}{\partial x^2} - \beta\tilde{C}\frac{\partial^2 \bar{C}}{\partial x^2} = \tilde{R} \tag{3.18}$$

$$\frac{\partial \tilde{C}_\mu}{\partial t} + k_{des}\tilde{C}_\mu = k_{des}\left(\overline{K}\tilde{C} + \tilde{K}\bar{C} + \tilde{K}\tilde{C} - \overline{\tilde{K}\tilde{C}}\right)$$

where we defined $\bar{R}$ and $\tilde{R}$ as

$$\bar{R} = \bar{\alpha}\frac{\partial \bar{C}}{\partial x} + \beta\bar{\alpha}'\frac{\partial \bar{C}}{\partial x} + \beta\bar{C}\frac{\partial^2 \bar{C}}{\partial x^2} + \overline{\tilde{\alpha}\frac{\partial \tilde{C}}{\partial x}} + \overline{\tilde{D}\frac{\partial^2 \tilde{C}}{\partial x^2}} + \beta\overline{\tilde{\alpha}'\frac{\partial \tilde{C}}{\partial x}} - \overline{\tilde{\Phi}\frac{\partial \tilde{C}_\mu}{\partial t}} \tag{3.19}$$

$$\tilde{R} = -\tilde{\Phi}\frac{\partial \bar{C}_\mu}{\partial t} - \tilde{\Phi}\frac{\partial \tilde{C}_\mu}{\partial t} + \overline{\tilde{\Phi}\frac{\partial \tilde{C}_\mu}{\partial t}} + \tilde{\alpha}\frac{\partial \bar{C}}{\partial x} + \tilde{\alpha}\frac{\partial \tilde{C}}{\partial x} - \overline{\tilde{\alpha}\frac{\partial \tilde{C}}{\partial x}} + \tilde{D}\frac{\partial^2 \bar{C}}{\partial x^2} + \tilde{D}\frac{\partial^2 \tilde{C}}{\partial x^2} - \overline{\tilde{D}\frac{\partial^2 \tilde{C}}{\partial x^2}} \tag{3.20}$$

$$+\beta\tilde{\alpha}'\frac{\partial \bar{C}}{\partial x} + \beta\tilde{\alpha}'\frac{\partial \tilde{C}}{\partial x} - \beta\overline{\tilde{\alpha}'\frac{\partial \tilde{C}}{\partial x}} + \beta\tilde{C}\frac{\partial^2 \tilde{C}}{\partial x^2} - \beta\overline{\tilde{C}\frac{\partial^2 \tilde{C}}{\partial x^2}}$$

Next, we implement the assumption of small-perturbations. Accordingly, the porosity fluctuations are so small that the terms including fluctuation correlations higher than second order are neglected. In homogeneous porous media, $\bar{\alpha}$, and $\bar{\alpha'}$ are defined as (L'Heureux, 2004)

$$\bar{\alpha} \cong \overline{\tilde{D}\frac{\partial \tilde{\phi}}{\partial x}} - \left(\frac{\bar{D}}{\bar{\phi}}\right)\overline{\tilde{\phi}\frac{\partial \tilde{\phi}}{\partial x}}$$
$$\bar{\alpha}' \cong \overline{\tilde{C}\frac{\partial \tilde{\phi}}{\partial x}} - \left(\frac{\bar{C}}{\bar{\phi}}\right)\overline{\tilde{\phi}\frac{\partial \tilde{\phi}}{\partial x}}$$

which are already second order in porosity fluctuations; therefore, $\bar{\alpha}\partial\tilde{C}/\partial x \cong 0$ and $\bar{\alpha'}\partial\tilde{C}/\partial x \cong 0$ are taken.

Introducing the notation of $\xi_1 = \tilde{\alpha}$ and $\xi_2 = \tilde{D}$ and taking space-Fourier and time-Laplace transform of the equations (3.17) leads to Fourier-Laplace solution of the mean concentrations:

$$(s + k^2\bar{D})\,\bar{C}_{ks} - \bar{C}_{k,t=0} + s\,\bar{\Phi}\,(\bar{C}_\mu)_{ks} - \bar{\Phi}\,(\bar{C}_\mu)_{k,t=0} = \bar{R}_{ks} \tag{3.21}$$

$$(\bar{C}_\mu)_{ks} = (s + k_{des})^{-1}\left[(\bar{C}_\mu)_{k,t=0} + k_{des}(\bar{K}\bar{C} + \overline{\tilde{K}\tilde{C}})_{ks}\right]$$

where k is the wave number, s the Laplace transform variable, $\bar{C}_{k,t=0}$ and $(\bar{C}_\mu)_{k,t=0}$ are the Fourier transform of the initial mean concentration of free and adsorbed gas respectively. Here $\bar{R}_{ks}$ is defined as

$$\bar{R}_{ks} = \left(\bar{\alpha}\frac{\partial\bar{C}}{\partial x} + \beta\bar{\alpha}'\frac{\partial\bar{C}}{\partial x} + \beta\bar{C}\frac{\partial^2\bar{C}}{\partial x^2} + \sum_{m=1,2}\overline{\frac{\xi_m\partial^m\tilde{C}}{\partial x^m}} + \beta\overline{\frac{\tilde{\alpha}'\partial\tilde{C}}{\partial x}} - \overline{\frac{\tilde{\Phi}\partial\tilde{C}_\mu}{\partial t}}\right)_{ks} \tag{3.22}$$

First and second terms in equation (3.22) are corrections to drift velocity, the third term is related to diffusive transport, and the last three terms indicate non-trivial cross-correlations between the fluctuating porosity, transport and kinetic coefficients with free and adsorbed gas concentration fields. Combining conservation of gas mass equations (3.21) for the free and adsorbed gas we have:

$$\left[s\left(1 + \frac{\bar{\Phi}k_{des}\bar{K}}{s + k_{des}}\right) + k^2\bar{D}\right]\bar{C}_{ks} = \bar{C}_{k,t=0} + \left(\bar{\Phi} - \frac{s\bar{\Phi}}{s + k_{des}}\right)\bar{C}_{\mu k,t=0} - \frac{s\bar{\Phi}k_{des}}{s + k_{des}}\left(\overline{\tilde{K}\tilde{C}}\right)_{ks} + \bar{R}_{ks}$$

Hence, formal solution of the Fourier-Laplace transform of the mean concentration $\bar{C}_{ks}$ is

$$\bar{C}_{ks} = \hat{G}_{ks}^{-1}\cdot\bar{R}_{ks} + \hat{G}_{ks}^{-1}\cdot \mathrm{X}_{ks} \tag{3.23}$$

where $\hat{G}_{ks}$ and X_{ks} are defined as

$$\hat{G}_{ks} = \left[s\left(1 + \frac{\bar{\Phi}k_{des}\bar{K}}{s + k_{des}}\right) + k^2\bar{D}\right]$$

$$\mathrm{X}_{ks} = \left[\bar{C}_{k,t=0} + \left(\bar{\Phi} - \frac{s\bar{\Phi}}{s + k_{des}}\right)(\bar{C}_\mu)_{k,t=0} - \frac{s\bar{\Phi}k_{des}}{s + k_{des}}\left(\overline{\tilde{K}\tilde{C}}\right)_{ks}\right]$$

In order to find the equivalent expression for free gas fluctuation $\tilde{C}$ in Fourier–Laplace domain, first we need to use the mean-field approximation for the terms $\beta\bar{C}\partial^2\tilde{C}/\partial x^2$ and $\beta\tilde{C}\partial^2\bar{C}/\partial x^2$. Assuming the average concentration is replaced by its value averaged over a large space domain L and time interval τ: $\bar{\bar{C}} = \int_0^\tau \int_0^L C(x,t)dxdt/L\tau \equiv g$ and $\partial\bar{\bar{C}}/\partial\overline{\phi} = g'$. Equivalently, we take $\bar{C}_{ks} = g$ in Fourier–Laplace domain. Figure 3.4 shows the effect of tight matrix porosity on the mean field approximation of free gas concentration g and its derivative g'.

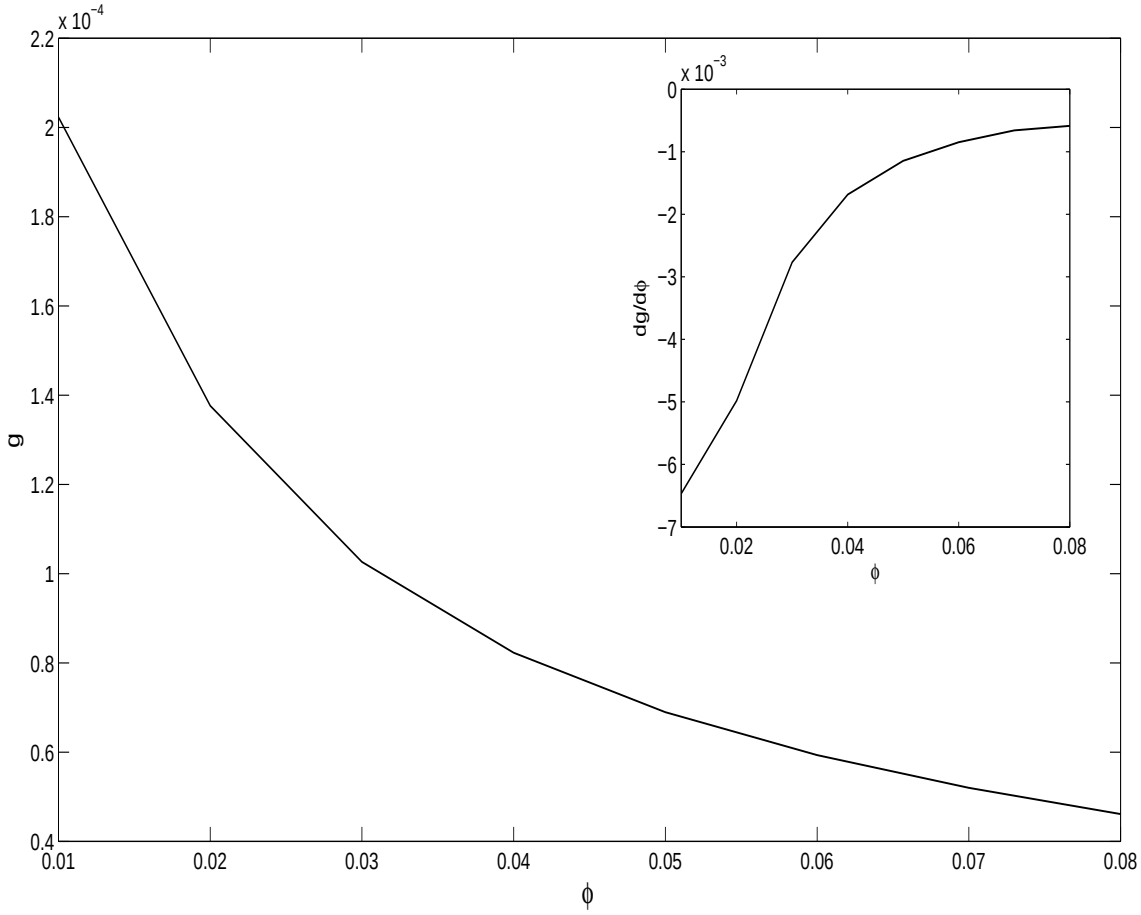

Figure 3.4: Effect of tight matrix porosity on the mean field approximation of free gas concentration g and its derivative g'

Next, we apply Fourier–Laplace transform to the perturbation equations (3.18):

$$\left(s + k^2\bar{D} + 2\beta g k^2\right)\tilde{C}_{ks} + \bar{\Phi}s\tilde{C}_{\mu ks} = \tilde{R}_{ks} \tag{3.24}$$

$$\tilde{C}_{\mu ks} = (k_{des}+s)^{-1} k_{des}\bar{K}\tilde{C}_{ks} + (k_{des}+s)^{-1} k_{des}\left[\tilde{K}\bar{C} + \tilde{K}\tilde{C} - \overline{\tilde{K}\tilde{C}}\right]_{ks}$$

where $\tilde{R}_{ks}$ is defined as

$$\tilde{R}_{ks} = \left(\begin{array}{c} -\tilde{\Phi}\dfrac{\partial \bar{C}_\mu}{\partial t} - \tilde{\Phi}\dfrac{\partial \tilde{C}_\mu}{\partial t} + \overline{\dfrac{\tilde{\Phi}\partial \tilde{C}_\mu}{\partial t}} + \tilde{\alpha}\dfrac{\partial \bar{C}}{\partial x} + \tilde{\alpha}\dfrac{\partial \tilde{C}}{\partial x} - \overline{\dfrac{\tilde{\alpha}\partial \tilde{C}}{\partial x}} + \tilde{D}\dfrac{\partial^2 \bar{C}}{\partial x^2} + \tilde{D}\dfrac{\partial^2 \tilde{C}}{\partial x^2} \\ -\overline{\dfrac{\tilde{D}\partial^2 \tilde{C}}{\partial x^2}} + \beta\tilde{\alpha}'\dfrac{\partial \bar{C}}{\partial x} + \beta\tilde{\alpha}'\dfrac{\partial \tilde{C}}{\partial x} - \beta\overline{\dfrac{\tilde{\alpha}'\partial \tilde{C}}{\partial x}} + \beta\tilde{C}\dfrac{\partial^2 \tilde{C}}{\partial x^2} - \beta\overline{\dfrac{\tilde{C}\partial^2 \tilde{C}}{\partial x^2}} \end{array} \right)_{ks} \tag{3.25}$$

In the derivation of Equations (3.25), terms higher order than quadratic are neglected, and $\tilde{C}(x,0) = \tilde{C}_\mu(x,0)$=0 are taken. Combining the free and adsorbed gas fluctuation equations in (3.24) gives

$$\left[s\left(1 + \frac{\bar{\Phi}k_{des}\bar{K}}{s+k_{des}}\right) + (\bar{D} + 2\beta g)k^2\right]\tilde{C}_{ks} = \tilde{R}_{ks} - \frac{s\bar{\Phi}k_{des}}{s+k_{des}}\left[\tilde{K}\bar{C} + \tilde{K}\tilde{C} - \overline{\tilde{K}\tilde{C}}\right]_{ks}$$

Hence, the formal solution to the Fourier–Laplace transform of the concentration fluctuation $\tilde{C}_{ks}$ is given by

$$\tilde{C}_{ks} = G_{ks}^{-1}\tilde{R}_{ks} - L_{ks}M_{ks} \tag{3.26}$$

in which

$$G_{ks} = \left[s\left(1 + \frac{\bar{\Phi}k_{des}\bar{K}}{s+k_{des}}\right) + (\bar{D} + 2\beta g)k^2\right]_{ks}$$

$$L_{ks} = \left(\frac{s\bar{\Phi}k_{des}}{s+k_{des}}\right)G_{ks}^{-1}$$

$$M_{ks} = \left[\tilde{K}\bar{C} + \tilde{K}\tilde{C} - \overline{\tilde{K}\tilde{C}}\right]_{ks}$$

In the space–time domain, the fluctuating concentration field is given by the convolution integral

$$\tilde{C}(x,t) = \int_0^t \int G^{-1}(x-x', t-t')\,\tilde{R}(x',t')\,dx'dt' \tag{3.27}$$

$$-\int_0^t \int L\left(x-x',t-t'\right) M\left(x',t'\right) dx'dt' \equiv G^{-1}_{x-x',t-t'} * \tilde{R}_{x',t'} - L_{x-x',t-t'} * M_{x',t'}$$

Substituting $\tilde{C}$ in adsorbed gas fluctuation equation gives

$$\left(\tilde{C}_\mu\right)_{ks} = \left(k_{des}+s\right)^{-1} k_{des}\bar{K}\tilde{C}_{ks} + \left(k_{des}+s\right)^{-1} k_{des}\left[\tilde{K}\bar{C} + \tilde{K}\tilde{C} - \overline{\tilde{K}\tilde{C}}\right]_{ks}$$

$$\left(\tilde{C}_\mu\right)_{ks} = \left(k_{des}+s\right)^{-1} k_{des}\bar{K}\left(G^{-1}_{ks}\cdot\tilde{R}_{ks} - L_{ks}.M_{ks}\right) + \left(k_{des}+s\right)^{-1} k_{des}\left[\tilde{K}\bar{C} + \tilde{K}\tilde{C} - \overline{\tilde{K}\tilde{C}}\right]_{ks}$$

$$= \breve{G}^{-1}_{ks}\,\tilde{R}_{ks} + \breve{L}_{ks}\,M_{ks} \tag{3.28}$$

in which $\breve{G}^{-1}_{ks} = \left(\dfrac{\bar{K}k_{des}}{s+k_{des}}\right) G^{-1}_{ks}$ and $\breve{L}_{ks} = \left(\dfrac{-\bar{K}k_{des}}{s+k_{des}} L_{ks} + \dfrac{k_{des}}{s+k_{des}}\right)$

In the space–time domain, the fluctuating adsorbed gas concentration field is given by the convolution integral

$$\tilde{C}_\mu\left(x,t\right) = \int_0^t \int \breve{G}^{-1}\left(x-x',t-t'\right)\tilde{R}\left(x',t'\right) dx'dt' \tag{3.29}$$

$$-\int_0^t \int \breve{L}\left(x-x',t-t'\right) M\left(x',t'\right) dx'dt' \equiv \breve{G}^{-1}_{x-x',t-t'} * \tilde{R}_{x',t'} - \breve{L}_{x-x',t-t'} * M_{x',t'}$$

The cross-correlation terms in equation (3.22), i.e., the last three terms, are obtained using $\tilde{C}$ and $\tilde{C}_\mu$. The summation term can be obtained by multiplying the proper spatial derivative of the concentration fluctuation $\tilde{C}$ with the fluctuating transport term $\xi_m(x)$ neglecting the third order porosity fluctuation terms and taking the expectation.

$$\sum_{m=1,2} \overline{\frac{\xi_m \partial^m \tilde{C}}{\partial x^m}} = \sum_{m=1,2} \frac{\partial^m G^{-1}_{x-x',t-t'}}{\partial x^m} * \overline{\xi_m \tilde{R}_{x',t'}} - \sum_{m=1,2} \frac{\partial^m L_{x-x',t-t'}}{\partial x^m} * \overline{\xi_m M_{x',t'}} \tag{3.30}$$

The fourth term in equation (3.22) is obtained similarly using the definition of $\tilde{C}$:

$$\beta\overline{\frac{\tilde{\alpha}'\partial\tilde{C}}{\partial x}} = \frac{\partial G^{-1}_{x-x',t-t'}}{\partial t} * \beta\overline{\tilde{\alpha}'\tilde{R}} - \frac{\partial L_{x-x',t-t'}}{\partial t} * \beta\overline{\tilde{\alpha}' M} \tag{3.31}$$

And the last term is obtained multiplying the time derivative of the adsorbed gas concentration fluctuation $\tilde{C}_\mu$ with $\tilde{\Phi}$ and taking the average over realizations.

$$\overline{\frac{\tilde{\Phi}\partial\tilde{C}_\mu}{\partial t}} = \frac{\partial \breve{G}^{-1}_{x-x',t-t'}}{\partial t} * \overline{\tilde{\Phi}\tilde{R}} + \frac{\partial \breve{L}_{x-x',t-t'}}{\partial t} * \overline{\tilde{\Phi} M} \tag{3.32}$$

where the third order terms in the porosity fluctuations have been dropped. Taking the space-Fourier and time-Laplace transformation of equations (7.13), (7.14) and (7.15) gives

$$\sum_{m=1,2} \overline{\frac{\xi_m \partial^m \tilde{C}}{\partial x^m}} = P_{ks}\bar{C}_{\mu\, k,t=0} + Q_{ks}\bar{C}_{ks} + S_{ks}\bar{C}_{ks} - T_{ks}\bar{C}_{ks} \tag{3.33}$$

$$\beta\overline{\frac{\tilde{\alpha}'\partial\tilde{C}}{\partial x}} = U_{ks}\bar{C}_{\mu\, k,t=0} + V_{ks}\bar{C}_{ks} + W_{ks}\bar{C}_{ks} - Y_{ks}\bar{C}_{ks} \tag{3.34}$$

$$\overline{\frac{\tilde{\Phi}\partial\tilde{C}_{\mu}}{\partial t}} = Z_{ks}\bar{C}_{\mu\, k,t=0} + M_{ks}\bar{C}_{ks} + N_{ks}\bar{C}_{ks} + O_{ks}\bar{C}_{ks} \tag{3.35}$$

Now substituting all these equations back to equation (3.22), $\bar{R}_{ks}$ becomes

$$\bar{R}_{ks} = \left(\bar{\alpha}\frac{\partial\bar{C}}{\partial x} + \beta\bar{\alpha}'\frac{\partial\bar{C}}{\partial x} + \beta\bar{C}\frac{\partial^2\bar{C}}{\partial x^2}\right)_{ks} + P_{ks}\bar{C}_{\mu k,t=0} + Q_{ks}\bar{C}_{ks} + S_{ks}\bar{C}_{ks} - T_{ks}\bar{C}_{ks}$$

$$+U_{ks}\bar{C}_{\mu k,t=0} + V_{ks}\bar{C}_{ks} + W_{ks}\bar{C}_{ks} - Y_{ks}\bar{C}_{ks} + Z_{ks}\bar{C}_{\mu k,t=0} + M_{ks}\bar{C}_{ks} + N_{ks}\bar{C}_{ks} + O_{ks}\bar{C}_{ks} \tag{3.36}$$

where a series of integral terms appear and are tabulated in Table 1, in Appendix A. In the table, Q is dummy wave number label. In addition, we can express the cross-correlation $\overline{\tilde{K}\tilde{C}}$ in equation (3.17) using the definition of $\tilde{C}$ (equation 7.16) in the following form

$$\overline{\tilde{K}\tilde{C}} = G^{-1} * \overline{\tilde{K}\tilde{R}} - L * \overline{\tilde{K}M} \tag{3.37}$$

Taking space–Fourier and time–Laplace transform of equation (7.17) leads to

$$\left(\overline{\tilde{K}\tilde{C}}\right)_{ks} = I_{ks}\bar{C}_{\mu\, k,t=0} + E_{ks}\bar{C}_{ks} + F_{ks}\bar{C}_{ks} - J_{ks}\bar{C}_{ks} \tag{3.38}$$

which, also includes a set of integral terms given in Table 2 in the Appendix A. In order to evaluate these integrals, the porosity fluctuations $\tilde{\phi}$ around the mean porosity $\bar{\phi}$ assumed to be Gaussian random variable with zero mean and variance

σ_ϕ^2, and the spatial correlation function defined as $\overline{\tilde{\phi}(x)\tilde{\phi}(y)} = \sigma_\phi^2 f(|x-y|)$. The auto– and cross–covariances appearing in the integrals are defined using Gaussian correlation function and the assumption of second order stationarity. Then $\overline{\tilde{\alpha}_x\tilde{\alpha}_{x'}} = \left(D' + \bar{D}/\bar{\phi}\right)^2 \overline{\partial_x\tilde{\phi}(x)\partial_{x'}\tilde{\phi}(x')}$=-$\left(D' + \bar{D}/\bar{\phi}\right)^2 \sigma_\phi^2 d^2 f(x)/dx^2$
is defined in space and time domain which is $\overline{\xi_{Q1}\xi_{-Q1}} = \overline{\tilde{\alpha}_Q\tilde{\alpha}_{-Q}} = \left(D' + \bar{D}/\bar{\phi}\right)^2 \sigma_\phi^2 Q^2 f_Q$ in Fourier space domain where σ_ϕ^2 is the variance of porosity, f_Q is the Fourier transform of the porosity correlation function $f(x)$. Assuming Gaussian random variable with Gaussian model of spatial covariance porosity, characterized by correlation length λ, we have $f_x = \exp\left(-x^2/2\lambda^2\right)$ and $f_Q = \sqrt{2\pi}\lambda \exp\left(-Q^2\lambda^2/2\right)$ in the real and spectral domains, respectively. Therefore we defined a set of auto– and cross–covariance in Table 3, Appendix B. Using conventional approximations s=k=0 in Q–dependent terms of the integrands, the following solutions are obtained for the integrals defined in Tables 1 and 2 Appendix A:

$$P_{ks} = \frac{\bar{D}\sigma_\phi^2}{\bar{\phi}(\bar{D}+2\beta g)}; \quad Q_{ks} = \frac{D'\sigma_\phi^2}{(\bar{D}+2\beta g)}(2D' + \frac{\bar{D}}{\bar{\phi}})k^2; \quad S_{ks} = T_{ks} = Y_{ks} = 0;$$

$$U_{ks} = \frac{\beta(g' + \frac{g}{\bar{\phi}})\sigma_\phi^2}{(\bar{D}+2\beta g)}; \quad V_{ks} = \frac{\beta D'(g' + \frac{g}{\bar{\phi}})\sigma_\phi^2}{(\bar{D}+2\beta g)}k^2; \quad W_{ks} = Z_{ks} = M_{ks} = N_{ks} = 0;$$

$$O_{ks} = k_{des}K'\sigma_\phi^2; \quad I_{ks} = -K'\sigma_\phi^2\frac{\lambda^2}{\bar{D}}; \quad F_{ks} = K'D'\sigma_\phi^2\frac{\lambda^2}{\bar{D}}k^2; \quad E_{ks} = J_{ks} = 0;$$

in which $\breve{G}_{k(0)}^{-1} = 0$ and $\breve{L}_{k(0)} = k_{des}$. Thus, the $\bar{R}_{ks}$ becomes

$$\bar{R}_{ks} = \left(\bar{\alpha}\frac{\partial\bar{C}}{\partial x} + \beta\bar{\alpha}'\frac{\partial\bar{C}}{\partial x} + \beta\bar{C}\frac{\partial^2\bar{C}}{\partial x^2}\right)_{ks} + \frac{\bar{D}\sigma_\phi^2}{\bar{\phi}(\bar{D}+2\beta g)}(\bar{C}_\mu)_{k,t=0} + \left(\frac{D'\sigma_\phi^2}{\bar{D}+2\beta g}\right)\left(2D' + \frac{\bar{D}}{\bar{\phi}}\right)$$

$$\times k^2\bar{C}_{ks} + \frac{\beta\left(g' + g/\bar{\phi}\right)\sigma_\phi^2}{\bar{D}+2\beta g}(\bar{C}_\mu)_{k,t=0} + \frac{\beta D'\left(g' + g/\bar{\phi}\right)\sigma_\phi^2}{\bar{D}+2\beta g}k^2\bar{C}_{ks} + k_{des}K'\sigma_\phi^2\bar{C}_{ks} \tag{3.39}$$

Taking the inverse Laplace-Fourier transform, $\bar{R}_{ks}$ becomes:

$$\bar{R} = \bar{\alpha}\frac{\partial\bar{C}}{\partial x} + \beta\bar{\alpha}'\frac{\partial\bar{C}}{\partial x} + \beta\bar{C}\frac{\partial^2\bar{C}}{\partial x^2} + \left(\frac{\bar{D}\sigma_\phi^2}{\bar{\phi}(\bar{D}+2\beta g)}\right)(\bar{C}_\mu)_{x,t=0} - \left(\frac{D'(2D' + \bar{D}/\bar{\phi})\sigma_\phi^2}{\bar{D}+2\beta g}\right)\frac{\partial^2\bar{C}}{\partial x^2}$$

$$+\left(\frac{\beta(g'+g/\bar{\phi})\sigma_\phi^2}{(\bar{D}+2\beta g)}\right)(\bar{C}_\mu)_{x,t=0}-\left(\frac{\beta D'(g'+g/\bar{\phi})\sigma_\phi^2}{\bar{D}+2\beta g}\right)\frac{\partial^2\bar{C}}{\partial x^2}+k_{des}K'\sigma_\phi^2\ \bar{C} \quad (3.40)$$

and also $\left(\overline{\tilde{K}\tilde{C}}\right)_{ks}$ is given by:

$$\left(\overline{\tilde{K}\tilde{C}}\right)_{ks}=-\left[K'\sigma_\phi^2\lambda^2/(\bar{D}+2\beta g)\right]\bar{C}_{\mu\,k,t=0}+\left[K'D'\sigma_\phi^2\lambda^2/(\bar{D}+2\beta g)\right]k^2\bar{C}_{ks} \quad (3.41)$$

which, in the time-space domain results in:

$$\overline{\tilde{K}\tilde{C}}=-\left[K'\sigma_\phi^2\lambda^2/(\bar{D}+2\beta g)\right](\bar{C}_\mu)_{x,t=0}-\left[K'D'\sigma_\phi^2\lambda^2/(\bar{D}+2\beta g)\right]\frac{\partial^2\bar{C}}{\partial x^2} \quad (3.42)$$

3.3 Upscaled Governing Equations

Substituting equations (7.18) and (7.19) into the mean governing equations given in (3.17), using the definitions of $\bar{\alpha}$, $\bar{\alpha'}$, and β, and re-arranging leads to the following form of the governing equations:

$$\bar{\phi}\frac{\partial \bar{C}}{\partial t} + (1-\bar{\phi})\frac{\partial \bar{C}_{\mu}}{\partial t} = \frac{\partial}{\partial x}\left(\bar{\phi}\mathcal{D}\frac{\partial \bar{C}}{\partial x}\right) + \frac{\partial}{\partial x}\left(\bar{\phi}\bar{C}\frac{k}{\mu}\frac{\partial \bar{p}}{\partial x}\right) + \Gamma_1 + \Gamma_2$$

$$\frac{\partial \bar{C}_{\mu}}{\partial t} = k_{des}\left[\bar{K}\bar{C} - \left(\bar{C}_{\mu} + \Gamma_3\right)\right] \tag{3.43}$$

in which new quantities reflecting the effects of local heterogeneities appear. These are defined as:

$$\mathcal{D} = \bar{D} - D'\sigma_{\phi}^2 \left(\frac{2D' + \beta g' + \dfrac{\bar{D} + \beta g}{\bar{\phi}}}{\bar{D} + 2\beta g}\right) \tag{3.44}$$

$$\Gamma_1 = \left[\bar{D} + \beta(\bar{\phi}g' + g)\right]\frac{\sigma_{\phi}^2 \bar{C}_{\mu 0}}{(\bar{D} + 2\beta g)} \tag{3.45}$$

$$\Gamma_2 = k_{des}K'\bar{\phi}\sigma_{\phi}^2\bar{C} \tag{3.46}$$

$$\Gamma_3 = \frac{K'\sigma_{\phi}^2\lambda^2}{\bar{D} + 2\beta g}\left(\bar{C}_{\mu 0} + D'\frac{\partial^2 \bar{C}}{\partial x^2}\right) \tag{3.47}$$

where $D' = d\bar{D}/d\bar{\phi} > 0$ and $K' = d\bar{K}/d\bar{\phi} < 0$ in agreement with our discussion in § 4.2.1.

Based on the analytical part of our investigation, the following fundamental observations on the structure of the upscaled differential equations can be made:

1. Upscaling introduces clearly defined new terms into the governing equations. These are the diffusive term, involving apparent diffusivity $\mathcal{D}$, and the source/sink terms Γ_1, Γ_2 and Γ_3 in equation (3.43).

2. In the homogeneous limit, the parameters σ_ϕ^2 is nil; hence, the apparent diffusion coefficient $\mathcal{D}$ reduces to $\bar{D}$ and Γ_i terms all disappear. Thus, equations (3.43) become identical with the equations (3.11), i.e., the homogeneous case.

3. $\mathcal{D}$ is influenced by the presence of viscous transport and its physical interpretation appears complex.

4. Γ_i increases with the variance of porosity, σ_ϕ^2.

5. Γ_2 and Γ_3 show dependence on the free gas concentration and therefore they are expected to change in time and space.

6. Γ_1 and Γ_3 increases with the initially available mean adsorbed gas amount, $\bar{C}_{\mu 0}$

In the following section, the obtained upscaled governing equations given in (3.43) are numerically analyzed using a time-implicit finite difference approach based on Newton method and using gas/matrix system parameters given in Table 4.1, and considering the initial/boundary value problem defined in Figure 3.5. The data set includes the local (or laboratory measured) viscous and diffusive transport, and kinetics parameters for a symmetric matrix block (slab) with a half-length of 10.0 cm and surrounded by fracture; in addition, it introduces a mildly heterogeneous matrix as base-case for the sensitivity analysis. At a particular time-step during the simulation, as part of the Newton iteration, the mean field approximation of the free gas concentration g and it's derivative with respect to porosity g' are computed. Results are presented in terms of the free and adsorbed gas concentration profiles, and fractional recovery curves through Figures 3.6 through 3.9.

Table 3.1: Problem parameters for the heterogeneous gas/matrix system

Parameter	Unit	Value
$\bar{\phi}$	fraction	1.0E-2
σ_{ϕ}^2	-	5.3E-7
$\bar{C}_0$	mol/cc	2.0E-3
k_{des}	1/sec	1.0E-5
$\bar{K}$	fraction	0.1
g	mol/cc	2.028E-4
k	cm^2	4.934E-14
μ_g	Kg/cm.s	2.0E-7
K'	fraction	-5.0E2
$\bar{D}$	cm^2/sec	1.0E-3
D'	cm^2/sec	3.3E-2
g'	mol/cc	-0.00835
$\hat{\alpha}$	cm/sec	6.0E-9
λ	cm	1.0
L	cm	10.0
T	Kelvin	293.15

3.4 Results and Discussion

Our analysis involves two types of numerically obtained data, which correspond to a matrix considered to be (i) homogeneous, or (ii) heterogeneous. In the later case, the analysis requires that the simulations are run under varying conditions of heterogeneity. Heterogeneous matrix properties with the base-state values are also given in Table 4.1. Figure 3.6 shows direct comparison of the heterogeneous case with the equivalent homogeneous case, in terms of free/adsorbed gas concentration profiles and fractional gas recovery curve. It is observed that heterogeneity retards gas release from the matrix and influences gas recovery adversely. The ultimate recovery, which was 100% in the homogeneous case, drops to a value around 87.0% in the mildly heterogeneous case. Understanding how the matrix heterogeneity influences the gas behavior, as depicted in Figure 3.6, requires several steps of analysis. For the purpose, first a sensitivity analysis is performed numerical simulation and comparing the magnitudes of the terms appearing in (3.43). Based on the sensitivity analysis, it is found that $\mathcal{D} \cong \bar{D}$, hence mild fluctuations in porosity has negligible effect on molecular diffusion in porous media. In addition, it is found that Γ_2 is negligible for the typical coalbed and shale gas conditions, and Γ_3 safely reduces to the following form:

$$\Gamma_3 \cong \frac{K'\lambda^2\sigma_\phi^2\bar{C}_{\mu 0}}{\bar{D} + 2\beta g} \tag{3.48}$$

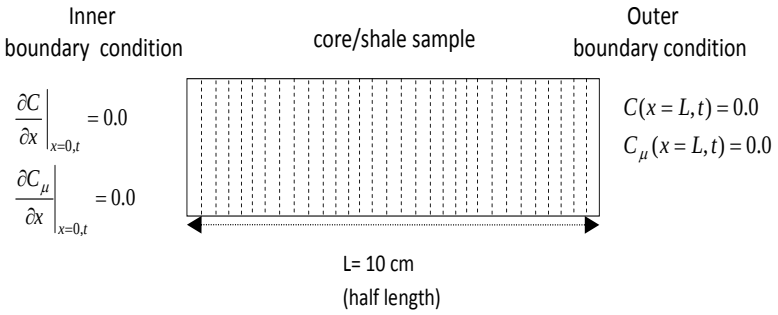

Figure 3.5: A schematic showing the setup for numerical simulation. δx_i=10/500 cm and δt_i=1.4 minutes for i=1,2,...,500, $C(x,t=0)$ = 2.0E-3, $C_\mu(x,t=0)$ = 2.0E-4 mol/cc

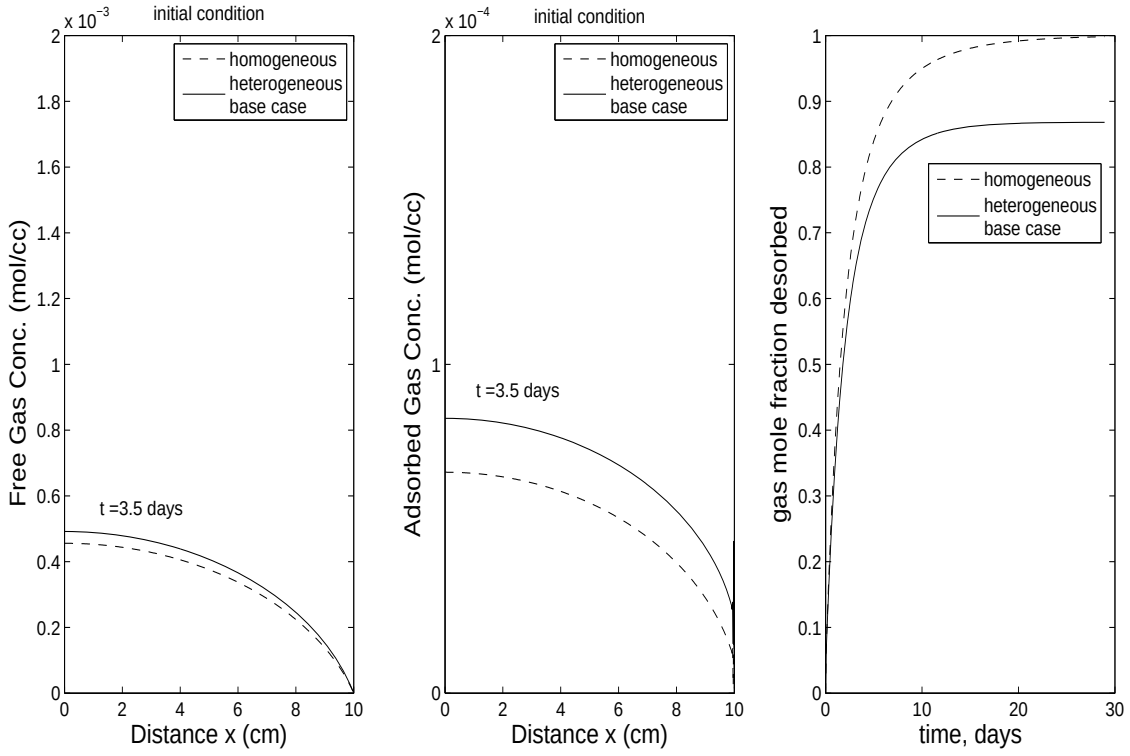

Figure 3.6: Effect of porosity heterogeneity on gas recovery. Left: free gas concentration profile versus distance from the center of matrix. Middle: adsorbed gas concentration profile versus distance from the center of the matrix. Right: gas mole fraction desorbed versus time.

3.4.1 Macro-transport Effects

Further, it is observed that typically $\bar{\phi}g' << g$ condition is satisfied across the matrix block; hence, Γ_1 simplifies to

$$\Gamma_1 \cong \left(\frac{\bar{D}}{\bar{D}+2\beta g}+\frac{\beta g}{\bar{D}+2\beta g}\right)\sigma_\phi^2\bar{C}_{\mu 0}. \tag{3.49}$$

Substituting the definitions of β and g into this approximation and re-arranging, the following expression is obtained:

$$\Gamma_1 \cong \left[\frac{1}{1+\dfrac{2k\bar{\bar{p}}}{\bar{D}\mu}}+\frac{1}{2+\dfrac{\bar{D}\mu}{k\bar{\bar{p}}}}\right]\sigma_\phi^2\bar{C}_{\mu 0}=\frac{\sigma_\phi^2\bar{C}_{\mu 0}}{1+N_{Pe}/(1+N_{Pe})}. \tag{3.50}$$

Here, $\bar{\bar{p}}=R_gT\bar{\bar{C}}$ is average pressure across the matrix and the denominator includes a dimensionless quantity N_{Pe} commonly known as P*é*clet number. It is a measure of the rate of viscous transport of a flow to its rate of molecular diffusion. Hence, for typical coal and shale matrices, Γ_1 increases with the matrix permeability. However, note that it does not disappear in the zero permeability limit; instead, it changes with the average initial adsorbed gas amount and with the porosity variance. (This limit will be further discussed in §3.4.3). Thus, Γ_1 is truly a term corresponding to macro-transport effect of the heterogeneous matrix.

3.4.2 Macro-kinetics Effects

Similarly, one can re-visit the expression of Γ_3 by substituting the definitions of β and g into the approximation:

$$\Gamma_3 \cong \frac{K'\sigma_\phi^2\lambda^2\bar{C}_{\mu 0}}{\bar{D}+\dfrac{2k\bar{\bar{p}}}{\mu}}=\frac{K'\lambda^2}{\bar{D}\left(1+\dfrac{2k\bar{\bar{p}}}{\bar{D}\mu}\right)}\sigma_\phi^2\bar{C}_{\mu 0}=\frac{N_{Th}}{k_{des}(1+2N_{Pe})}\sigma_\phi^2\bar{C}_{\mu 0}, \tag{3.51}$$

which now includes a modified Thiele modulus, $N_{Th}=(d\bar{K}/d\bar{\phi})k_{des}\lambda^2/\bar{D}$ for the heterogeneous matrix. In our case, Thiele modulus is a measure of the porosity dependence of the adsorption rate with respect to the rate of diffusion and, interestingly,

its definition now includes the correlation length of the heterogeneous porosity field. As in the case of macro-transport term, Γ_3 increases with the average initial adsorbed gas amount and with the porosity variance. Hence Γ_3 reflects macro-kinetics effect of the heterogeneous matrix.

One can have a more insightful look at the macro-kinetics effect in the equilibrium adsorption limit. Note that under the equilibrium conditions, we now have

$$\bar{K}\bar{C} - \left(\bar{C}_\mu + \Gamma_3\right) = 0 \tag{3.52}$$

which gives

$$\bar{C}_\mu = \bar{K}\bar{C} - \Gamma_3 \tag{3.53}$$

when re-organized. A schematic representation of the macro-kinetics effect is shown in Figure 3.7 for both gas uptake and release cases. For a given free gas amount, the macro-kinetics effect (or Γ_3) causes the matrix to retain a larger amount of adsorbed gas, which creates trapping effect during the gas release and a threshold effect during the gas uptake. These observations are confirmed using numerical results, which are shown in Figure 3.8.

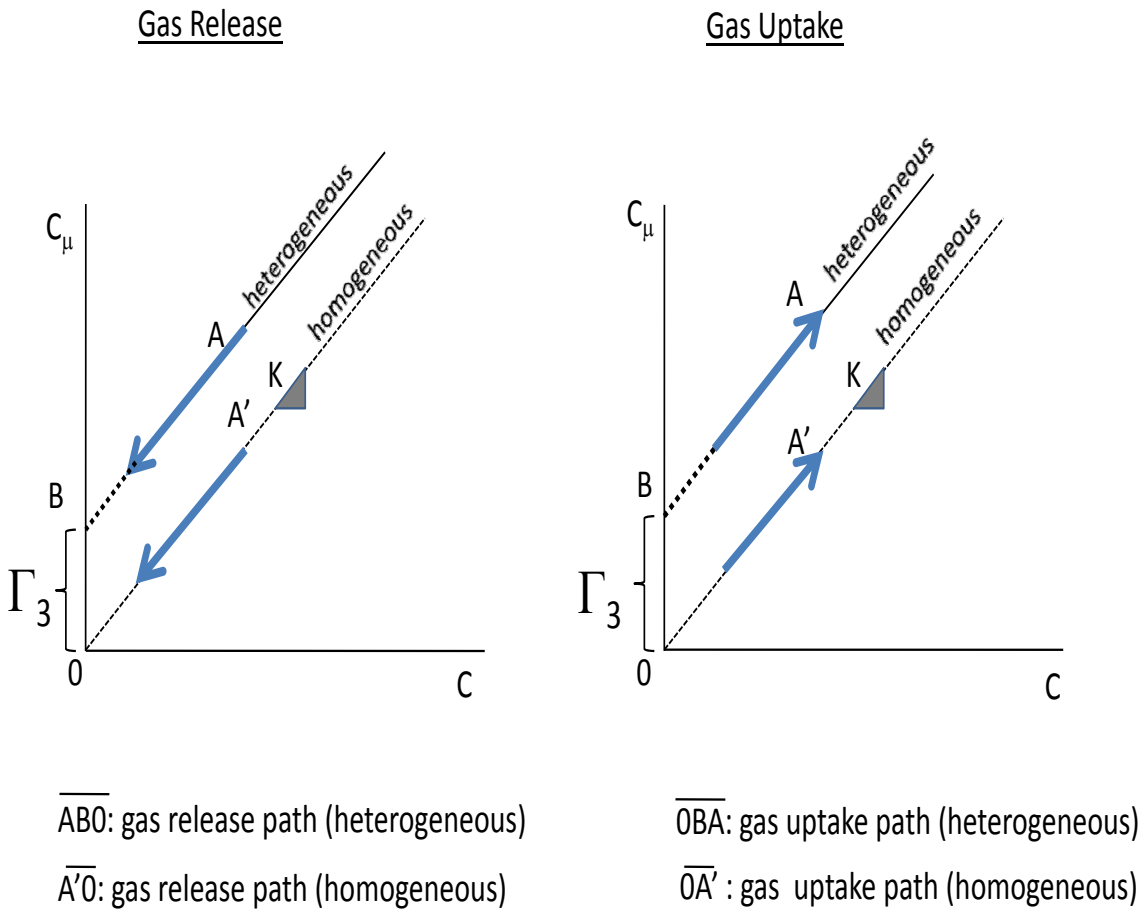

Figure 3.7: Effect of Γ_3 on gas release (left) and gas uptake (right) under the equilibrium adsorption condition

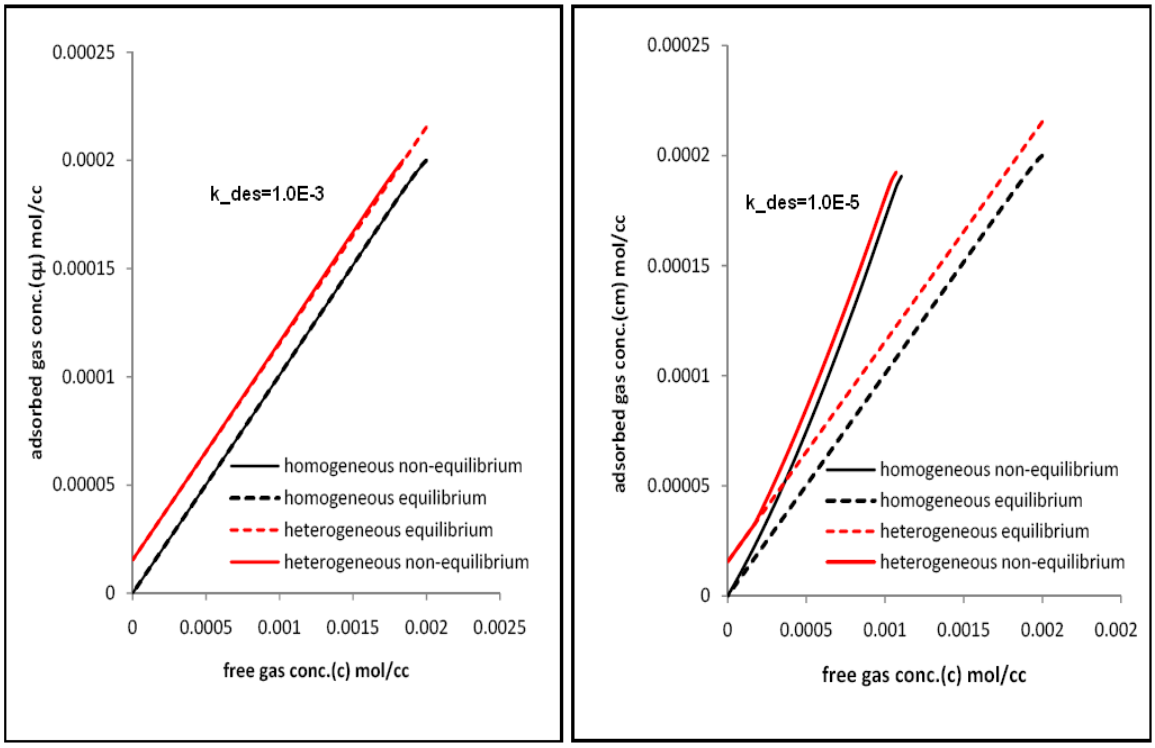

Figure 3.8: Effect of sorption on gas behavior in homogeneous and heterogeneous porous media. Free gas versus adsorbed gas concentrations at the center of the matrix block

Figure 3.9 (left) delineates the macro-transport and macro-kinetics effects of heterogeneity. It investigates the influences of Γ_1 and Γ_3 on the fractional gas recovery curve separately. Obviously, macro-transport and -kinetics both play an active role on the reduction in gas recovery observed earlier, see Figure 3.6 (right).

3.4.3 Diffusive limit: $N_{Pe} \to 0$

When permeability is low, typically in the order of nano-darcy, the convective transport term in our upscaled free gas mass balance vanishes. In this limit, equations (3.50), and (3.51) reduces to

$$\Gamma_{1,\text{diff}} = \sigma_\phi^2 \bar{C}_{\mu 0}$$

$$\Gamma_{3,\text{diff}} = \frac{N_{Th}}{k_{des}} \sigma_\phi^2 \bar{C}_{\mu 0} \tag{3.54}$$

Substituting equations (3.54) into the upscaled equation (3.43), and considering $\mathcal{D}$ and Γ_2 are negligible, the upscaled equation for diffusive system becomes:

$$\bar{\phi} \frac{\partial \bar{C}}{\partial t} + (1 - \bar{\phi}) \frac{\partial \bar{C}_\mu}{\partial t} = \frac{\partial}{\partial x} \left(\bar{\phi} \bar{D} \frac{\partial \bar{C}}{\partial x} \right) + \sigma_\phi^2 \bar{C}_{\mu 0}$$

$$\frac{\partial \bar{C}_\mu}{\partial t} = k_{ads} \bar{C} - k_{des} \bar{C}_\mu + N_{Th} \sigma_\phi^2 \bar{C}_{\mu 0} \tag{3.55}$$

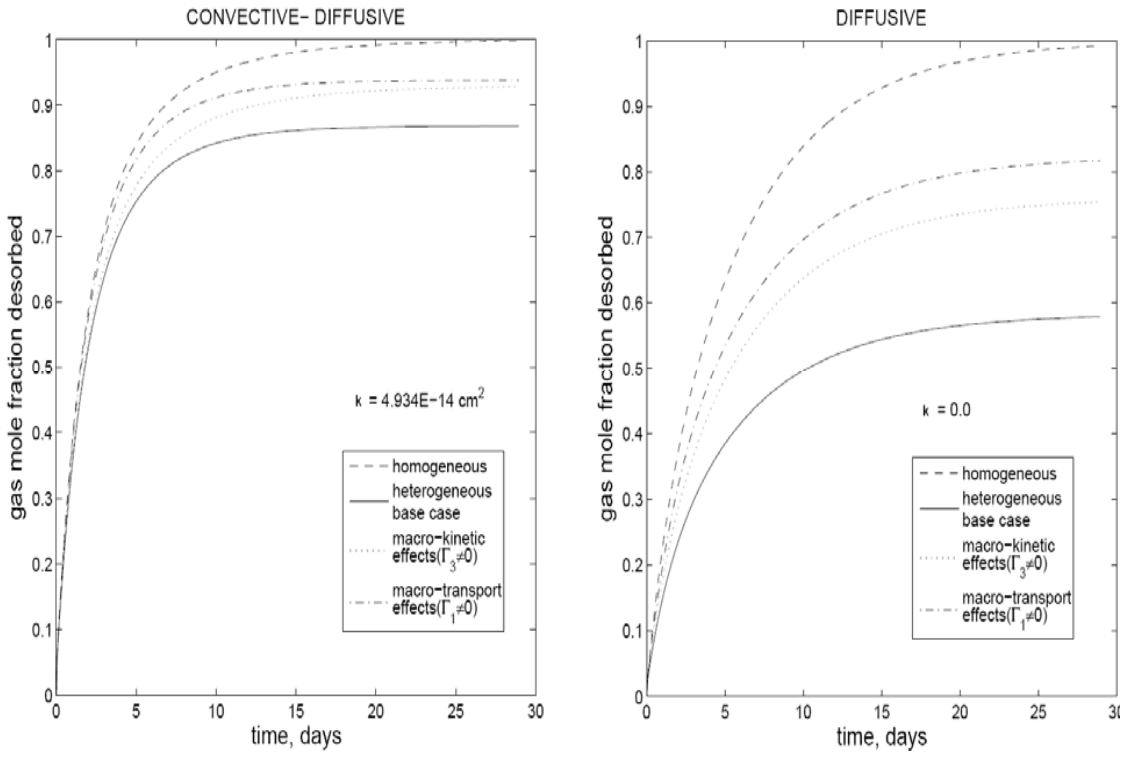

Figure 3.9: Macro-kinetics and macro-transport effects on the ultimate gas recovery. Fractional gas recovery versus time for a convective-diffusive (left) and for a diffusive (right) system with zero permeability.

Figure 3.9 (right) shows the diffusive system response in terms of gas recovery. We note that the absence of viscous transport does not influence the homogeneous response significantly because, during the same time period, almost the same amount of gas is ultimately recovered using diffusion as the only transport mechanism, see slightly lower dashed line on Figure 3.9 (right) and compare with the other dashed line on Figure 3.9 (left) . Intuitively, one would expect such behavior in the case of coal and shale matrices because these environments maintain relatively low permeability. Interestingly, however, the same argument may not be raised when the matrix is considered to be heterogenous (see the solid lines in Figure 3.9). Less than 60% of the gas initially in-place could be recovered during the same time period when the gas transport is due to diffusion only. This reduction is due to macro-transport and, more importantly, macro-kinetics effects of the porosity heterogeneity, as they persist in the diffusive limit. Furthermore, depending on Thiele modulus, the macro-kinetics effect has the potential to dominate the ultimate gas recovery.

3.5 Summary

Here, gas flow, diffusive transport and adsorption in heterogeneous porous media resembling coal and shale matrices are investigated using a theoretical approach. In addition, unlike previous theoretical works, the sorption rates are explicitly introduced to a mathematical framework in this context.

Random local variations in matrix pore structure and material content are considered and their influence on gas sorption and transport are investigated using small perturbations theory, a proven technique widely used in various other disciplines where analysis of multi-physics problems are required in the presence of *a priori* fluctuations induced by non-uniform fields. In conclusion, the homogenized gas-matrix system behavior can be described using the following upscaled governing equations

$$\phi\frac{\partial C}{\partial t}+(1-\phi)\frac{\partial C_\mu}{\partial t}=\frac{\partial}{\partial x}\left(\phi D\frac{\partial C}{\partial x}\right)+\frac{\partial}{\partial x}\left(\phi C\frac{k}{\mu}\frac{\partial p}{\partial x}\right)+\frac{\sigma_\phi^2\bar{C}_{\mu 0}}{1+N_{Pe}/(1+N_{Pe})}$$

$$\frac{\partial C_\mu}{\partial t}=k_{ads}C-k_{des}C_\mu+\frac{N_{Th}}{1+2N_{Pe}}\sigma_\phi^2\bar{C}_{\mu 0} \tag{3.56}$$

Further, it is founded that the matrix heterogeneity generates non-trivial macro-transport and macro-kinetics effects on the system. The system behavior is investigated numerically and it is found that macro-kinetics and macro transport has the potential to reduce the ultimate gas recoveries significantly.

As mentioned earlier in §3.1.1 we simplified the adsorption kinetics by assuming that the adsorption rate is independent of the adsorbed gas concentration. Therefore linear sorption kinetics for fundamental studies of gas sorption behavior in coal and shale matrices is used. More importantly the resistance in micropores is assumed to be only due to sorption behavior of the gas and we neglected the adsorbed gas transport in the micropores, i.e., surface or solid diffusion. Now having good fundamental understanding of the local heterogeneity effects on gas storage and transport in tight

formations, in next chapter the non-equilibrium, non-linear sorption kinetics is used to describe the sorption behavior of the gas in the matrices that could simplify to well known Langmuir isotherm kinetics. Furthermore, surface diffusion recognized to be one of the important gas transport mechanisms in micro-porous materials (Carman and Raal, 1951; Ash *et al.*, 1963; Aylmotre and Barrer 1966; Do and Wang 1998; Siemons *et al.*, 2007), where the adsorption of the gases are taking place, is used to describe the adsorbed gas transport at the solid surface of the matrices.

CHAPTER IV

MASS TRANSPORT OF ADSORBED-PHASE IN STOCHASTIC POROUS MEDIUM WITH FLUCTUATING POROSITY FIELD AND NONLINEAR GAS ADSORPTION KINETICS

Physical adsorption of gaseous phase fluid components in porous materials is commonly associated with separation processes (McCabe *et al.*, 1993). In physical sciences and modern engineering fields, however, a large number of cases and applications exist where gas adsorption and its related phenomena find other important roles. In the energy sector, in particular, they are often closely related to storage of natural gases and hydrogen. In addition, adsorption is more frequently at the center of discussions involving natural gas in-place estimation and production from thermally-mature coal seams and organic-rich gas shale reservoirs (Ambrose *et al.*, 2010). These same natural gas resources are in parallel being considered as the places of CO_2 sequestration, in this case using adsorption as the means of trapping the greenhouse gases.

Separation, storage and entrapment are the consequences of certain gas molecules (with a certain molecular weight, shape, or polarity) being transferred to and held more strongly on the surfaces than others. Hence, these processes involve intricate mass transfer phenomena in porous media in addition to –often nonlinear– adsorption kinetics. Due to short lengths of the characteristic pore size and low permeability, mass transport mechanisms of the adsorbed and free gas are considered to be mainly diffusive in these porous materials.

A vast literature exists on transport of free gas in porous media. It is well-recognized that the free gas transport is due to viscous –Darcian– flow and molecular diffusion and that the overall movement of the gas could be significantly retarded in the presence of adsorption. If large enough voids are available, diffusive transport of free gas could take place in pores and throats due to random movement and collisions of molecules from high- to low-concentration regions, i.e., bulk (or pore) diffusion. With the decreasing pore sizes, however, and depending on the pore pressure and temperature, molecular streaming (or Knudsen diffusion) could develop as an additional transport mechanism indicating the dominant effect of collisions between the gas and pore wall molecules. Surface and solid (or interstitial) diffusion, on the other hand, are often associated with mass transport of the sorbed (adsorbed and dissolved, respectively) phase. The later transport mechanisms have been the subjects of research for several decades, see (Tiselius, 1934, 1935) for the earliest discussion. Carman and Raal (1951), Ash *et al.*, (1963), Aylmotre and Barrer (1966), Do and Wang (1998), and Siemons *et al.*, (2007) independently performed experiments using different gases to investigate the magnitude of gas transport mechanisms in microporous materials such as carbon and coal. They found that the sorption rate in porous media cannot be accounted for only by free gas diffusion and there must be an additional transport of the adsorbed-phase. In several experiments, although a slow mechanism of transport, surface diffusion is quantified as the dominant one, in some cases with a significantly larger contribution than viscous gas flow.

A simple approach to describe surface diffusion of the adsorbed-phase is to consider a net adsorbed-phase mass flux as molecules jumping from one adsorption site to another adjacent site due to thermal motion of the molecules under the influence of pore walls. Accordingly, the adsorbed-phase transport is an activated diffusion that could be described as Fickian where the flux is proportional to the adsorbed-phase concentration gradient with a diffusivity in Arrhenius form ($D_s = \nu\, Exp(-E/RT)$).

Hence only the activated adsorbed molecules with a desorption energy beyond the activation energy threshold could participate in the transport process. This may be an appropriate approach to model the adsorbed-phase transport in geological formations such as coal and shale, since the local reservoir conditions are typically below the capillary condensation threshold. When loading exceeds monolayer adsorption limit, one needs to consider a hydrodynamics model such as the one earlier proposed by Gilliland *et al.*, (1958).

Solid diffusion represents the movement of small gas molecules inside the macromolecular openings of the solid phase that make up the matrix. As a transport mechanism it has been proposed to consider transient solid dissolution of the gases. It may be distinguished from the surface diffusion by investigating changes in the rate of mass transport due to changes in gas type. Solid diffusion rate decreases (while surface diffusion increases) as molecular size of the gas becomes larger and heavier (Do, 1998). Depending on the porous material, diffusive mechanisms could act individually or simultaneously (Sevenster 1959, Thimons *et al.*, 1973).

Natural or synthetic porous materials involving adsorption-related phenomena are often characterized by a network of relatively small pores. The common characteristics are large internal surface area, providing enough adsorption sites to store significant amounts of fluid, and very low matrix porosity and permeability. In some of these studies the porous materials have adjustable characteristics that could be a symmetry in pore sizes and homogeneity in porosity, while in the others (such as natural gas resources and CO_2 sequestration) the porous material is fairly large and heterogeneous in its petro-physical qualities. Particularly in the later case, the porous material shows complexity in pore structure and material content. In this study, we consider such case in which the porosity of the porous material is considered heterogeneous with spatially-correlated random fluctuations. Complexity in structure and material content of the porous material is considered introducing random porosity field that

holds assumption of first and second-order stationarity.

Using an upscaling approach based on small perturbation theory, we have previously investigated the influence of small-scale heterogeneities in matrix porosity on Darcy flow and Fickian-type pore diffusion in the presence of linear non-equilibrium gas adsorption (Fathi and Akkutlu, 2009). We identified non-trivial macro-transport and -kinetics effects of the heterogeneity which significantly retard gas release from the matrix and influence the ultimate gas recovery adversely. The work was a unique fundamental approach for our understanding of the gas production and sequestration behavior in unconventional reservoirs; however, it was simplified and did not consider (i) the presence of nonlinear sorption kinetics and (ii) a transport mechanism for the adsorbed-phase. Here, we incorporate the sorption nonlinearity and surface diffusion into formulations and apply the same upscaling approach. Gas sorption involves the so-called Langmuir kinetics, which reduces to the well-known Langmuir isotherm in the equilibrium limit. In our mathematical formulation, the adsorbed-phase behavior is due to a mass balance equation with non-linear adsorption kinetics. We consider that surface diffusion is the only mechanism of transporting the adsorbed phase and that its mass flux is proportional to the gradient of the adsorbed-phase concentration. The assumption of having monolayer gas adsorption is held and the amount of gas as condensate and at a dissolved state in the solid is assumed to be negligible. In addition, for clarity during the analysis, we consider the effects of bulk and Knudsen diffusion combined in one effective pore diffusion which accounts for the overall free gas transport. It is found that the nonlinearity participates into both macro–transport and –kinetics, promoting primarily the surface diffusion effects. Whereas surface diffusion, although commonly ignored, brings an intricate nature to the gas release dynamics in heterogeneous media. Through macro–transport effect of the heterogeneity, it increases ultimate gas recovery and, through the macro-kinetics effect of the heterogeneity, it significantly decreases the time needed to reach the ultimate

recovery. The enhancement is beyond the levels that can be explained using the adsorbed-phase concentration gradient arguments and therefore brings new insight to previous experimental observations on how a slow transport process such as surface diffusion can dominate the overall gas mass transfer across porous materials. As the consequence of these effects, it is shown that the gas-matrix system practically does not reach the equilibrium adsorption limit during any stage of the gas release.

4.1 Local Governing Equations Describing Gas Behavior in The Homogeneous Matrix

2.1 Kinetics of Gas Sorption in Porous Media

In this study we introduce surface diffusion as the mechanism of transport for the adsorbed phase under the isothermal conditions. Previously, linear approach for the adsorption kinetics of fluids in porous media have been used by several authors, see for example Brusseau and Rao (1991), Hu *et al.*, (1995), Alvarado *et al.*, (1998), and Fathi and Akkutlu (2009), assuming that the adsorption rate is independent of the adsorbed gas concentration. However, when single-component sorption rates are considered, it is more realistic to consider that adsorption follows the so-called Langmuir kinetics. Koss *et al.*, (1986), showed that gas behavior in carbons may not be diffusion-limited, however it can be accurately modeled using adsorption kinetics type of rate expressions. The nonlinear sorption kinetics behavior of gas has been studied by several authors Srinivasan *et al.*, (1995), Schlebaum *et al.*, (1999). They showed that the nonlinear sorption behavior of the adsorbed gas influences the diffusive processes. The non-linearity can be seen as concentration dependency of the diffusion coefficients (S. Farooq and D. M. Ruthven 1991). Here we introduce nonlinear sorption kinetics where the rate of interchange between the adsorbed and free gas can be described using the following mass balance:

$$\frac{\partial C_\mu}{\partial t} = k_f(C_{\mu s} - C_\mu)C - k_r C_\mu \tag{4.1}$$

Here, C is the molar density of the free gas in moles per unit pore volume, whereas C_μ the molar density of the adsorbed-phase in moles per unit solid volume. k_f and k_r are the adsorption and desorption rate coefficients, respectively. $C_{\mu s}$ is maximum monolayer gas adsorption of the matrix solid surface. When equilibrium is reached, equation (5.4) simplifies to well known Langmuir equation:

$$C_\mu = \frac{C_{\mu s} K C}{1 + KC} \tag{4.2}$$

$K = k_f/k_r$ is often referred to as the equilibrium partition (or, distribution) coefficient.

2.2 Conservation of Gas Mass in Porous Media

Both bulk diffusion and viscous flow considered for free gas transport in the matrix. Consequently, local equations describing the gas transport in matrix using nonlinear sorption kinetics and transport mechanism of the adsorbed gas (i.e., surface diffusion) becomes:

$$\phi\frac{\partial C}{\partial t}+(1-\phi)\frac{\partial C_\mu}{\partial t}=\frac{\partial}{\partial x}\left(\phi\, D\frac{\partial C}{\partial x}\right)+\frac{\partial}{\partial x}\left(\phi C\frac{B_0}{\mu}\frac{\partial p}{\partial x}\right)+\frac{\partial}{\partial x}\left[(1-\phi)\, D_s\frac{\partial C_\mu}{\partial x}\right] \tag{4.3}$$

$$\frac{\partial C_\mu}{\partial t}=k_r\left[K(C_{\mu s}-C_\mu)C-C_\mu\right] \tag{4.4}$$

Here, x-t are the space-time coordinates, ϕ the interconnected porosity, $D(\phi)$ the tortuosity-corrected coefficient of molecular diffusion, B_0 the absolute permeability of the porous medium, p the pore pressure, and μ the dynamic gas viscosity. Note that the formulation contains a diffusive transport term which is Fickian in nature. This roughly corresponds to bulk (pore) diffusion as the mechanism of transport. The existence of other mechanisms (e.g., Knudsen and surface diffusion) will not be considered in this work. According to this new formulation the resistance controlling adsorption dynamics is due to surface diffusion D_s, i.e., adsorbed-phase diffusion. The later indicates that, although the adsorbed gas molecules are always under the restrictive influence of the solid walls, the concentration gradient $\partial C_\mu/\partial x$ is high such that significant surface fluxes are possible in the matrix (Yi *et al.*,2008). Next, equations (4.3-4.4) are reorganized and written in the following form:

$$\frac{\partial C}{\partial t}+\Phi\frac{\partial C_\mu}{\partial t}=\alpha_1\frac{\partial C}{\partial x}+D\frac{\partial^2 C}{\partial x^2}+\beta\alpha'\frac{\partial C}{\partial x}+\beta C\frac{\partial^2 C}{\partial x^2}+\alpha_2\frac{\partial C_\mu}{\partial x}+\Phi D_s\frac{\partial^2 C_\mu}{\partial x^2} \tag{4.5}$$

$$\frac{\partial C_\mu}{\partial t}=k_r\left[K(C_{\mu s}-C_\mu)C-C_\mu\right] \tag{4.6}$$

Here, we introduce $\alpha_1=\dfrac{\partial(\phi D)}{\phi\partial x}$ as an effective drift velocity, reflecting changes in free gas concentration due to a non-constant diffusivity with a gradient and $\alpha_2=\dfrac{\partial[(1-\phi)D_s]}{\phi\partial x}$ as an effective drift velocity of adsorbed phase due to non-constant surface diffusion coefficient with a gradient. In addition, we defined $\alpha'=\dfrac{\partial(\phi C)}{\phi\partial x}$, $\beta=B_0R_gT/\mu$ (the gas mobility), and $\Phi=(1-\phi)/\phi$ as the solid-to-bulk volume ratio.

4.2 Gas Behavior in Heterogeneous Matrix

Consider a porous medium where medium heterogeneity is defined by a time-independent, spatially fluctuating porosity field. The porous medium still maintains an average porosity and absolute permeability. Application of the random porosity field, instead of random permeability, is more appropriate because the transport is mainly diffusive. Next, the classical perturbation theory was employed where porosity ϕ is defined in terms of its mean $\bar{\phi}$ and small fluctuation $\tilde{\phi}$ such that $\phi = \bar{\phi} + \tilde{\phi}$. The later is assumed to be Gaussian random number of zero average around the mean porosity. Further, the assumption of first and second order of stationarity, i.e., mean and variance of porosity kept constant, is held with a well-defined spatial covariance function. The dependent variables, transport and rate coefficients will be affected by the random porosity field; therefore, they are also considered to be random variables. We thus have

$$\alpha_1 = \bar{\alpha_1} + \tilde{\alpha_1} \qquad \alpha_2 = \bar{\alpha_2} + \tilde{\alpha_2} \qquad \alpha' = \bar{\alpha}' + \tilde{\alpha}'$$

$$C = \bar{C} + \tilde{C} \qquad C_\mu = \bar{C}_\mu + \tilde{C}_\mu \qquad D = \bar{D} + \tilde{D}$$

$$D_s = \bar{D}_s + \tilde{D}_s \qquad \Phi = \bar{\Phi} + \tilde{\Phi} \qquad K = \bar{K} + \tilde{K}$$

Where, a bar and a tilde over a quantity denote its average value and its fluctuations about the mean, respectively. Note that the partition coefficient K is considered as a random variable. This means the porosity fluctuations have the potential to create variations in gas adsorption and desorption rates. This is a reasonable and important consideration since porous media are often mixtures of various organic and inorganic materials exhibiting an intricate pore-network. Variations in the material properties add to structurally complex nature of a porous medium, influencing gas retention (adsorption) capacity. Substituting these expressions into the governing equations (4.5-4.6) and taking the expectations of the equations, the mean equations for the free and adsorbed gas are obtained.

$$\frac{\partial \bar{C}}{\partial t} + \bar{\Phi}\frac{\partial \bar{C}_\mu}{\partial t} - \bar{D}\frac{\partial^2 \bar{C}}{\partial x^2} - \bar{\Phi}\bar{D}_s\frac{\partial^2 \bar{C}_\mu}{\partial x^2} = \bar{R} \tag{4.7}$$

$$\frac{\partial \bar{C}_\mu}{\partial t} = k_r\left[\bar{K}\bar{C}(C_{\mu s} - \bar{C}_\mu) - \bar{C}_\mu + (C_{\mu s} - \bar{C}_\mu)\overline{\tilde{K}\tilde{C}} - \bar{C}\overline{\tilde{K}\tilde{C}_\mu} - \bar{K}\overline{\tilde{C}_\mu\tilde{C}}\right] \tag{4.8}$$

where we defined $\bar{R}$ as

$$\begin{aligned}\bar{R} = \; & \bar{\alpha_1}\frac{\partial \bar{C}}{\partial x} + \beta\bar{\alpha}'\frac{\partial \bar{C}}{\partial x} + \bar{\alpha_2}\frac{\partial \bar{C}_\mu}{\partial x} + \beta\bar{C}\frac{\partial^2 \bar{C}}{\partial x^2} \\ & + \sum_{m=1,2}\overline{\frac{\xi_m \partial^m \tilde{C}}{\partial x^m}} + \beta\overline{\frac{\tilde{\alpha}'\partial \tilde{C}}{\partial x}} - \overline{\frac{\tilde{\Phi}\partial \tilde{C}_\mu}{\partial t}} + \overline{\tilde{\alpha}_2\frac{\partial \tilde{C}_\mu}{\partial x}} + \bar{D}_s\overline{\tilde{\Phi}\frac{\partial^2 \tilde{C}_\mu}{\partial x^2}} + \bar{\Phi}\overline{\tilde{D}_s\frac{\partial^2 \tilde{C}_\mu}{\partial x^2}}\end{aligned} \tag{4.9}$$

Here, for simplicity we also defined $\xi_1 = \tilde{\alpha_1}$ and $\xi_2 = \tilde{D}$. First, second and third terms in equation (4.9) are corrections to drift velocities, the fourth term is related to viscous transport, and the remaining terms indicate non-trivial cross-correlations due to fluctuating porosity. Importantly, a series of auto- and cross-correlations appeared in the formulation, such as cross-correlation between the partition coefficient and free gas and adsorbed phase amount in equation (4.8), indicating the impact of local porosity fluctuations on the adsorption kinetics and gas transport. Subtracting the obtained mean equations (4.7)-(4.8) from the original ones (i.e., equations 4.5 and 4.6), the mean-removed equations are derived:

$$\frac{\partial \tilde{C}}{\partial t} + \bar{\Phi}\frac{\partial \tilde{C}_\mu}{\partial t} - \bar{\alpha_1}\frac{\partial \tilde{C}}{\partial x} - \bar{D}\frac{\partial^2 \tilde{C}}{\partial x^2} - \beta\bar{\alpha}'\frac{\partial \tilde{C}}{\partial x} - \beta\bar{C}\frac{\partial^2 \tilde{C}}{\partial x^2} - \beta\tilde{C}\frac{\partial^2 \bar{C}}{\partial x^2} - \bar{\alpha_2}\frac{\partial \tilde{C}_\mu}{\partial x} - \bar{\Phi}\bar{D}_s\frac{\partial^2 \tilde{C}_\mu}{\partial x^2} = \tilde{R} \tag{4.10}$$

$$\frac{\partial \tilde{C}_\mu}{\partial t} + k_r\tilde{C}_\mu + k_r\bar{K}\bar{C}\tilde{C}_\mu = k_r\bar{K}\left(C_{\mu s} - \bar{C}_\mu\right)\tilde{C} + k_r M \tag{4.11}$$

where $\tilde{R}$ and M are defined as follows:

$$\begin{aligned}\tilde{R} = & -\tilde{\Phi}\frac{\partial \bar{C}_\mu}{\partial t} - \tilde{\Phi}\frac{\partial \tilde{C}_\mu}{\partial t} + \overline{\frac{\tilde{\Phi}\partial \tilde{C}_\mu}{\partial t}} + \tilde{\alpha_1}\frac{\partial \bar{C}}{\partial x} + \tilde{\alpha_1}\frac{\partial \tilde{C}}{\partial x} - \overline{\frac{\tilde{\alpha}_1\partial \tilde{C}}{\partial x}} + \tilde{D}\frac{\partial^2 \bar{C}}{\partial x^2} + \tilde{D}\frac{\partial^2 \tilde{C}}{\partial x^2} \\ & - \overline{\frac{\tilde{D}\partial^2 \tilde{C}}{\partial x^2}} + \beta\tilde{\alpha}'\frac{\partial \bar{C}}{\partial x} + \beta\tilde{\alpha}'\frac{\partial \tilde{C}}{\partial x} - \beta\overline{\frac{\tilde{\alpha}'\partial \tilde{C}}{\partial x}} + \beta\tilde{C}\frac{\partial^2 \tilde{C}}{\partial x^2} - \beta\overline{\frac{\tilde{C}\partial^2 \tilde{C}}{\partial x^2}} + \tilde{\alpha}_2\frac{\partial \tilde{C}_\mu}{\partial x} \\ & + \tilde{\alpha}_2\frac{\partial \bar{C}_\mu}{\partial x} - \overline{\frac{\tilde{\alpha}_2\partial \tilde{C}_\mu}{\partial x}} + \bar{\Phi}\tilde{D}_s\frac{\partial^2 \tilde{C}_\mu}{\partial^2 x} + \bar{\Phi}\tilde{D}_s\frac{\partial^2 \bar{C}_\mu}{\partial^2 x} + \tilde{\Phi}\bar{D}_s\frac{\partial^2 \bar{C}_\mu}{\partial^2 x} + \tilde{\Phi}\tilde{D}_s\frac{\partial^2 \bar{C}_\mu}{\partial^2 x} \\ & - \overline{\tilde{\Phi}\tilde{D}_s}\frac{\partial^2 \bar{C}_\mu}{\partial^2 x} - \bar{\Phi}\overline{\frac{\tilde{D}_s\partial^2 \tilde{C}_\mu}{\partial^2 x}} + \tilde{\Phi}\bar{D}_s\frac{\partial^2 \tilde{C}_\mu}{\partial^2 x} + \tilde{\Phi}\tilde{D}_s\frac{\partial^2 \tilde{C}_\mu}{\partial^2 x} - \bar{D}_s\overline{\frac{\tilde{\Phi}\partial^2 \tilde{C}_\mu}{\partial^2 x}}\end{aligned} \tag{4.12}$$

$$\begin{aligned}M = & C_{\mu s}\left(\tilde{K}\bar{C} + \tilde{K}\tilde{C} - \overline{\tilde{K}\tilde{C}}\right) - \bar{C}\bar{C}_\mu\tilde{K} - \bar{K}\tilde{C}_\mu\tilde{C} - \bar{C}_\mu\tilde{K}\tilde{C} - \bar{C}\tilde{K}\tilde{C}_\mu + \overline{\tilde{K}\tilde{C}}\bar{C}_\mu \\ & + \overline{\tilde{C}_\mu\tilde{C}}\bar{K} + \overline{\tilde{C}_\mu\tilde{K}}\bar{C}\end{aligned} \tag{4.13}$$

As stated earlier the fluctuations are assumed to be Gaussian random numbers with zero mean, (i.e., $\overline{\tilde{C}} = \overline{\tilde{C}_\mu} = \overline{\tilde{D}} = \overline{\tilde{D}_s} = \overline{\tilde{K}} = \overline{\tilde{\Phi}} = \overline{\tilde{\alpha}_1} = \overline{\tilde{\alpha}_2} = \overline{\tilde{\alpha}'} = 0$); however, their auto– and cross–correlations (e.g., $\overline{\tilde{\alpha}_1\tilde{\alpha}_1}$ and $\overline{\tilde{\alpha}_1\tilde{D}}$) are non-trivial.

The assumption of small-perturbations was implemented. Accordingly, the porosity fluctuations are so small that the terms including fluctuation correlations higher than second order are neglected. Also, $\tilde{C}(x, t = 0) = \tilde{C}_\mu(x, t = 0)$=0 are taken. The upscaled governing equations describing gas behavior in the heterogeneous matrix can be obtained by substituting explicit expressions for the auto– and cross–correlation terms in the mean equations (4.7-4.8). We approached the problem by first finding the general solutions for the free and adsorbed gas fluctuations, $\tilde{C}$ and $\tilde{C}_\mu$ in Fourier -Laplace domain. Next, the correlation terms in the mean equation (4.7) are obtained by multiplying the proper spatial and temporal derivative of the concentration fluctuations (free or adsorbed) with the fluctuating term and keeping only up to second order terms; whereas the correlation terms in the mean equation (4.8) are obtained by multiplying the concentration fluctuations with the fluctuating term and keeping only up to second order terms. The auto- and cross-correlation terms include a set of convolution integral terms in Fourier–Laplace domain. In order to evaluate these integrals, spatial correlation function is defined as $\overline{\tilde{\phi}(x)\tilde{\phi}(y)} = \sigma_\phi^2 f(|x - y|)$. We assume Gaussian model for the spatial covariance of porosity, characterized by correlation length λ: $f_x = \exp\left(-x^2/2\lambda^2\right)$. The model can be written as $f_Q = \sqrt{2\pi}\lambda \exp\left(-Q^2\lambda^2/2\right)$ in the spectral domain. Complete details of the mathematical procedure are presented in Appendix C. Details on the methodology and the correlation functions can be found in Forster (1977), Gelhar(1993), L'Heureux (2004), and more recently in Fathi, and Akkutlu (2009).

4.2.1 Upscaled Governing Equations for the Nonlinear Problem with Surface Diffusion

Using the definitions of $\bar{\alpha_1}$, $\bar{\alpha_2}$, $\bar{\Phi}$, $\bar{\alpha'}$, and β, in the upscaled governing equations (7.40-7.41) presented in Appendix C, after simplifying and re-arranging the following form of the upscaled governing equations describing gas mass transport and nonlinear sorption kinetics are obtained as follows:

$$\bar{\phi}\frac{\partial \bar{C}}{\partial t} + (1-\bar{\phi})\frac{\partial \bar{C}_\mu}{\partial t} = \frac{\partial}{\partial x}\left(\bar{\phi}\mathcal{D}_{\mathit{eff}}\frac{\partial \bar{C}}{\partial x}\right) + \frac{\partial}{\partial x}\left(\bar{\phi}\bar{C}\frac{B_0}{\mu}\frac{\partial \bar{p}}{\partial x}\right) + \frac{\partial}{\partial x}\left[(1-\bar{\phi})\,\bar{D}_{s,\mathit{eff}}\frac{\partial \bar{C}_\mu}{\partial x}\right] + \Gamma_{tr} \tag{4.14}$$

$$\frac{\partial \bar{C}_\mu}{\partial t} = k_r\left[\bar{K}(\bar{C}_{\mu s} - \bar{C}_\mu)\bar{C} - (\bar{C}_\mu + \Gamma_{kn})\right] \tag{4.15}$$

in which new quantities reflecting the macro-effects of local heterogeneities appear. These are defined as follows:

$$\mathcal{D}_{\mathit{eff}} = \bar{D} - D'\sigma_\phi^2\left\{\frac{\dfrac{2D' + \beta g' + \dfrac{\bar{D}+\beta g}{\bar{\phi}}}{\bar{D}+2\beta g}}{1+\dfrac{\upsilon_1\bar{\Phi}\bar{D}_s\bar{K}}{\bar{D}+2\beta g}} + \frac{\bar{K}\upsilon_1\left[1/\bar{\phi}(D'_s+\bar{D}_s)+\bar{D}_s\right]}{\bar{D}+2\beta g+\upsilon_1\bar{\Phi}\bar{D}_s\bar{K}}\right\} \tag{4.16}$$

$$\mathcal{D}_{s,\mathit{eff}} = \bar{D}_s - \frac{\sigma_\phi^2}{\bar{\Phi}}\left\{\begin{array}{l}\dfrac{2D'D'_s\bar{\Phi} + (\bar{\Phi}D'_s - \bar{D}_s)\left(\beta g' + \dfrac{\bar{D}+\beta g}{\bar{\phi}}\right)}{\bar{D}+2\beta g+\upsilon_1\bar{\Phi}\bar{D}_s\bar{K}} \\ \qquad + \dfrac{\bar{K}\upsilon_1\left[(D'_s+\dfrac{\bar{D}_s}{\bar{\phi}})(\bar{\Phi}D'_s-\bar{D}_s)+(\bar{\Phi}D'_s+\bar{D}_s)^2\right]}{\bar{D}+2\beta g+\upsilon_1\bar{\Phi}\bar{D}_s\bar{K}}\end{array}\right\} \tag{4.17}$$

$$\Gamma_{tr} = \left\{\frac{\beta g' + \left(\dfrac{\bar{D}+\beta g}{\bar{\phi}}\right) + \bar{K}\upsilon_1\left[D'_s + (\bar{D}_s - D'_s)\bar{\Phi}\right]}{\bar{D}+2\beta g+\upsilon_1\bar{K}\bar{\Phi}\bar{D}_s}\right\}\left(1-\upsilon_2\upsilon_1\bar{C}\right)\bar{\phi}\sigma_\phi^2\bar{C}_{\mu,0} + \frac{K'\upsilon_1\left[D'_s+\left(\bar{D}_s-D'_s\right)\right]}{\lambda^2}\bar{\phi}\sigma_\phi^2\bar{C} \tag{4.18}$$

$$\Gamma_{kn} = \left(\frac{\upsilon_1 \sigma_\phi^2 \lambda^2 \bar{C}_{\mu,0} K'}{\bar{D} + 2\beta g + \upsilon_1 \bar{K} \bar{\Phi} \bar{D}_s} \right) \left(1 + \upsilon_2 \upsilon_1 \bar{C} + \frac{2\bar{\Phi} \bar{D}_s \bar{K}^2 \upsilon_1 \bar{C}}{\bar{D} + 2\beta g + \upsilon_1 \bar{K} \bar{\Phi} \bar{D}_s} \right) \tag{4.19}$$

In the above upscaled governing equations, we defined $D' = d\bar{D}/d\bar{\phi} > 0$, $D'_s = d\bar{D}_s/d\bar{\phi} > 0$ and $K' = d\bar{K}/d\bar{\phi} < 0$. In addition, υ_1 and υ_2 are identified as new common parameters of our analysis:

$$\upsilon_1 = \frac{C_{\mu s} - \bar{C}_\mu}{1 + \bar{K}\bar{C}} \tag{4.20}$$

$$\upsilon_2 = \frac{(1 - \bar{\phi}) \bar{D}_s K'}{\bar{\phi} \lambda^2 \bar{C}_{\mu 0}} \tag{4.21}$$

They appear in the upscaled formulation purely due to introduction of adsorption nonlinearity and surface diffusion.

4.3 Results and Discussion

Based on the analytical part of our investigation, the following fundamental observations on the structure of the upscaled differential equations can be made:

(i) Upscaling introduces clearly defined new terms into the governing equations. These are the diffusive terms (involving apparent pore diffusivity $\mathcal{D}_{eff}$ and apparent surface diffusivity $\mathcal{D}_{s,eff}$) and the source/sink terms Γ_{tr} , and Γ_{kn}. The later can also be considered as decay terms because they depend on the gas amounts in porous medium.

(ii) Upscaled equations show the gas amount dependency of pore and surface diffusion in the presence of nonlinear adsorption kinetics. It also shows that gas desorption rate depends on the initial adsorbed gas amount. This effect is known as loading effect discussed earlier by D. Do (1998).

(iii) In the homogeneous limit Γ terms all disappear and the apparent diffusion coefficients reduce to their homogeneous value due to the fact that the variance σ_ϕ^2 of the porosity field become nil. Hence, the upscaled equations (4.14-4.15) become identical with the local equations (4.3-4.4), i.e., the homogeneous case.

(iv) Nonlinearity in sorption kinetics and surface diffusion introduces new terms υ_1 and υ_2 into the upscaled equations. Interestingly, when both υ_1 and υ_2 go to zero, the equations are reduced to the form earlier reported by Fathi and Akkutlu (2009), i.e., the linear case.

Second part of our work involves numerical analysis of the upscaled governing equations describing gas adsorption and transport in a heterogeneous porous media using a time-implicit finite difference approach based on Newton method and using gas/matrix system parameters given in Table 1. The data set includes the local (or laboratory measured) viscous and diffusive transport, and kinetics parameters for a symmetric matrix block (slab) with a half-length of 10.0 cm and surrounded by fractures; in addition, it introduces a mildly heterogeneous matrix as a base-case for the sensitivity analysis. For the purpose, gas release from a matrix is considered and presented as a one-dimensional initial/boundary value problem defined in Figure 4.1. Results showing the influence of porosity heterogeneity on gas release rates are demonstrated using fractional gas recovery curves and comparing

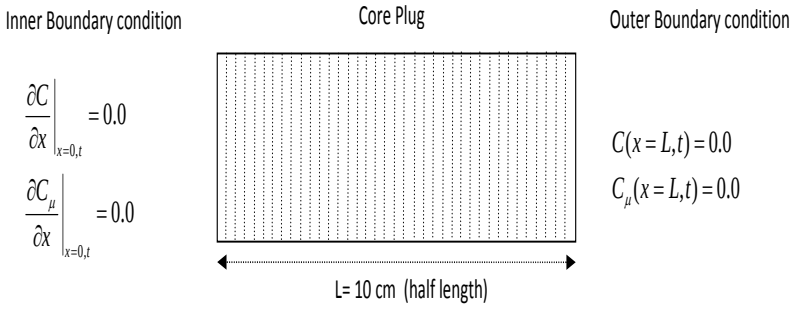

Figure 4.1: A schematic showing the setup for numerical simulation. δx_i=10/500 cm and δt_i=1.4 minutes for i=1,2,...,500, $C(x, t = 0) = 2.0\text{E-}3, C_\mu(x, t = 0) = 2.0\text{E-}4$ mol/cc

with the equivalent homogeneous case. Below, we take a closer look at the influence of local porosity fluctuations on the system behavior in terms of macro-transport and -kinetics effects. Sensitivity analysis of the upscaled equations using the numerical method showed that the heterogeneity does not have any significant impact on the effective pore and surface diffusivity values. Therefore $\mathcal{D}_{eff}$ and $\mathcal{D}_{s,eff}$, can be safely reduced to their local mean values of $\bar{D}$ and $\bar{D}_s$. We use the local mean values for the later quantities in our analysis.

4.3.1 Macro-kinetics Effects

Our numerical investigation based on the sensitivity of the upscaled quantities to gas release dynamics showed that the expression of macro-kinetics, Γ_{kn}, i.e. ,the right-hand-side of equation (4.19) can be simplified. The last term in second parenthesis is takes small values during the simulation so that it can be ignored for the analysis. Furthermore, substituting the definition of β, we obtain:

$$\Gamma_{kn} \cong \upsilon_1 \left(\frac{K' \sigma_\phi^2 \lambda^2 \bar{C}_{\mu 0}}{\bar{D} + \frac{2k\bar{\bar{p}}}{\mu}} \right) \left(1 + \upsilon_1 \upsilon_2 \bar{C}\right) = \upsilon_1 \left[\frac{N_{Th} \sigma_\phi^2 \bar{C}_{\mu 0}}{k_r (1 + 2N_{Pe})} \right] \left(1 + \upsilon_1 \upsilon_2 \bar{C}\right) \tag{4.22}$$

$$= \upsilon_1 \left(1 + \upsilon_1 \upsilon_2 \bar{C}\right) \Gamma_{kn,linear}$$

Here, $\bar{\bar{p}} = R_g T \bar{\bar{C}}$ is average pressure across the matrix. We also introduced N_{Th} and N_{Pe} as Thiele modulus and P*é*clet number in the upscaled formulation:

$$N_{Th} = \frac{k_r \lambda^2}{\bar{D}} \frac{d\bar{K}}{d\bar{\phi}}$$

$$N_{Pe} = \frac{B_0 \bar{\bar{p}}}{\mu \bar{D}}$$

In our case, Thiele modulus is a measure of the porosity dependence of the adsorption rate with respect to the rate of diffusion and, interestingly, its definition now includes the correlation length of the heterogeneous porosity field. P*é*clet number, on the other hand, is a measure of the rate of viscous transport of a flow to its rate of molecular diffusion. In equation (4.22), $\Gamma_{kn,linear}$ is a constant defined with the ratio in bracket and corresponds to the linear sorption kinetics case in the absence of the adsorbed-phase transport, which has previously been introduced as the macro-kinetics effect by Fathi and Akkutlu (2009). In this formulation Γ_{kn} increases with the initial adsorbed gas amount and with the porosity variance. Equation (4.22) shows two new factors υ_1 and υ_2 contributing to the macro-kinetics as the sorption nonlinearity and surface diffusion effect, respectively. In Figure 4.2 we quantified the contributions of these factors. The new contributions improve the ultimate recovery up to %93.7 and decrease the time it takes to reach this recovery from nearly 20 days (for linear case) to about 6 days. This is a significant improvement in gas production rate specifically due to macro kinetics effect.

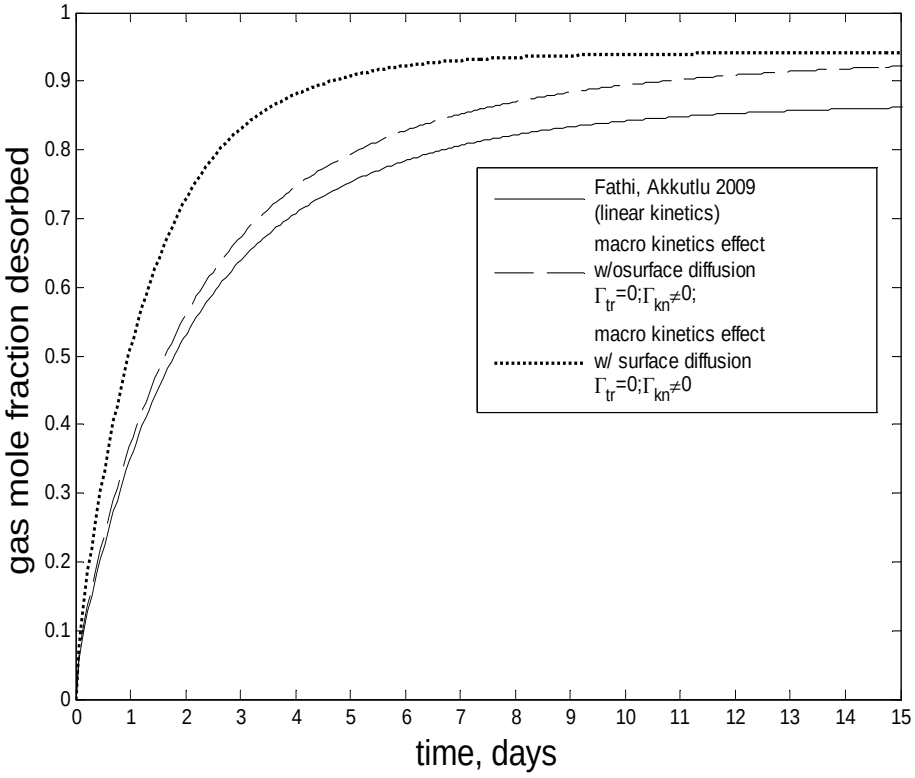

Figure 4.2: The effect of macro-kinetics on matrix gas release

If we were to include only the nonlinearity in sorption kinetics in the absence of surface diffusion, i.e., υ_2=0, the macro-kinetics equation (4.22) then simplifies to

$$\Gamma_{kn} \cong \upsilon_1 \Gamma_{kn,linear} \tag{4.23}$$

The dashed line in Figure 4.2 shows this isolated effect. Clearly, the improvement in ultimate recovery is primarily due to nonlinearity in sorption kinetics. In the presence of surface diffusion, however, the gas release takes place at significantly higher rates. (e.g., 6 days for %93.7 recovery instead of 20 days in the absence of D_s), see the dotted line in the figure. Note that, for the simulations, the input values of the diffusivities are $\bar{D} = 1.0E\text{-}3$ cm^2/s for the pore diffusion and $\bar{D}_s = 2.5E\text{-}5$ cm^2/s for the surface diffusion. Given the fact that the adsorbed-phase diffusivity has a two orders of magnitude smaller value, the enhancement in the gas release rate due to heterogeneity effect is a somewhat unexpected behavior. To find the source of this significant impact on the gas release, we revisited the mathematical formulation and back-traced the derivation of Γ_{kn}. In equation (4.8), it is the $(C_{\mu s} - \bar{C}_\mu)\overline{\tilde{K}\tilde{C}} - \bar{C}\overline{\tilde{K}\tilde{C}_\mu}$ terms that cause the impact on gas release, i.e., the nonlinearity effect (first term) and the cross-correlations between partition coefficient, K, and the molar gas densities. In essence, we theoretically observe new transport effects in the presence of adsorbed-phase which may explain the earlier experimental observations suggesting that the gas release cannot be accounted for only by free gas diffusion and there must be an additional transport associated with the adsorbed phase. Figure 4.3 further confirms these observations numerically by showing sensitivity of gas recovery to the changes in surface diffusivity values for the homogeneous and heterogeneous cases. Figure 4.3 (top) shows the sensitivity of homogeneous matrix to the surface diffusion. In the homogeneous case the surface diffusion does not play an important role in the gas release dynamics. However, Figure 4.3 (middle) shows significant improvement on the gas release rate with the heterogeneous case. Changes in the surface diffusion indeed impact the gas release from the heterogeneous matrix. Figure 4.3 (bottom) compares the times required to reach %90 gas recovery for both homogeneous and heterogeneous cases. It shows that the adsorbed-phase transport becomes significantly important dealing with heterogeneous

systems. we also note that, unlike the linear case presented by Fathi and Akkutlu (2009), the contributions of nonlinearity and surface diffusion to the overall macro-kinetics effect are not constant. Therefore macro-kinetics effect now vary in time and space depending on the free and adsorbed gas amounts.

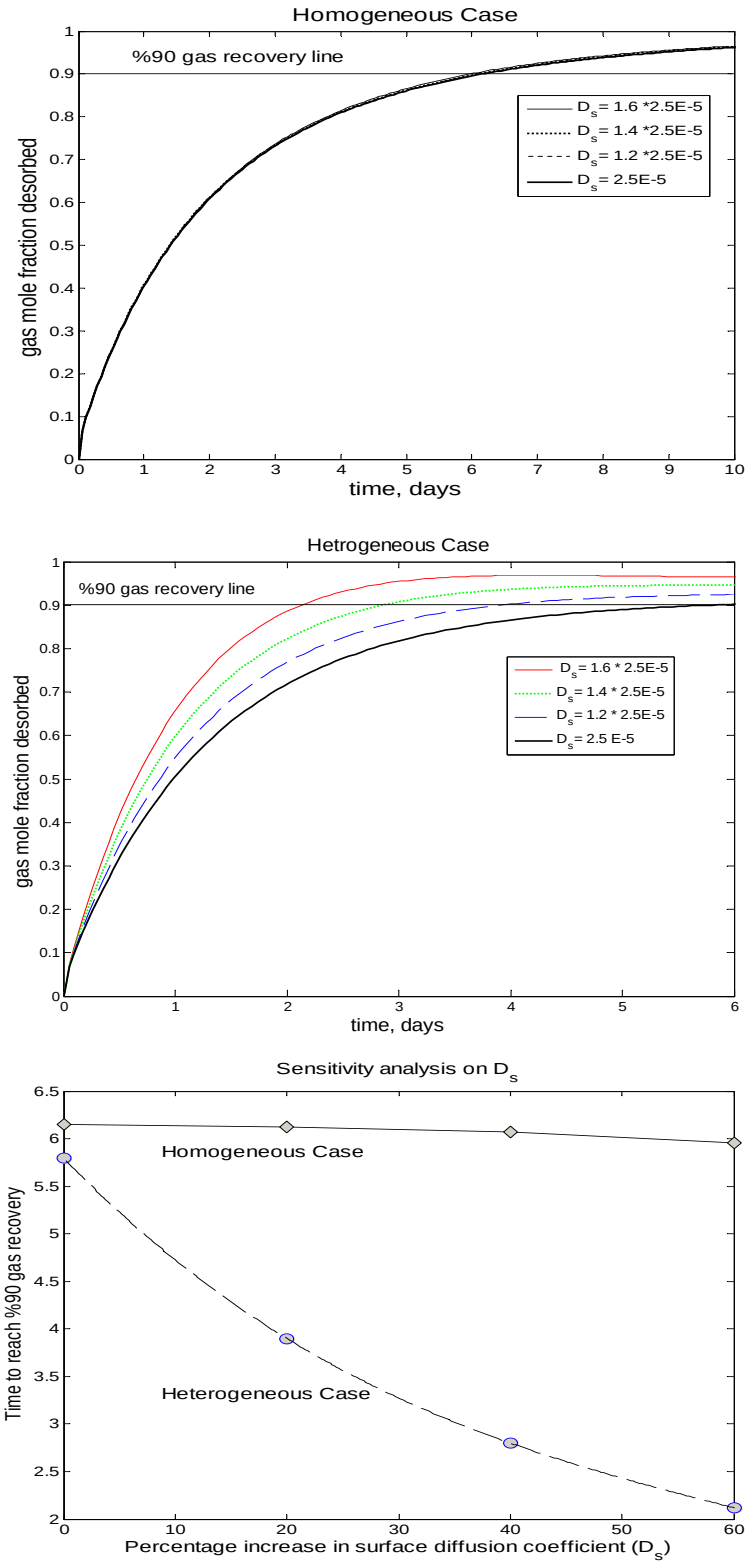

Figure 4.3: The effect of adsorbed-phase transport in homogeneous(top) and heterogeneous (middle) porous media

4.3.2 Macro-transport Effects

Based on the sensitivity analysis on equation (4.18), we omit last term in equation (4.18). Furthermore, typically $\bar{\phi}g' << g$ condition is satisfied across the matrix block. Substituting the definitions of β and g in equation (4.18), re-arranging and using the definitions of υ_1 and υ_2, the macro-transport effect Γ_{tr} is written in the following simple form:

$$\begin{aligned}
\Gamma_{tr} &\cong \left(1-\upsilon_1\upsilon_2\bar{C}\right)\left(\frac{\bar{D}}{\bar{D}+2\beta g}+\frac{\beta g}{\bar{D}+2\beta g}\right)\bar{\phi}\sigma_{\phi}^{2}\bar{C}_{\mu,0} \\
&= \left(1-\upsilon_1\upsilon_2\bar{C}\right)\left(\frac{1}{1+\dfrac{2B_0\bar{\bar{p}}}{\bar{D}\mu}}+\frac{1}{2+\dfrac{\bar{D}\mu}{B_0\bar{\bar{p}}}}\right)\bar{\phi}\sigma_{\phi}^{2}\bar{C}_{\mu,0} \\
&= \left(1-\upsilon_1\upsilon_2\bar{C}\right)\frac{1}{1+N_{Pe}/(1+N_{Pe})}\bar{\phi}\sigma_{\phi}^{2}\bar{C}_{\mu,0} \\
&= \left(1-\upsilon_1\upsilon_2\bar{C}\right)\Gamma_{tr,linear}
\end{aligned} \tag{4.24}$$

In this form we can clearly identify the contribution of sorption nonlinearity and surface diffusion as a correction term to the linear-case earlier obtained by Fathi and Akkutlu (2009). Note that the bracket term in the last line of equation (4.24) is larger than unity, because $K' < 0$ taken; therefore $\Gamma_{tr} > \Gamma_{tr,linear}$. Note that Γ_{tr} is denpendent on the P*é*clet number and, hence, increases with the matrix permeability. It does not disappear in the zero permeability limit, however; instead, it changes with the average initial adsorbed gas amount, with the porosity and with the porosity variance. If we were to include only the nonlinearity in sorption kinetics in the absence of surface diffusion in local governing equations (4.3-4.4) then Γ_{tr} in upscaled equation (4.14) simplifies to

$$\Gamma_{tr} \cong \Gamma_{tr,linear} \tag{4.25}$$

suggesting that contribution of heterogeneity is a combined effect and by removing the surface diffusion the sorption non-linearity effect in macro-transport diminishes too. Figure 4.4 shows the contribution of only the macro-transport term (i.e., $\Gamma_{tr} \neq 0$ and $\Gamma_{kn} = 0$) on the gas release by comparing the numerical results with respect to the linear case. Based on the simulation, it is predicted that the ultimate gas recovery is increased slightly, to nearly %90, due to pure macro-transport effect. However, no significant improvement on the recovery time is observed.

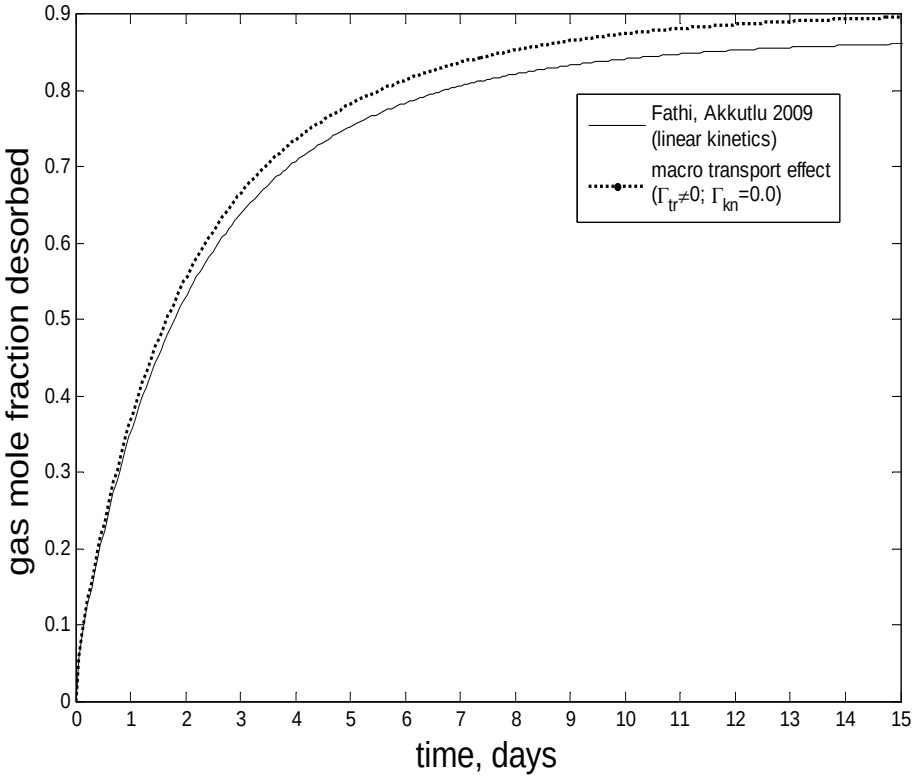

Figure 4.4: The effect of macro-transport on matrix gas release

4.3.3 Sensitivity analysis on sorption non-linearity and adsorbed-phase transport

Auto- and cross– correlations in the mean equations (4.7-4.8) regarding the adsorbed-phase transport and non-linearity in sorption kinetics leads to common parameters υ_2 and υ_1 in the upscaled equations (4.14-4.15). In this section sensitivity to these parameters will be studied using the gas release simulation. In Figure 4.5 the solid black line is related to gas release based on the linear sorption kinetics of Fathi and Akkutlu (2009). Note that in this case υ_1=0. The dashed line corresponds to the heterogeneous base-case corresponding to data set from Table 1. The red dashed line, on the other hand, presents the heterogeneous case where nonlinearity effect has been reduced %90. Two distinct observations can be made in Figure 4.5. First, comparing the solid black line with black dotted line shows significant improvement on gas release rate and ultimate gas recovery due to presence of adsorbed-phase transport and nonlinear sorption kinetics. This observation is made earlier using desorption experiment by Schlebaum *et al.*, (1999). They interpreted this as the presence of a limited number of high-affinity adsorption sites that cause nonlinear sorption behavior(heterogeneity in adsorption sites). Second, the nonlinearity in sorption kinetics υ_1 has a significant effect on gas release rate, while it's effect on ultimate gas recovery is minimal. It is also important to notice that υ_1 has a dynamic effect on gas recovery as it changes with the average free and adsorbed-phase amounts (equation 4.20). υ_2, on the other hand, i.e., the adsorbed-phase transport effect, does not change during the gas release. Figure 4.6 illustrates the sensitivity analysis of the adsorbed-phase transport on the gas release. It clearly shows that, as the adsorb-phase transport effect decreases, both rate of gas release and ultimate gas recovery decrease significantly. These observations also highlights the importance of adsorbed-phase transport and its combined effect with nonlinearity in sorption kinetics on the rate of gas release and ultimate gas recovery in the heterogeneous porous media.

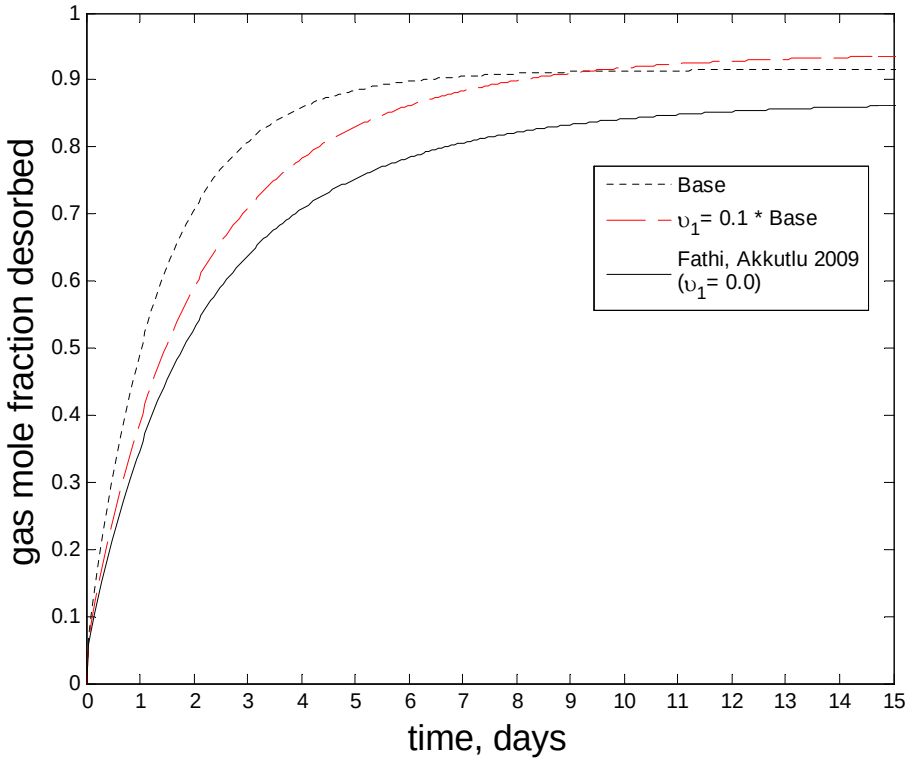

Figure 4.5: Sensitivity analysis of υ_1

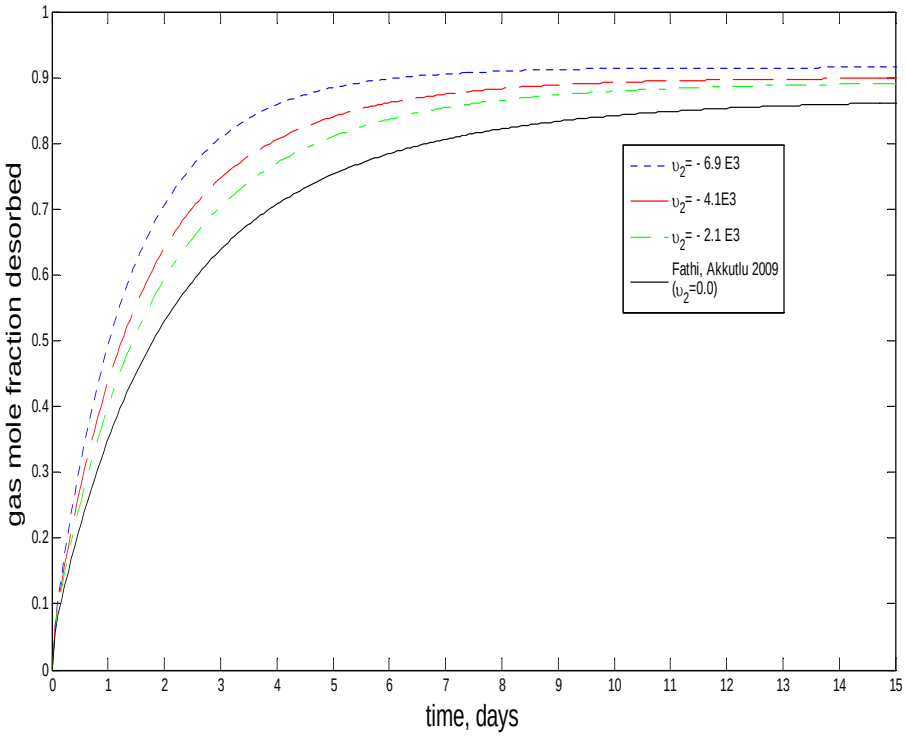

Figure 4.6: Sensitivity analysis of υ_2

4.3.4 Adsorption Equilibrium Limit

One can have a more insightful look at the importance of macro-kinetics effect in the equilibrium adsorption limit. Note that under the equilibrium conditions, we now have $\partial \bar{C}_\mu / \partial t = 0$, thus:

$$\bar{K}(C_{\mu s} - \bar{C}_\mu)\bar{C} - \left(\bar{C}_\mu + \Gamma_{kn}\right) = 0 \tag{4.26}$$

which gives the well-known expression for the Langmuir adsorption isotherm with an additional term purely related to the heterogeneity of the matrix block:

$$\bar{C}_\mu = \frac{\bar{K} C_{\mu s} \bar{C}}{1 + \bar{K}\bar{C}} - \frac{\Gamma_{kn}}{1 + \bar{K}\bar{C}} \tag{4.27}$$

Accordingly, the macro-kinetics effect of heterogeneity appears in equation (4.27) as a gas trapping mechanism that leads to residual adsorbed gas in the matrix.

Figure 4.7 shows the time evolution of the estimated free gas versus adsorbed-phase densities at two fixed locations of the matrix block (points 1 and 2) during the gas release. The x-coordinate represents the pore pressure at a location in the matrix. The pressure is obtained converting molar density of the free gas using compressibility equation of state, $\bar{p} = zRT\bar{C}$. In Figure 4.7, first, the nonlinear sorption kinetics case with and without surface diffusion is compared. The dotted blue line is obtained using equations (4.3-4.4) for the homogeneous Langmuir kinetics, the solid black line corresponds to the heterogeneous case using equations (4.14-4.15), and the dashed red line is the heterogeneous case where adsorbed-phase transport is ignored (i.e., $\bar{D}_s = 0$). It shows that behavior of the isotherm is more like the homogeneous case in the absence of surface diffusion, however, heterogeneity acts as trapping mechanism for the adsorbed gas (i.e., at large times, when the matrix pressure goes to zero, some adsorbed gas amount trapped in the matrix). In the presence of surface diffusion, on the other hand, the heterogeneity leads to accelerated transport of the adsorbed phase while its trapping effect at large times persists. In this case the gas release from the matrix takes place much faster due to the presence of adsorbed-phase transport. Siemons *et al.*, (2007) using a volumetric experimental set up also showed that gas retardation decreases as the adsorbed-phase amount increases. This is likely due to fast surface diffusion transport.

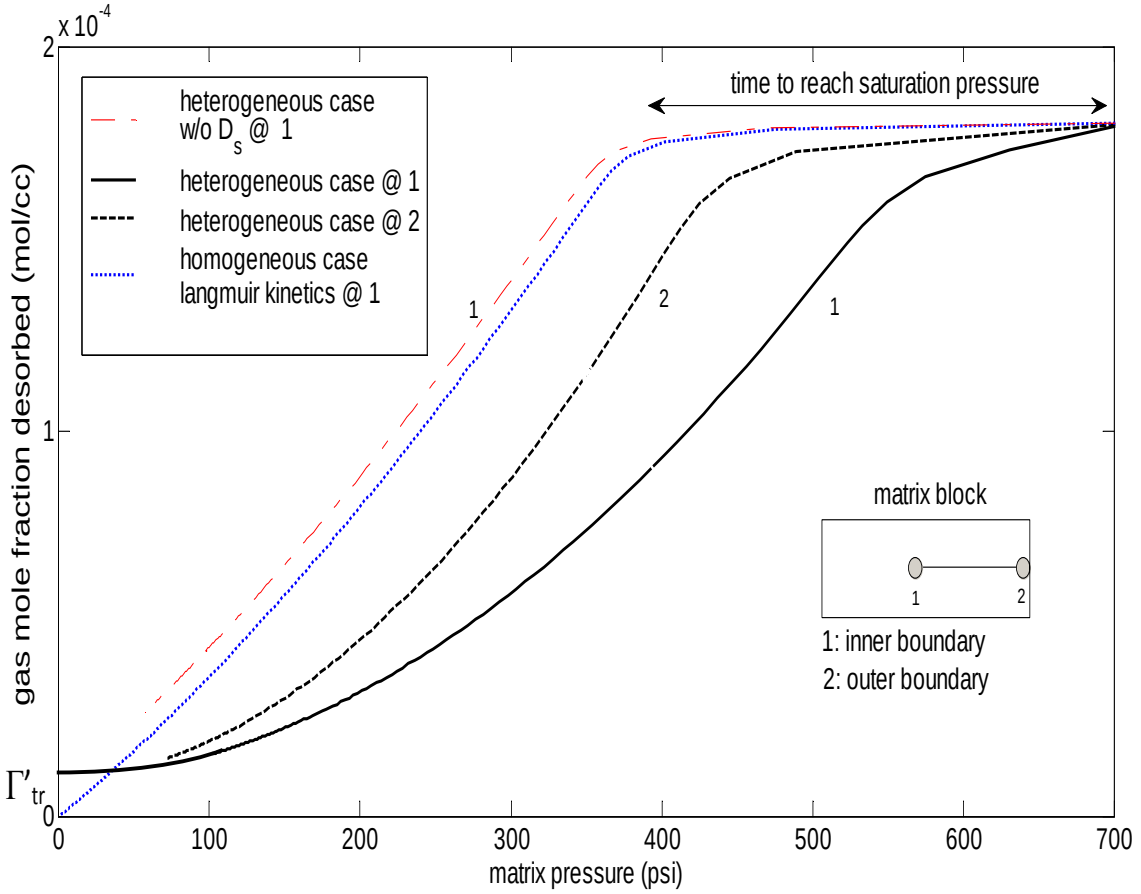

Figure 4.7: Time evolution of free gas versus adsorbed-phase molar densities at fixed locations of the matrix block during the gas release.Free gas amount is shown in terms of matrix pore pressure at the fixed points

Figure 4.7 also shows a significant difference between profiles at different locations. At the outer boundary the gradient of the adsorbed phase with respect to free gas is less than that at the inner boundary, in particular at early times:

$$\left(\frac{\partial \bar{C}_\mu}{\partial \bar{C}}\right)_{innerboundary} > \left(\frac{\partial \bar{C}_\mu}{\partial \bar{C}}\right)_{outerboundary}$$

The effect can be described easily, if one considers the pressure transient at the inner and outer boundary conditions and also using the definition of $\frac{\partial \bar{C}_\mu}{\partial \bar{C}}$ based on the Langmuir kinetics:

$$\frac{\partial \bar{C}_\mu}{\partial \bar{C}} = \frac{\bar{K} C_{\mu s}}{(1 + \bar{K}\bar{C})^2} \tag{4.28}$$

Figure 4.8 compares the pressure transients at the inner and outer boundaries during the gas release. It shows that the free gas amount drops much faster with respect to time at the inner boundary. Therefore, in equation (4.28), $\frac{\partial \bar{C}_\mu}{\partial \bar{C}}$ is larger at the inner boundary, in particular at early times.

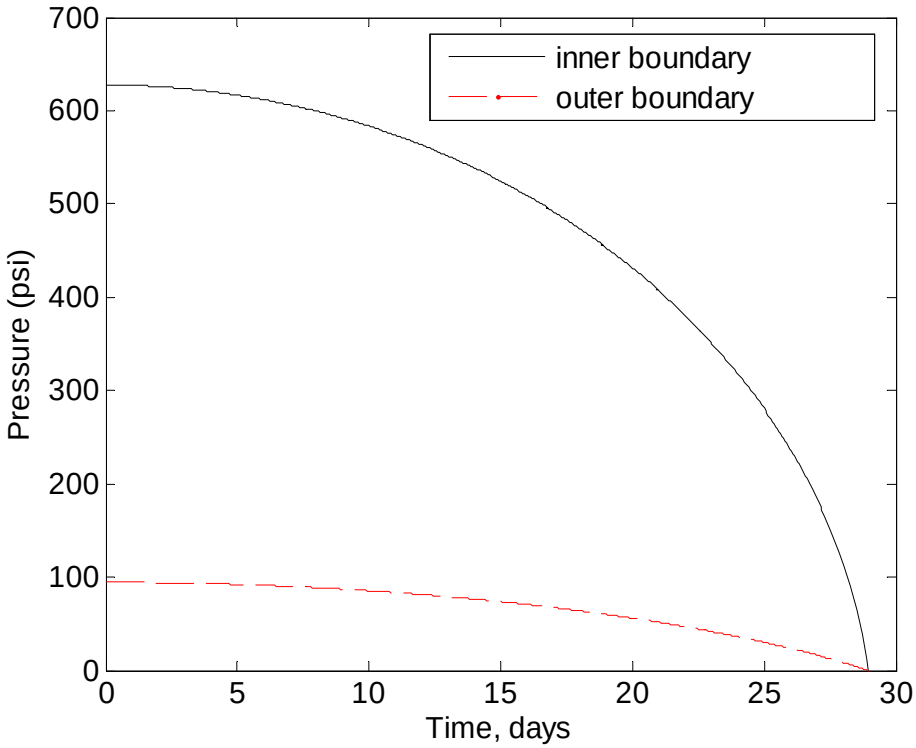

Figure 4.8: Comparison of the pressure profiles at the inner and outer boundaries

Figure 4.7 also shows that, once the system reaches the residual gas saturation, the difference between homogeneous and heterogenous case is not a function of free gas amount and it reduces to the constant, i.e., Γ'_{kn}. The residual adsorbed gas amount in nonlinear case is much less than the linear case purely due to presence of surface diffusion. When the free gas amount approaches to zero, i.e., $\bar{C} \to 0$, equation (4.27) reduces to:

$$\left(\bar{C}_\mu\right)_{\bar{C}=0} = \Gamma'_{kn} = -\left(\Gamma_{kn}\right)_{\bar{C}=0} = \left(-\upsilon_1 \Gamma_{kn,linear}\right)_{\bar{C}=0} \tag{4.29}$$

substituting the definitions of υ_1 and Γ_{kn} at $\bar{C} = 0$ and rearranging the equation leads to

$$\left(\bar{C}_\mu\right)_{\bar{C}=0} = -\frac{C_{\mu s}\Gamma'_{linear}}{1 - \Gamma'_{linear}} \tag{4.30}$$

where Γ'_{linear} is defined as

$$\Gamma'_{linear} = \left(\Gamma_{linear}\right)_{\bar{C}=0} = \frac{N_{Th}\sigma_\phi^2 \bar{C}_{\mu 0}}{k_r} \tag{4.31}$$

Table 4.1: Problem parameters for the heterogeneous gas/matrix system

Parameter	Unit	Value
$\bar{\phi}$	fraction	1.0E-2
σ_{ϕ}^2	-	5.3E-7
$\bar{C}_0$	mol/cc	2.0E-3
k_r	1/sec	1.0E-5
$\bar{K}$	fraction	0.1
$\bar{C}_{\mu s}$	mol/cc	0.9
g	mol/cc	2.028E-4
B_0	cm^2	4.934E-14
μ_g	Kg/cm.s	2.0E-7
K'	fraction	-5.0E2
$\bar{D}$	cm^2/sec	1.0E-3
$\bar{D}_s$	cm^2/sec	2.5E-5
D'	cm^2/sec	3.3E-2
D'_s	cm^2/sec	3.3E-5
g'	mol/cc	-0.00835
λ	cm	1.0
L	cm	10.0
T	Kelvin	293.15

4.4 Summary

Here, gas flow, diffusive transport and adsorption in heterogeneous porous media with low permeability and porosity is investigated using a theoretical approach. In addition, unlike previous theoretical works, the sorption rates are explicitly introduced to a mathematical framework in this context.

Random local variations in matrix pore structure is considered and their influence on gas sorption and transport are investigated using small perturbations theory, a proven technique widely used in various other disciplines where analysis of multi-physics problems are required in the presence of *a priori* fluctuations induced by non-uniform fields. In conclusion, the homogenized gas-matrix system behavior can be described using the following upscaled governing equations

$$\bar{\phi}\frac{\partial \bar{C}}{\partial t} + (1-\bar{\phi})\frac{\partial \bar{C}_\mu}{\partial t} = \frac{\partial}{\partial x}\left(\bar{\phi}\mathcal{D}_{eff}\frac{\partial \bar{C}}{\partial x}\right) + \frac{\partial}{\partial x}\left(\bar{\phi}\bar{C}\frac{B_0}{\mu}\frac{\partial \bar{p}}{\partial x}\right) + \frac{\partial}{\partial x}\left[(1-\phi)\,\bar{D}_s\frac{\partial \bar{C}_\mu}{\partial x}\right] \tag{4.32}$$

$$+ \frac{\sigma_\phi^2 \bar{C}_{\mu 0}}{1 + N_{Pe}/(1+N_{Pe})}(1 - \upsilon_1\upsilon_2\bar{C})$$

$$\frac{\partial \bar{C}_\mu}{\partial t} = k_f\left(C_{\mu s} - \bar{C}_\mu\right)\bar{C} - k_r\bar{C}_\mu - \frac{N_{Th}}{1+2N_{Pe}}\sigma_\phi^2 C_{\mu 0}\upsilon_1(1+\upsilon_1\upsilon_2\bar{C}) \tag{4.33}$$

Further, it is founded that the matrix heterogeneity defined by random porosity field generates non-trivial macro-transport and macro-kinetics effects on the system that includes well known dimensionless numbers, i.e., P*é*clet number and Thiele modulus. It is also shown that the heterogenous porosity field leads to a significant improvement in adsorbed-phase transport when non-linear sorption kinetics is considered in very low permeability porous medias, that can explain earlier experimental observations suggesting significant adsorbed phase transport in microporous materials such as carbon and coal (Carman and Raal (1951), Ash *et al.*, (1963), Aylmotre and Barrer (1966), Do and Wang (1998), and Siemons *et al.*, (2007)). Our upscaling approach clearly shows the importance of initially adsorbed amount of gas on macro-transport and macro kinetics, known as the loading effect on gas sorption and adsorbed-phase transport (D.Do 1990). The system behavior is investigated numerically and it is found that macro–kinetics significantly increases the gas release rate and

macro–transport increases the ultimate gas recovery compare to the case where adsorbed-phase transport is ignored. Most importantly, our theoretical investigation shows that the nonlinear gas dynamics does not allow the system to reach equilibrium adsorption limit, even at large times.

Chapters 3 and 4 are dedicated to investigating the effects of small scale heterogeneities defined by random porosity field on gas storage and transport in coal and shale core samples, where we did not take into account the presence of macro fractures and cleats around the matrices and mass exchange between matrix and fractures. We also assumed the single gas component, i.e., methane, in the matrix while in coalbed methane and shale gas reservoirs multi-component gas is presented. This might not be an important issue dealing with primary production from coalbed and shale gas reservoirs, due to the fact that, more than %90 of gas component is methane (Hewitt *et al.*, 1984; Satriana M., 1980; Saghafi A., 2001). However, if we were to consider the CO_2 sequestration in these reservoirs, we need to consider multi-component nature of the problem that in micro-scale pore structure of coal and shale initiates the competitive sorption behavior and co- and counter-diffusion effects. In next chapter, we are investigating the CO_2 injection and methane production from a single well injection and production sector, where counter diffusion and competitive adsorption is considered in homogeneous reservoir with fixed porosity and permeability.

CHAPTER V

COUNTER-DIFFUSION AND COMPETITIVE ADSORPTION DURING CO_2 INJECTION AND COALBED METHANE PRODUCTION

When subsurface storage of anthropogenic carbon dioxide (CO_2) is considered, among the geological formations, coal seams keep a unique place with a distinct gas trapping mechanism: physical adsorption. Under the subsurface conditions and depending on the thermal maturity of coal, CO_2 sorption capacity of coals is typically 2-10 times that for methane (CH_4)(Shi and Durucan, 2008). This is a remarkable observation not only for sequestration but also from coalbed methane production point of view as it implicitly points out that stronger affinity of CO_2 to the coal material could initiate a mechanism of displacement of the originally in-place CH_4, when CO_2 is introduced to the coalbed environment. Thus, CO_2-enhanced coalbed methane recovery, CO_2-ECBM, was proposed as an improved natural gas recovery technique. Although CO_2-ECBM technique has not been commercialized yet, several pilot projects exist: the Allison Unit pilot in San Juan Basin, New Mexico, USA; the flue gas micro-pilot in Alberta, Canada; Yubari CO_2 injection site in Ishikari Basin, Japan; Kaniw injection site in Silesian Coal Basin, Poland. In addition, several coal basins in Australia, Russia, China, India, and Indonesia are determined to have large CO_2-ECBM potentials. The total worldwide gas production potential is estimated at approximately 68 Tscf, with about 7.1 billion metric tons of associated CO_2 sequestration potential. If viewed purely as a non-commercial CO_2 sequestration technology, the worldwide sequestration potential of deep coal seams may be 20 to 50 times greater.

Previous investigations have shown that carbon dioxide injection and enhanced coalbed

methane production (CO_2-ECBM) involves several viscous and diffusive transport mechanisms, raising challenging questions related to the chemically and structurally intricate nature of coalbeds. CO_2-ECBM recovery involves phenomena of fundamental interest in a chemically and structurally intricate porous medium. In general, the technique involves three stages: (1) convective/dispersive two-phase flow of the gas phase (injected CO_2 and released CH_4 molecules) with the coalbed water, in particular in the fractures and often during an early de-watering stage; (2) diffusive/dispersive gas transport in the secondary pore structure of the coalbed, i.e., fractures and the macropores; and (3) multi-component sorption phenomena, in particular in the primary (microporous) pore structure of the coalbed, e.g., co- and counter diffusion and competitive adsorption. These simultaneously take place in the coalbed within at least three different characteristic times of mass transport (flow, diffusion and sorption times) and several characteristic length scales, i.e., the scales of injector/producer well-spacing, of coal matrices bounded by the fractures and of the internal surface area of the matrices. As the consequence of these stages, the incoming CO_2 molecules are expected to activate and displace the in-place CH_4 molecules in coalbed. Injection of gas in a network of natural fractures initiates counter-diffusive transport and competitive (and often selective) sorption processes among the gas molecules in coal. Consequently, the incoming CO_2 molecules activate and displace the in-place CH_4 molecules. Competitive sorption rates, however, could be controlled by the counter-diffusive mass fluxes during the gas injection and production operations. Nature of the multi-component diffusive transport processes should therefore be understood clearly. Earlier theoretical attempts investigating coalbed methane production involved numerical simulators developed in the 'spirit' of modeling the naturally fractured conventional gas reservoirs with single permeability and dual porosity fields (Barenblatt *et al.*, 1960; Warren and Root, 1963; Closmann, 1975; and Gwo *et al.*, 1998). Often the gas mass balance appeared in these approaches in terms of a gas quality such as concentration or pressure, which is averaged over unipore coalbed matrix block. When it is written in one-dimensional space for the concentration of the gas

component, the balance for a finite-size matrix block typically reads as

$$\phi\frac{\partial C}{\partial t}+(1-\phi-\phi_f)\frac{\partial C_\mu}{\partial t}=\frac{\partial}{\partial x_1}\left(\phi\, D\frac{\partial C}{\partial x_1}\right) \tag{5.1}$$

where ϕ and ϕ_f are the constants of matrix and fracture porosity, and C and Cμ are the free and adsorbed gas concentrations in the matrix block, respectively. Notice that equation (5.1) is another form of Fick's second law written for a fluid adsorbing in porous medium. The adsorbed amount is often estimated during the calculations using a nonlinear equilibrium adsorption isotherm, e.g., the Langmuir isotherm, (Clarkson C.R., and Bustin, 1999):

$$C_\mu=\frac{C_m b' C}{1+b' C} \tag{5.2}$$

The presence of a diffusive mass transport with a constant diffusivity, D_m, was assumed next at the matrix-fracture interface and the averaging is performed using a priori parabolic concentration profile across the half-length R of the matrix block (Shi and Durucan 2005)

$$\phi\frac{\partial \bar{C}}{\partial t}+(1-\phi-\phi_f)\frac{\partial \bar{C}_\mu}{\partial t}=\frac{3}{R}\phi D_m\left(\frac{\partial C}{\partial x_1}\right)_{x_1=R} \tag{5.3}$$

with the block-averaged free and adsorbed gas concentrations are assigned to symbols with an over bar. The balance is based on an inner boundary condition dictating that no concentration gradient exists at the center of the matrix block (i.e., $\partial C(0,t)/\partial x_1$ =0). Consequently, the balance showing the time evolution of the averaged concentration was coupled to the mass balance equation for the fracture network using the diffusive mass exchange term at the matrix-fracture interface as a source/sink terms in the later:

$$\phi\frac{\partial \bar{C}}{\partial t}+(1-\phi-\phi_f)\frac{\partial \bar{C}_\mu}{\partial t}=\phi\sigma D_m(C_f-\bar{C}) \tag{5.4}$$

$$\phi_f\frac{\partial C_f}{\partial t}+\frac{\partial\left(\phi\nu_f C_f\right)}{\partial x_2}=\phi_f\sigma D_m(\bar{C}-C_f) \tag{5.5}$$

Here, $\sigma = 15/R^2$ is the coefficient of mass exchange between the matrix and the fracture (i.e., the transfer function). The accompanying gas mass balance, equation (5.5), dictates that the fractures are the places of transient (darcian) flow with a corresponding coalbed

permeability field. When complemented with appropriate coalbed boundary and initial conditions, i.e., closure of the initial/boundary value problem, and solved, the formulation may capture certain behavior of gas production in the field. However, it ignores several aspects of the coalbed physics as it significantly reduces the size of the problem. Those are the emphasis of this chapter since they are important to coalbed methane production and they may become critical considerations for the design and application of CO_2-ECBM. First, the conventional model assumes that partitioning of the free and the adsorbed gas in the matrix block occurs instantaneously and that the only resistance to the free gas release from the matrix is due to the so-called transfer function, which is essentially an averaged diffusive mass flux at the matrix-fracture interface (Warren, and Root 1963, Gwo *et al.*, 1998, Sarma, and Aziz 2006). The resistance obviously takes a finite value when the matrix block is surrounded by a network of uniformly distributed dominant single fractures and maintains a finite size, R. In essence, the conventional approach (1) considers the existence of discrete matrix blocks in the coalbed, (2) treats the gas behavior in the matrices as a molecular diffusion (heat conduction) problem and (3) controls the gas release from the matrices using the transfer function as a valve. It is, however, true that the coalbed matrix blocks can be described and characterized suitably using a multi-scale pore structure: the total pore volume of a block is made not only of micro- and macropores but also due to a high-density fracture network, which may significantly contribute to gas release during the production. Although the characteristic dimensions of these fractures are small relative to the dominant single fractures of the coalbed, they may be considered as the places for convective transport. Thus, their presence in the matrices not only makes the identification and discretization of the blocks difficult, if not impossible, but also changes the nature of gas transport, modifying the traditional matrix problem to a convective-diffusive one. Second, the diffusive nature of the mass transport for the matrices has to be re-visited. It is well documented in the literature that bulk diffusion and Knudsen (molecular streaming) flow of the gas molecules are the main mechanisms for the free gas migration in the macropores; whereas surface diffusion is the mechanism for the adsorbed molecules through the physically adsorbed layer on the micropore walls. It is perhaps straightforward to incorporate

these mechanisms with the traditional approach using Fick's first law, although the problem becomes a challenging one when multi-component gas behavior is considered. Flow of the injected CO_2 in a complex multi-scale fracture network initiates counter-diffusive and competitive adsorption processes between the CO_2 and CH_4 molecules in the primary pore structure of the coal, modifying the gas transport, in particular, and the nature of the surface diffusion on the adsorption layer. The conventional model (with the mass balances written for each component of the gas), as well as a new generation of CBM simulators, does not consider such steric effects due to multi-component nature of the problem. Although competitive adsorption and multi-component (co- and counter-) diffusion processes are well recognized in the chemical engineering literature and they are considered important for practical reasons (e.g., gas separators), our understanding of the system dynamics is limited due to difficulties of measuring quantities related to transport in the mixture, (Yi *et al.*, 2008).

Purpose of this work is to investigate the CO_2-ECBM technique using a new multi-continuum modeling approach that does not have the above-mentioned matrix-averaging and multi-component transport limitations of the conventional approach. A new formulation is proposed for the coalbed gas transport using Maxwell-Stefan formulation and for kinetics of gas release from the pores using a linear relationships describing net rate of gas mass interchange between the fractures and the pores. The governing equations consider the fractures, macropores and micropores as continua with a serial coupling, each represented by its own flow and transport processes: fractures are the places where the injected and released gas flows (i.e., convective and dispersive flow), the macropores make up the portion of pore volume where convective-diffusive transport takes place for the free gas, and the micropores are considered as part of the solid coal material which retains the gas at an adsorbed state and allows their surface transport. The resistance in the micropores is due to surface diffusion. Here, we develop a new one-dimensional theoretical framework suitable for a fundamental level investigation of binary gas storage and transport in coal seams considering a serial multi-continuum porous medium with triple porosity and dual permeability. Total pore volume is due to micro- and macropores and due to a high-density fracture

network. Macropores and fractures are characterized by their own effective uniform permeability fields; hence, they are continua for fast viscous/diffusive transport of the free gas. Micropores, on the other hand, are primary pores retaining the bulk of the gas in-place at an adsorbed state. Resistence in the micropores is due to surface diffusion of the adsorbed binary mixture. The generalized Maxwell-Stefan formulation of multi-component transport is revisited and extended to describe gas behavior in bimodal (micro- and macro-) pore structures. We first show that the widely used single-component Langmuir gas behavior is, in fact, a limiting case of the generalized form. The later includes not only the anticipated binary effects (due to the existence of two components with different molecular size and adsorption capacity) but also additional nonlinear effects due to the direction of diffusive mass fluxes and to the lateral interactions of the adsorbed gas molecules in the micropores. Following, we incorporate the multi-component formulation to a reservoir flow model to consider CO_2-ECBM process in between an injector/producer pair. Dynamics of sequestration and production is then investigated varying initial/boundary conditions. It is shown that the counter diffusion and competitive adsorption effects in the micropores could generate nontrivial effects at the reservoir-scale such that methane production is significantly enhanced. The investigation is important for our understanding and the design of CO_2-ECBM processes.

5.1 Binary Gas Transport Model for CO_2-ECBM

One-dimensional gas-coalbed system consists of the following mass balances for the components 1(CH_4) and 2 (CO_2): in the micro- and macropores:

$$\phi\frac{\partial C_i}{\partial t}+(1-\phi-\phi_f)\frac{\partial C_{\mu i}}{\partial t}=\Im(C_i)+\frac{\partial}{\partial x}\left[(1-\phi-\phi_f)\,D_{si}\frac{\partial C_{\mu i}}{\partial x}\right];\quad i=1,2 \tag{5.6}$$

$$\phi_f\frac{\partial C_{fi}}{\partial t}=\frac{\partial}{\partial x}\left(\phi_f K_{Li}\frac{\partial C_{fi}}{\partial x}\right)+\frac{\partial}{\partial x}\left(\phi_f\,C_{fi}\frac{R_gTk_f}{\mu}\frac{\partial C_{fi}}{\partial x}\right)-\phi_f a_i(bC_{fi}-C_i);i=1,2 \tag{5.7}$$

$$\Im(C_i)=\frac{\partial}{\partial x}\left(\phi\,C_i\frac{R_gTk_p}{\mu}\frac{\partial C_i}{\partial x}\right)+\frac{\partial}{\partial x}\left(\phi\,D_{pi}\frac{\partial C_i}{\partial x}\right) \tag{5.8}$$

In equations (5.6-5.8) ϕ is the effective macroporosity of the coal; whereas ϕ_f is the coalbed fracture porosity. The observation that the solid volume (i.e., $1-\phi-\phi_f$) involves accumulation of the adsorbed gases and their Fickian diffusion in equation (5.6) suggests that the solid material contains voids for the gas-coal interactions. These voids are mainly pores with small dimensions (characteristic length scales less than 10 nm) and macromolecular openings. They allow the storage and transport (i.e., surface diffusion) of small adsorbed molecules in the solid material. Here, we will refer to these voids as micropores in general. Thus, in the following pages, we pursue the binary gas behavior in a triple-porosity medium with micropores, macropores and fractures. We consider the macropores as the places for the free gases (with concentrations C_1 and C_2) to accumulate, flow and diffuse only. Hence, the adsorption of gas molecules on the macropore walls is negligible. The transport is Darcian flow with an effective coal matrix block permeability k_p and molecular diffusion with a diffusivity D_{pi}. The later is a measure of the macropore diffusion which may involve the bulk and/or Knudsen diffusion depending on the local coalbed conditions. In this study, for simplicity, it will be taken as a constant given as

$$D_{pi}(T)=\frac{D_k}{q}=\frac{4\eta_0}{3q}\sqrt{\frac{8R_gT}{\pi M_i}} \tag{5.9}$$

under the isothermal conditions. Here, η_0 is the Knudsen flow parameter and q is the tortuosity factor. We note that the nature of diffusive transport in the micropores is different

than that in the macropores and fractures. In the micropores, the gas molecules are at a physically adsorbed state and, hence, their binary transport is under the influence of solid material which has different adsorption capacity for the components. In this case, the surface diffusivity D_{si} for the binary gas has the diagonal and off-diagonal components of a second order diffusivity tensor D_{ii}:

$$D_{s1} = D_{11} + D_{12}\frac{\partial C_{\mu 2}/\partial x}{\partial C_{\mu 1}/\partial x} \tag{5.10}$$

$$D_{s2} = D_{22} + D_{21}\frac{\partial C_{\mu 1}/\partial x}{\partial C_{\mu 2}/\partial x} \tag{5.11}$$

A detailed derivation of surface diffusivity D_{si} is presented in Appendix E. Here, we note that the contribution of the off-diagonal terms on the diffusivity of a component is dependent on the ratio of the concentration gradients of the adsorbed gas components. Hence, the mass flux of each component is related to the locally existing gradients of the binary system. The main- and cross-term diffusion coefficients are described as:

$$D_{ii} = \frac{C_m - C_{\mu j}}{C_m - C_{\mu i} - C_{\mu j}} D_{si0} + \alpha (D_{si0} D_{sj0})^{0.5} \frac{(C_{\mu i} C_{\mu j})^{0.5}}{C_m - C_{\mu i} - C_{\mu j}} \tag{5.12}$$

$$D_{ij} = \frac{C_{\mu i}}{C_m - C_{\mu i} - C_{\mu j}} D_{si0} + \alpha (D_{si0} D_{sj0})^{0.5} \left(\frac{C_{\mu i}}{C_{\mu j}}\right)^{0.5} \frac{C_m - C_{\mu j}}{C_m - C_{\mu i} - C_{\mu j}} \tag{5.13}$$

where α is the lateral molecular interaction coefficient taking values in between $-1 \leq \alpha \leq 1$. In the case of co-diffusion, for example, when the direction of fluxes for CH_4 and CO_2 are the same, α takes positive values. As it can be seen from equations (5.12-5.13), mass fluxes of the gas components in this case reach to a maximum when $\alpha = +1$; their values decrease with α and eventually reach to a minimum when $\alpha = 0$. $\alpha = +1$ corresponds to the case when there is no lateral interaction between the adsorbed molecules in the micropores, i.e., extended Langmuir-type adsorption; whereas, $\alpha = 0$ to the case when the lateral interaction reaches a maximum level. Thus, the lateral interaction in the adsorbed phase may decrease the fluxes and hence slow down the mass transport of the gas components from the micropores to the macropores. In our case, α will be calculated at each time and location step as described by Yang *et al.*,(1991). $\alpha(C_{\mu 1}, C_{\mu 2}, \nabla C_{\mu 1}, \nabla C_{\mu 2}, C_m, D_{p1}, D_{p2}, D_{s10}, D_{s20})$ and C_m is defined

as

$$\frac{1}{C_m} = \frac{c_{\mu 10}}{C_{\mu s1}} + \frac{c_{\mu 20}}{C_{\mu s2}} \tag{5.14}$$

$$c_{\mu i0} = \frac{C_{\mu i0}}{C_{\mu 10} + C_{\mu 20}}; \qquad i = 1, 2 \tag{5.15}$$

Here, we consider that the binary gas mixture obeys the multi-component (extended-) Langmuir adsorption isotherm:

$$C_{\mu i} = \frac{C_m b_i' C_i}{1 + b_1' C_1 + b_2' C_2}; \qquad i = 1, 2 \tag{5.16}$$

Finally, equation (5.7), describing the mass balances for the gas components in the fractures, involves convective-dispersive flow with velocity ν_{fi} and the dispersion coefficient K_{Li}.

$$\nu_{fi} = \frac{R_g T k_f}{\mu} \frac{\partial C_{fi}}{\partial x}; \qquad i = 1, 2 \tag{5.17}$$

The fracture mass balance for component (i) is coupled to the mass balance for that component in the pores using a source/sink term which dictates the kinetics of gas uptake by and release from the pores:

$$\Phi = a_i (b C_{fi} - C_i); \qquad i = 1, 2 \tag{5.18}$$

The formulation is based on the net rate of interchange between the gas in the fractures and in the pores, i.e.,$\Phi = k_{f \to m} C_{fi} - k_{m \to f} C_i$ with $a_i = k_{\to m} f$ and $b = k_{f \to m}/k_{m \to f}$ appearing as the coefficient of mass transfer rate from the matrix to fracture and the ratio of the mass transfer coefficients, respectively. In general, typical values the partition coefficient b takes is expected to be in the order of one, although the quantity a_i needs to be evaluated carefully. The later has the dimension of 1/time. In the terminology of the conventional approach (diffusion-dominated matrix blocks with finite-size, R), an expression for it, which is dependent on the free and adsorbed gas concentrations, can be given as follows

$$a_i = \frac{15 D_{mi}}{R^2} = \frac{15}{R^2} \left[\begin{array}{l} \phi D_{pi} + \phi C_i \dfrac{R_g T k_p}{\mu} + (1 - \phi - \phi_f) D_{si} \\ \qquad \left(\dfrac{C_m b_i' + C_m b_i' b_j' C_j}{(1 + b_i' C_i + b_j' C_j)^2} - \dfrac{C_m b_i' b_j' C_i}{(1 + b_i' C_i + b_j' C_j)^2} \dfrac{\partial C_j}{\partial C_i} \right) \end{array} \right] \tag{5.19}$$

Prior to setting up the initial/boundary value problems and numerically solving the governing equations (5.6-5.8), the later are written in the dimensionless form as follow:

$$\left(\delta_1 + \delta_2 g_1 - \delta_2 g_1' \frac{\partial c_2}{\partial c_1}\right) \frac{\partial c_1}{\partial \tau} = \frac{\partial}{\partial r}\left[\left(1 + \theta_1 c_1 + \varepsilon_1 g_1 - \varepsilon_1 g_1' \frac{\partial c_2}{\partial c_1}\right) \frac{\partial c_1}{\partial r}\right] \tag{5.20}$$

$$\left(\delta_1 + \delta_2 g_2 - \delta_2 g_2' \frac{\partial c_1}{\partial c_2}\right) \frac{\partial c_2}{\partial \tau} = \frac{\partial}{\partial r}\left[\left(1 + \theta_2 c_2 + \varepsilon_2 g_2 - \varepsilon_2 g_2' \frac{\partial c_1}{\partial c_2}\right) \frac{\partial c_2}{\partial r}\right] \tag{5.21}$$

$$\delta_1 \frac{\partial c_{f1}}{\partial \tau} = \frac{\partial}{\partial r}\left[\left(\xi_1 + \chi_1 c_{f1}\right) \frac{\partial c_{f1}}{\partial r}\right] - \gamma_1 (c_{f1} - c_1) \tag{5.22}$$

$$\delta_1 \frac{\partial c_{f2}}{\partial \tau} = \frac{\partial}{\partial r}\left[\left(\xi_2 + \chi_2 c_{f2}\right) \frac{\partial c_{f2}}{\partial r}\right] - \gamma_2 (c_{f2} - c_2) \tag{5.23}$$

Details of scaling and non-dimensionalization are presented in Appendix F.

5.1.1 Initial/Boundary Value Problem for CO_2-ECBM

As initial condition we will consider that the coalbed contains a mixture of the components:

$$\tau = 0 \qquad ; \qquad c_1(r,0) = c_{f1}(r,0) = 0.95 \qquad c_2(r,0) = c_{f2}(r,0) = 0.05$$

At the location of CO_2 injection, i.e., the left boundary, we consider that CH_4 does not have any gradient, although the former gradient is inversely related to its flux in the reservoir J_{c2}:

$$r = 0 \qquad ; \qquad \frac{\partial c_1}{\partial r} = \frac{\partial c_{f1}}{\partial r} = 0 \qquad \frac{\partial c_2}{\partial r} = \frac{\partial c_{f2}}{\partial r} = -0.005/J_{c2}$$

On the other hand, fixed concentration (partial pressure) conditions are specified for the components at the location of CH_4 production, i.e., the right boundary:

$$r = 1 \qquad ; \qquad c_1(L,\tau) = c_2(L,\tau) = 0, \qquad c_{f1}(L,\tau) = 0.05; c_{f2}(L,\tau) = 0.005$$

Equations (5.20-5.23) are coupled second order nonlinear partial differential equation, numerical approximation of which could be obtained using an implicit finite difference scheme and Newton iteration. Time integration of the ordinary differential equations resulting from the discretization in space is performed by a solver, which is based on an implicit linear multi-step method that chooses the time steps dynamically during the computations.

5.2 Results and Discussion

We consider single well coalbed methane production and the application of CO_2-ECBM technique using 100 m injector and producer spacing in a coalbed reservoir with properties given in Table 5.1. At these conditions, the coalbed maintains an estimated 1,558.2 psi of average reservoir pressure. The simulation of coalbed methane production continues 4 years until the reservoir is depleted.

First, comparison of the CO_2-ECBM model of this study with the conventional model is done. Figure 5.1 shows the differences between the models in terms of the estimated fractional methane recoveries versus time with varying D_{si0}/D_{pi} ratio. The difference between the models is due to the coalbed gas release kinetics approach and to the binary nature of the problem. Note that the quantity D_{si0} refers to surface diffusion in the absence of binary molecular interactions of the components and of their gradients. It is given a constant $D_{s0} = D_{s10} = D_{s20}$ values different than D_{si} which is estimated during the simulation using equations (5.10) and (5.11). Increasing D_{si0}/D_{pi} ratio leads to faster gas production rate at early times due to faster CO_2/CH_4 exchange rate between micro-, macro-pores. However, as CH_4 concentration decreases and CO_2 concentration increases in micropores at later time, increasing D_{si0}/D_{pi} ratio has a reverse effect reducing the rate of CH_4 release from the micropores decreasing the ultimate gas recovery. Figure 5.2 shows the influence of changing the coefficient of gas release rate. The methane produced during CO_2-ECBM is sensitive to gas release kinetics. Similarly, the influence of the coefficient of molecular interaction among the adsorbed molecules in the micropores is investigated in Figure 5.3. Here, two cases are compared: the base case where the interaction coefficient is estimated numerically (typically negative values close to zero) and the case where it is fixed to -1. The former corresponds to counter diffusion of the adsorbed molecules with high levels of molecular interaction, whereas the later is counter diffusion with minimum molecular interaction, i.e., the Langmuirian case. Hence, the small-scale steric effects are predicted to play a significant role enhancing methane production during a CO_2-ECBM process.

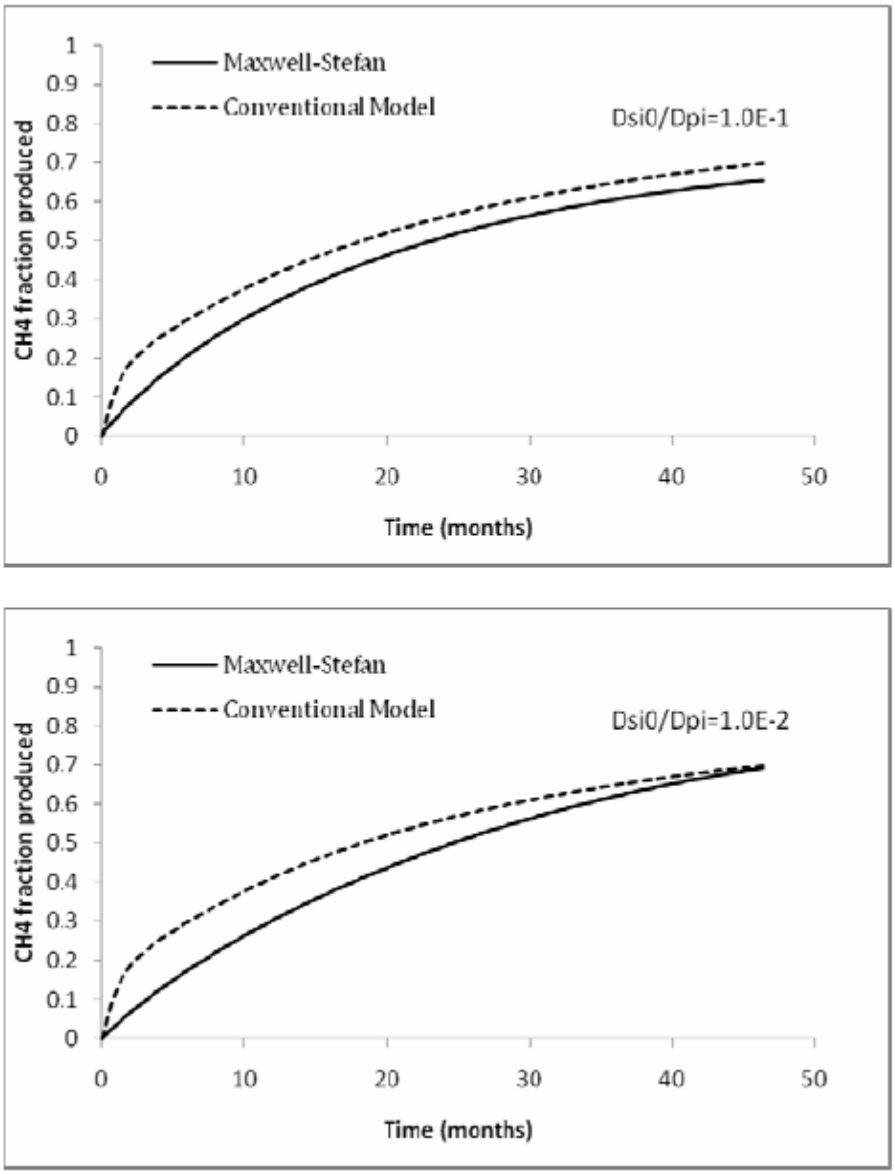

Figure 5.1: Comparison of the Maxwell-Stefan model with the conventional model for different D_{si0}/D_{pi0} ratio values

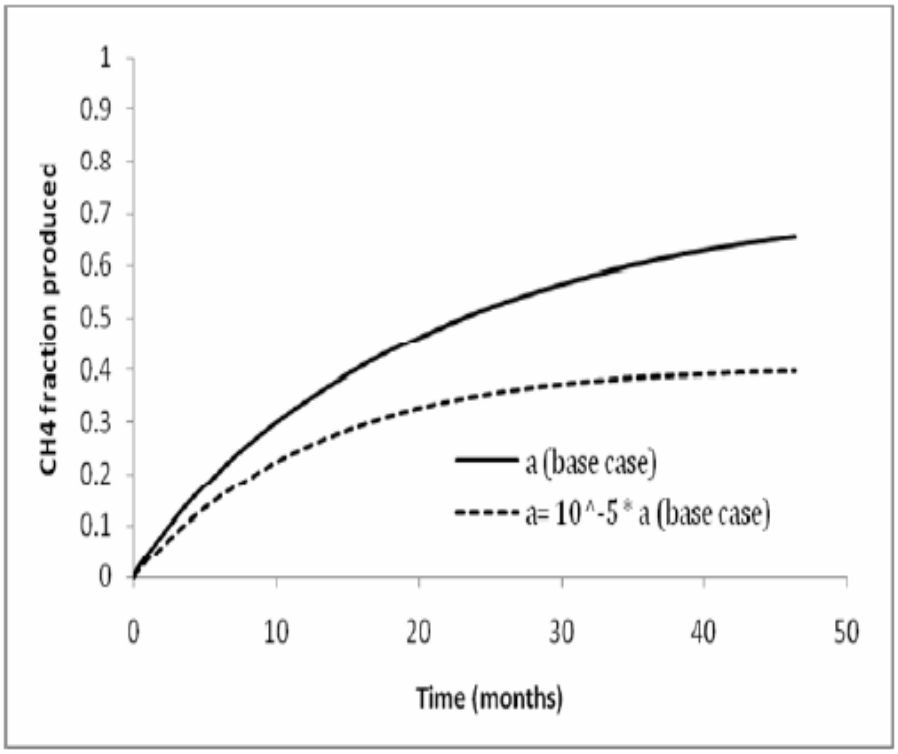

Figure 5.2: Sensitivity analysis of CH_4 production to reverse kinetic coefficient a_i

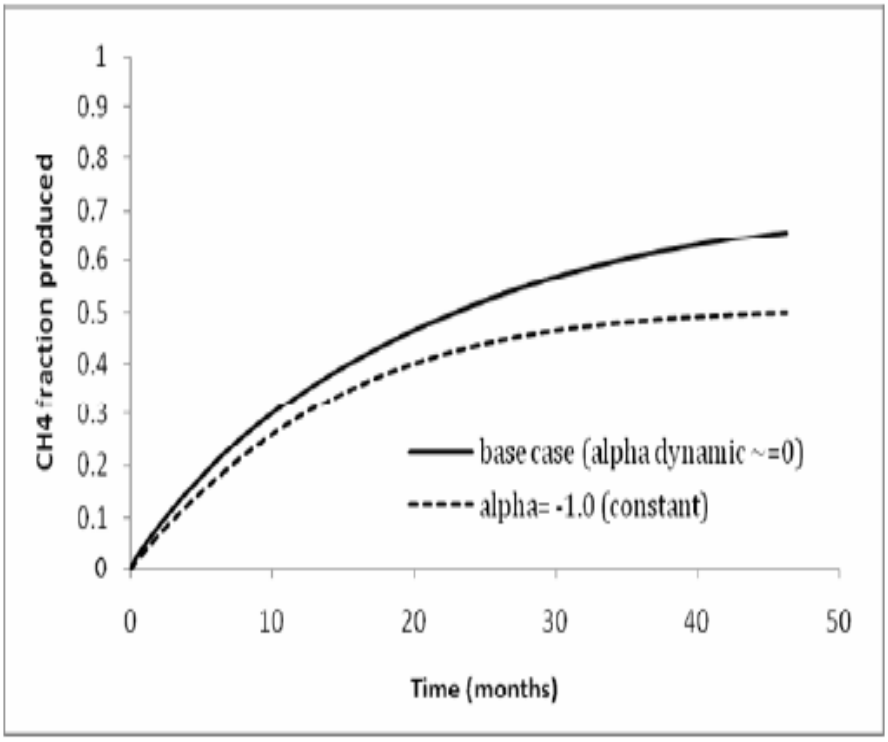

Figure 5.3: Sensitivity to the coefficient of lateral molecular interaction, α, during CO_2-ECBM production

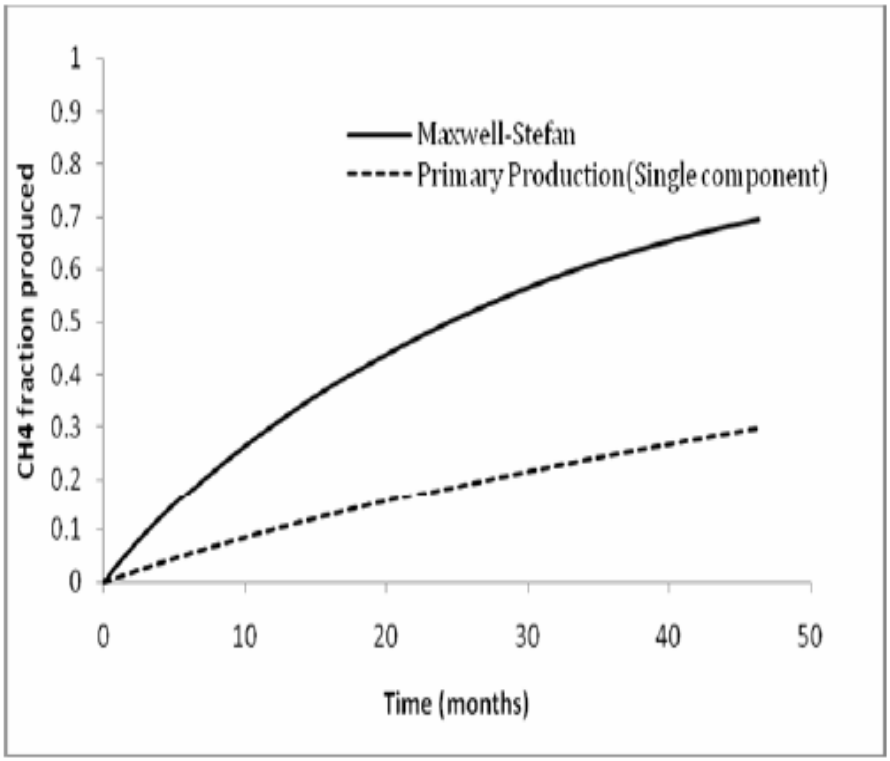

Figure 5.4: Fraction of CH_4 produced due to primary CBM (dashed line) and CO_2-ECBM (solid line) production

Figure 5.4 compares the first four years of primary methane production with the CO_2-ECBM production for the fixed drainage volume. Maxwell-Stefan formulation for CO_2-ECBM model predicts twice as much as gas produced using primary production scheme. Figure 5.5 shows the CO_2 influx to the reservoir at the injection well, which is nearly constant, receiving larger values when the CO_2 influx in the reservoir is smaller and smaller values when the influx is increased. It is clear that CO_2 injection is beneficial for methane recovery at every stage of methane production. This is due to positive counter diffusion and competitive adsorption effects of the CO_2 molecules and shown in terms of the estimated CH_4 and CO_2 profiles in the micropores, macropores and fractures in Figure 5.6.

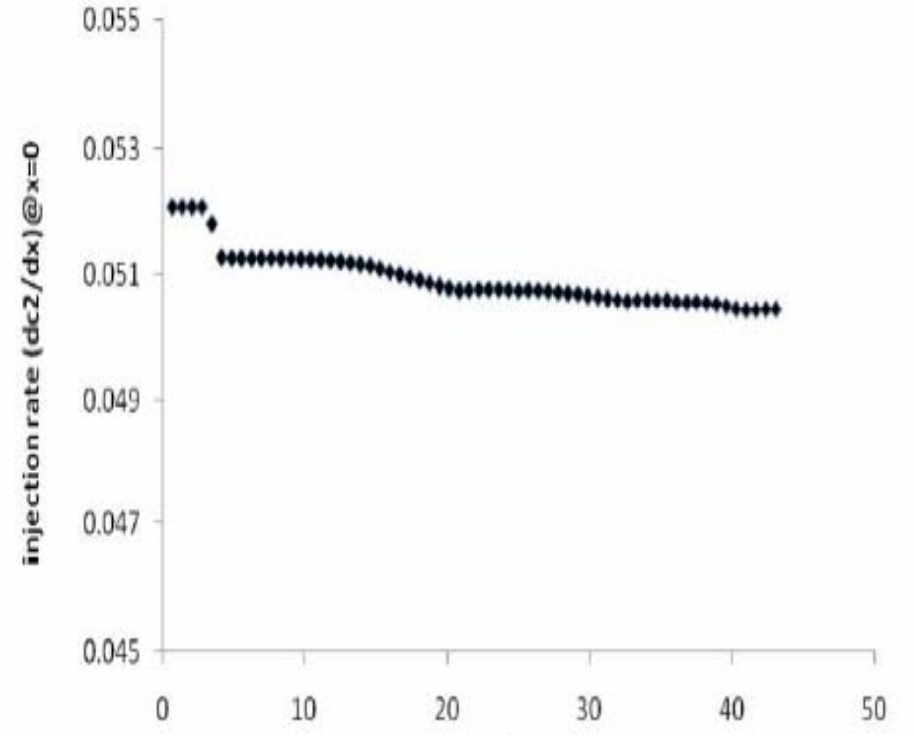

Figure 5.5: CO_2 injection rates versus time during CO_2-ECBM

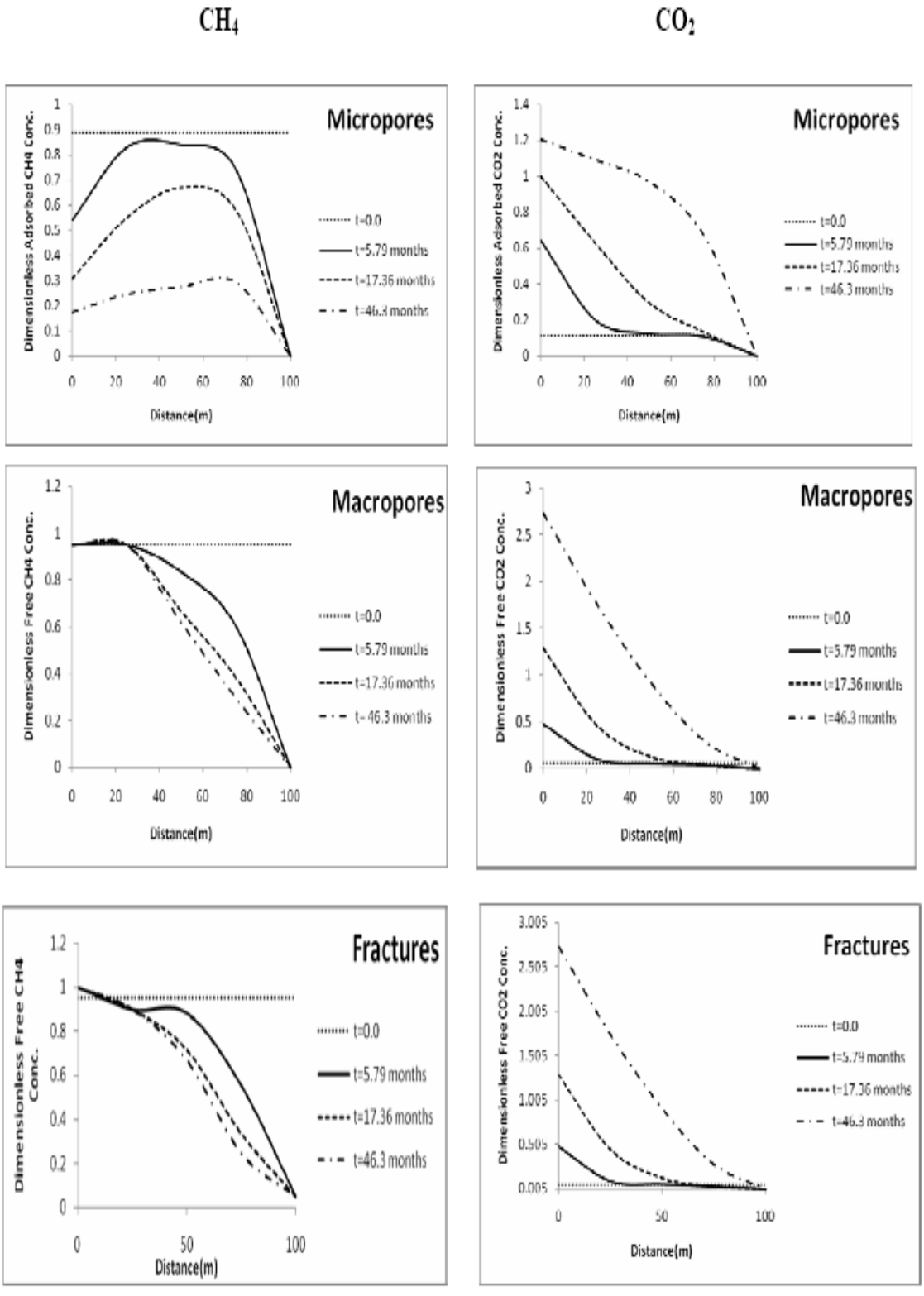

Figure 5.6: Dimensionless free and adsorbed gas concentration profiles in micropores, macropores and fractures

Table 5.1: Problem parameters for the heterogeneous gas/matrix system

Parameter	Unit	Value
ϕ	fraction	5.0E-2
ϕ_f	fraction	5.0E-3
k_p	μD	5.0
k_f	mD	10.0
$C_{10} = C_{f10}$	mol/cc	3.8E-3
$C_{20} = C_{f20}$	mol/cc	2.0E-4
$C_{\mu s1}$	mol/cc	2.0E-3
$C_{\mu s2}$	mol/cc	3.0E-3
a_1	$1/sec$	0.17
a_2	$1/sec$	0.28
b	$---$	1.0
b_1	cc/mol	5.0E2
b_2	cc/mol	1.2E3
D_p/R^2	$1/sec$	1.0E-2
$D_{s10}/D_{p1} = D_{s20}/D_{p2}$	—	1.0E-2
D_{s20}/D_{s10}	—	1.0
$K_{L1} = K_{L2}$	cm^2/sec	7.0E-2
L	cm	1.0E4
R	cm	10
T	Kelvin	322.04
R_g	$k_g cm^2/K/mol/sec^2$	8.314E4
μ	$k_g/cm/sec$	10.0

5.3 Summary

Injection and storage of anthropogenic CO_2 in coal seams have the benefit of producing additional coalbed methane which makes the sequestration a low-cost procedure in these subsurface environments. Conventional numerical simulators, however, have limited predictive capabilities for the design and development of CO_2-ECBM field projects because they neglect certain physical mechanisms intrinsic to the technique and its application to the coalbeds. Focus of the work here was to develop a new triple-porosity, dual-permeability flow simulation model which is based on a new kinetic approach for the description of gas release from the micro- and macropores into the fractures. It is shown that surface diffusion of the adsorbed gas molecules in the micropores is an important mechanism of transport during the CO_2-ECBM since it leads to important counter diffusion and competitive adsorption effects. These effects have the potential to change the dynamics of injection and production operations at the field scale and they may be critical during the evaluation of a CO_2-ECBM commercial project.

Fundamental investigation of the effects of heterogeneity on gas transport and storage in shale and coal samples are presented earlier in §3 and §4, where the single continuum including multi-scale pore structure is assumed for tight formations. However, recent microscopic investigations on shale gas samples using scanning electron microscopy have revealed finely-dispersed micro-porous organic material (i.e., kerogen) that is imbedded within the inorganic shale matrix (Ambrose *et al.*, 2010). Inorganic materials contain larger-size pores of varying geometries although it is the organic material that makes up the majority of gas pore volumes. It is shown that a significant portion of total gas in-place is associated with inter-connected large nano-pores within the organic material in certain gas shales. Therefore, to investigate the heterogeneity effects on this multi-continua multi-scale pore structure more detailed investigation considering multi-continua porous medium models are required. Multi-scale perturbation methods developed by Krylov and Bogoliubov and later popularized by Nayfeh (1970s) is a very popular method to approximate the solution of weakly non-linear differential equations for the cases with different time scale dynamics.

However, application of these methods for the case where different special scale properties also involved is very complicated. If the perturbations of the random field decays in large length scales then only short and intermediate length scale fluctuations are important, otherwise, one needs to investigate the behavior of the average random filed in large length scales, Van Horssen et al. (2008). In next chapter, we applied small perturbation theory to the problem where the heterogeneity effects of porous medium introduced by random permeability field on reactive flow. In this problem assumptions of one step nonlinear dissolution reaction and ideal liquid solution, i.e., the fluid properties of which is not significantly influenced by the dissolution reaction, are held.

CHAPTER VI

REACTIVE FLOW, MACROKINETICS, AND ADVECTIVE DISPERSION IN HETEROGENEOUS POROUS MEDIA

Reactive flow in a porous medium is influenced by the medium heterogeneities. The effective macroscopic equations must incorporate such information. In this chapter, upscaling of an isothermal advection-reaction problem in inert heterogeneous porous media is considered using spectral-based small perturbation theory (Gelhar and Axness 1983; Gelhar 1993; Wilhelm *et al.*,1997). The heterogeneity is in flow permeability (lnK) field, which is random and correlated in space. A one-step nonlinear dissolution reaction moderately takes place between an injected tracer and a stationary mineral residing in the pore space. In addition to the species concentrations, the local reaction kinetics is dependent on reactive mineral specific surface area, initial distribution of which is correlated to permeability with a linear slope b. Stochastic analysis of flow, transport and reaction is performed using first-order perturbations. Uniform reaction wave propagation is investigated on a moving coordinate system and upscaled governing equations are obtained with explicit macro-scale expressions for the coefficients of reaction, fluid flow and tracer macrodispersion. The reaction coefficient takes larger values than its mean and it is significantly influenced by the medium variances. Its profile along the reaction wave is strongly nonlinear, displaying a characteristic asymptotic behavior at central part of the wave. Macrodispersion coefficient is larger inside the reaction wave than its value in the absence of reaction. Fluid flow is under the combined influences of macrokinetics and macrodispersion. Consequently, the entering fluid accelerates ($b > 0$) and decelerates ($b < 0$) as it travels along the reaction wave. This hydrodynamic effect becomes more pronounced with the intensity of medium

heterogeneities and has a potential to induce reaction wave instabilities.

6.1 Local Governing Equations Describing Flow and Transport in the Presence of Fluid-Solid Interactions

Our investigation deals with a problem of flow and transport in porous media in the presence of fluid-solid interactions. The scope is limited to an isothermal reactive flow system. It is considered that a first-order heterogeneous reaction takes place between the injected liquid solution and a stationary solid such as flocculated clays, carbonates or some other solid particles residing on the grain surfaces of the inert porous matrix. An overall reaction scheme is anticipated for the purpose of investigation with the following representative components: $[\text{Mineral}]+\tilde{\nu}[\text{Tracer}]\rightarrow \tilde{\nu}_p[\text{product}]_{aq}$

Due to nature of this type of reactions, the main contributing factors for the chemical transformation, i.e., mineral dissolution, are the amount of initially available reactive mineral and its average specific surface area. Generally, the mineral has much larger surface area than the grains forming the framework of the matrix, hence, locally increasing the reaction rate and leaving the matrix minerals virtually untouched (Fogler *et al.*,1976). Since the process involves a heterogeneous reaction, a tracer-mineral reaction wave develops spontaneously and propagates at a velocity less than that of the injected fluid (Fan *et al.*,1976). It is within this moving boundary, where the mineral dissolution occurs at relatively high rates. Molecular diffusion of the tracer in the liquid phase is considered small relative to the gas phase diffusion; however, the rate of molecular transport could be sensitive to the tracer concentration gradients. Outside the reaction wave, the problem is mainly controlled by convective mass transport, initial and boundary conditions.

During the reactive fluid flow, although the porosity distribution of the medium may not change significantly, dissolution could cause significant variations in the absolute permeability of the medium. Subsequently, the reaction wave could suffer hydrodynamic instability due to preferential tracer flow through the generated high-permeability channels. Sherwood (1987)and Hinch and Bhatt (1990) have completed linear stability analysis of such reaction waves in homogeneous porous media. In this work, the reaction-induced permeability variations are not included; hence, we describe and analyze flow, transport and reaction

interactions in the presence of a porous medium with fixed, i.e., frozen, permeability heterogeneity. Dimensional form of the governing equations for a planar reaction wave propagating in a homogeneous porous medium is presented below. Tracer with concentration Y has the following mass balance

$$\phi\frac{\partial}{\partial t}(Y\rho)+\frac{\partial}{\partial x_i}(Y\rho v_i)=\frac{\partial}{\partial x_i}\left(D_{ij}\rho\frac{\partial Y}{\partial x_j}\right)-\nu\rho_m^0 W \tag{6.1}$$

Total liquid mass balance is

$$\phi\frac{\partial\rho}{\partial t}+\frac{\partial}{\partial x_i}(\rho v_i)=0 \tag{6.2}$$

The quantity of reactive mineral residing in porous medium is described in terms of its total volume density, i.e., dissolvable mineral mass per total volume ρ_m. Hence, the mineral mass balance reads:

$$\frac{\partial\eta}{\partial t}=W \tag{6.3}$$

with dependent variable, $\eta=\rho_m/\rho_m^0$ representing the depth of mineral conversion, and W the mineral dissolution rate. Hence, η corresponds to a normalized solid mass that is available for reaction at a particular time and location. Using the law of mass action, the dissolution rate will be taken in a general form as follows:

$$W=k_0 a_s^{n1}Y^{n2}\eta^{n3} \tag{6.4}$$

where k_0 is the coefficient of reaction; exponents ni represent the dependences on mineral surface area a_s and the concentrations of the reactants. Evaluation of these parameters, as well as the initial reactive mineral density ρ_m^0 requires elaborate pore-level study. It should be noted here that if the reaction rate had been found to change linearly with the reactant concentrations and had not involved any spatially varying parameters, such as the specific mineral surface area, then the average reaction rate would have been obtained simply using the mean concentrations in the calculations. Subsequently the mean rate of reaction could have been incorporated into the transport model of mean concentrations without any difficulty. In the above formulation, ρ is the density of the carrier liquid. Although this quantity could vary locally due to reaction-induced concentration gradients, it is considered

independent of tracer and aqueous product concentrations during the investigation. D_{ij} is the pore-scale tracer dispersion in liquid phase, while ν represents the mass-weighted stoichiometric coefficient for the tracer defined in terms of the stoichiometric coefficient $\tilde{\nu}$ as follows

$$\nu = \frac{\tilde{\nu} M_t}{M_m} \tag{6.5}$$

Here, M_t and M_m are molecular weights of the tracer and mineral respectively. Finally, the local flow is represented by

$$\upsilon = -\frac{K_{ij}}{\mu}\frac{\partial p}{\partial x_i} \tag{6.6}$$

where K_{ij} is the absolute permeability and μ is the concentration-independent liquid viscosity. During the investigation, the spatially varying fluid velocity field, υ_i, is taken as divergence free, i.e., fluid being incompressible, and obeys the Darcy's law. This assumption is reasonable for single-phase liquid flow in porous media and simplifies the system equations substantially. The reaction rate expression is further simplified by taking the exponents $n_i = 1$, and generating a new reaction rate coefficient:

$$\omega = k_0 a_s Y_0 \tag{6.7}$$

Hence, the reaction rate is now given as $W \approx \tilde{r} = \omega Y \eta$. Note that the reaction coefficient ω is an important quantity for the investigation since it is directly proportional to the specific surface area as of the solid reactant and it will be allowed to change only spatially, i.e., $\partial\omega/\partial t = 0$. In addition, we introduce a dimensionless parameter $\alpha = (\nu\rho_m^0)/(\rho_0 Y_0)$ representing the tracer reactant capacity. Thus, the governing equations describing reactive flow in a porous medium take the following form:

$$\phi\frac{\partial Y}{\partial t} + \frac{\partial}{\partial x_i}(\upsilon_i Y) = \frac{\partial}{\partial x_i}\left(D_{ij}\frac{\partial Y}{\partial x_i}\right) - \alpha\tilde{r} \tag{6.8}$$

$$\frac{\partial \eta}{\partial t} = \tilde{r} \tag{6.9}$$

$$\frac{\partial \upsilon_i}{\partial x_i} = 0 \tag{6.10}$$

6.2 Random Fields

Naturally occurring porous medium heterogeneities is represented by a time-independent, spatially variable random permeability field, which will be considered in terms of its mean $\bar{f}$ and its small perturbation f':

$$f(x_i) = \bar{f} + f'; \qquad E[f] = \bar{f}; \qquad E[f'] = 0$$

The spatial variations are quantified by a three dimensional statistically anisotropic exponential covariance with the following spectral density function:

$$S_{ff} = \frac{\sigma_f^2 \lambda_1 \lambda_2 \lambda_3}{\pi^2 \left[1 + (k_1\lambda_1)^2 + (k_2\lambda_2)^2 + (k_3\lambda_3)^2\right]^2} \tag{6.11}$$

Where λ_i and k_i are components of correlation length and wave number, respectively (Gelhar and Axness 1983). During the flow, the liquid velocity, tracer and mineral concentrations and reaction rate ω are influenced by the medium heterogeneity and hence are represented in terms of their means and perturbations accordingly:

$$\begin{aligned}
&Y = \bar{Y} + Y'; && E[Y] = \bar{Y}; && E[Y'] = 0 \\
&\eta = \bar{\eta} + \eta'; && E[\eta] = \bar{\eta}; && E[\eta'] = 0 \\
&\upsilon_i = \bar{\upsilon}_i + \upsilon_i'; && E[\upsilon_i] = \bar{\upsilon}_i; && E[\upsilon_i'] = 0 \\
&\omega = \bar{\omega} + \omega'; && E[\omega] = \bar{\omega}; && E[\omega'] = 0
\end{aligned}$$

Coefficient ω is assumed to have a partial linear correlation with $f(x_i)$; thus, it is also allowed to vary in space:

$$\omega = a + b(f - f_{min}) + \delta; \qquad \bar{\omega} = a + b(\bar{f} - f_{min}); \qquad \omega' = bf' + \delta$$

Where a and b represent the intercept and slope of the linear relationship. When a negative correlation is taken, for example, i.e., $b < 0$, a is equal to ω_{max} corresponding to its minimum counterpart in the permeability field. The correlation residual δ is assumed to be statistically homogeneous random field described by a three-dimensional anisotropic exponential autocovariance function, with a spectrum given in Appendix I.

6.2.1 Spectral Analysis

The coordinate system x_i is chosen such that x_1 is the direction of the mean flow, hence, we take:

$$\bar{\upsilon}_1 = \upsilon; \qquad \bar{\upsilon}_2 = \bar{\upsilon}_3 = 0$$

However, note that the velocity perturbations υ_2' and υ_3' are still non-zero. The local dispersion tensor is approximated as

$$D_{ij} = \alpha_t \upsilon \delta_{ij} + (\alpha_L - \alpha_T)\frac{\bar{\upsilon}_i \bar{\upsilon}_j}{\upsilon} \tag{6.12}$$

With α_L and α_T being the local longitudinal and transverse dispersivity values and δ_{ij} the Kronecker delta function. For the reaction term, Taylor series expansion centered on the mean concentrations is used as a function of the mean and perturbed quantities:

$$\tilde{r}(\omega, Y, \eta) \approx \omega \left(r + r_Y Y' + r_\eta \eta' + r_{YY} Y'^2 + r_{\eta\eta} \eta'^2 + r_{Y\eta} Y' \eta' \right) \tag{6.13}$$

with

$$r = \frac{1}{\omega} \tilde{r}(\bar{Y}, \bar{\eta}, \omega) \tag{6.14}$$

$$r_Y = \frac{1}{\omega} \left(\frac{\partial \tilde{r}}{\partial Y} \right)_{\bar{Y}, \bar{\eta}, \omega} \tag{6.15}$$

$$r_\eta = \frac{1}{\omega} \left(\frac{\partial \tilde{r}}{\partial \eta} \right)_{\bar{Y}, \bar{\eta}, \omega} \tag{6.16}$$

$$r_{YY} = \frac{1}{2\omega} \left(\frac{\partial^2 \tilde{r}}{\partial Y^2} \right)_{\bar{Y}, \bar{\eta}, \omega} \tag{6.17}$$

$$r_{\eta\eta} = \frac{1}{2\omega} \left(\frac{\partial^2 \tilde{r}}{\partial \eta^2} \right)_{\bar{Y}, \bar{\eta}, \omega} \tag{6.18}$$

$$r_{Y\eta} = \frac{1}{\omega} \left(\frac{\partial^2 \tilde{r}}{\partial Y \partial \eta} \right)_{\bar{Y}, \bar{\eta}, \omega} \tag{6.19}$$

Note that the functions described in equations (6.14-6.19) are independent of ω since the reaction rate is considered linear in ω. Next, the perturbed quantities are substituted into the tracer and mineral mass balances given in equations (6.8-6.10):

$$\phi\frac{\partial(\bar{Y}+Y')}{\partial t}+\frac{\partial}{\partial x_i}\left[(\bar{\upsilon}+\upsilon')(\bar{Y}+Y')\right]=\frac{\partial}{\partial x_i}\left(D_{ij}\frac{\partial(\bar{Y}+Y')}{\partial x_i}\right) \\ -\alpha\psi\left[(\bar{Y}+Y'),(\bar{\eta}+\eta'),(\bar{\omega}+\omega')\right] \tag{6.20}$$

$$\frac{\partial(\bar{\eta}+\eta')}{\partial t}=\psi\left[(\bar{Y}+Y'),(\bar{\eta}+\eta'),(\bar{\omega}+\omega')\right] \tag{6.21}$$

Taking expectations of the equations in (6.20-6.21) and retaining up to the second order perturbations, the mean transport equations are obtained as follows:

$$\phi\frac{\partial\bar{Y}}{\partial t}+\bar{\upsilon}_i\frac{\partial\bar{Y}}{\partial x_i}+\frac{\partial\overline{\upsilon_i'Y'}}{\partial x_i}=\frac{\partial}{\partial x_i}\left(D_{ij}\frac{\partial\bar{Y}}{\partial x_j}\right)-\alpha\psi(\bar{Y},\bar{\eta}) \tag{6.22}$$

$$\frac{\partial\bar{\eta}}{\partial t}=\psi(\bar{Y},\bar{\eta}) \tag{6.23}$$

Here, we define the reaction rate $\psi(\bar{Y},\bar{\eta})$:

$$\psi(\bar{Y},\bar{\eta})=\bar{\omega}r+r_Y\overline{\omega'Y'}+r_\eta\overline{\omega'\eta'}+\bar{\omega}\left(r_{YY}\bar{Y'}^2+r_{\eta\eta}\bar{\eta'}^2+r_{Y\eta}\overline{Y'\eta'}\right) \tag{6.24}$$

By subtracting the mean transport equations (6.22-6.23) from the original equations given in (6.20-6.21), respectively, and adopting the small perturbation approach, the following first order perturbation equations are obtained:

$$\phi\frac{\partial Y'}{\partial t}+\bar{\upsilon}_i\frac{\partial Y'}{\partial x_i}+\upsilon_i'\frac{\partial\bar{Y}}{\partial x_i}=\frac{\partial}{\partial x_i}\left(D_{ij}\frac{\partial Y'}{\partial x_j}\right)-\alpha(\omega'r+r_Y\bar{\omega}Y'+r_\eta\bar{\omega}\eta') \tag{6.25}$$

$$\frac{\partial\eta'}{\partial t}=\omega'r+r_Y\bar{\omega}Y'+r_\eta\bar{\omega}\eta' \tag{6.26}$$

Next, a coordinate system moving with the reaction wave is introduced using the mean propagation speed $\bar{V}$ of the reaction wave:

$$\xi_1=x_1-\bar{V}t;\qquad \xi_2=x_2;\qquad \xi_3=x_3$$

An expression for the wave propagation speed is determined in terms of the fluid velocity υ in the main flow direction in Appendix H and found that the reaction wave speed differs from the fluid flow velocity in the main direction:

$$\bar{V} = \frac{\upsilon}{\varphi + \alpha} \tag{6.27}$$

Hinch and Bhatt (1990) recognized $1/\alpha$ as the reactant capacity number for the tracer. The later is defined as the ratio of inlet tracer concentration to the required concentration in a pore space to transform all the minerals in the corresponding solid. The capacity number is usually less than 1.0 and, therefore, the reaction wave is expected to propagate slower than the fluid. In the moving coordinate system the mean equations are

$$\phi\left(\frac{\partial \bar{Y}}{\partial t} - \bar{V}\frac{\partial \bar{Y}}{\partial \xi_1}\right) + \upsilon\frac{\partial \bar{Y}}{\partial \xi_1} + \frac{\partial \overline{\upsilon_i' Y'}}{\partial \xi_i} = \frac{\partial}{\partial \xi_i}\left(D_{ij}\frac{\partial \bar{Y}}{\partial \xi_j}\right) - \alpha\psi(\bar{Y}, \bar{\eta}) \tag{6.28}$$

$$\frac{\partial \bar{\eta}}{\partial t} - \bar{V}\frac{\partial \bar{\eta}}{\partial \xi_1} = \psi(\bar{Y}, \bar{\eta}) \tag{6.29}$$

and the first-order perturbation equations are

$$\phi\left(\frac{\partial Y'}{\partial t} - \bar{V}\frac{\partial Y'}{\partial \xi_1}\right) + \upsilon_i'\frac{\partial \bar{Y}}{\partial \xi_i} = \frac{\partial}{\partial \xi_i}\left(D_{ij}\frac{\partial Y'}{\partial \xi_j}\right) - \alpha(\omega' r + r_Y \bar{\omega} Y' + r_\eta \bar{\omega}\eta') \tag{6.30}$$

$$\frac{\partial \eta'}{\partial t} - \bar{V}\frac{\partial \eta'}{\partial \xi_1} = \omega' r + r_Y \bar{\omega} Y' + r_\eta \bar{\omega}\eta' \tag{6.31}$$

The cross-correlation term $\overline{\upsilon_i' Y'}$ in equation (6.28) includes the field-scale heterogeneity effects on the mean tracer transport and represents macroscopic dispersive flux due to random variations in the fluid velocity υ_i and tracer concentration Y. Estimation of this and the other five reaction-related cross-correlation terms given in equation (6.24) involves solving the stochastic transport equations using spectral approach described in References (Gelhar and Axness 1983; Gelhar 1993). The perturbation quantities are assumed locally stationary in space and their spectral representation is given as the following:

$$Y'(\xi_i, t) = \int_{-\infty}^{\infty} exp\left[ik_1(\xi_1 + \bar{V}t) + ik_2\xi_2 + ik_3\xi_3\right] dZ_Y(k_i, t) \tag{6.32}$$

$$\eta'(\xi_i, t) = \int_{-\infty}^{\infty} exp\left[ik_1(\xi_1 + \bar{V}t) + ik_2\xi_2 + ik_3\xi_3\right] dZ_\eta(k_i, t) \tag{6.33}$$

$$Y'(\xi_i,t) = \int_{-\infty}^{\infty} exp\left[ik_1(\xi_1+\bar{V}t)+ik_2\xi_2+ik_3\xi_3\right] dZ_Y(k_i,t) \tag{6.34}$$

$$v_i'(\xi_i,t) = \int_{-\infty}^{\infty} exp\left[ik_1(\xi_1+\bar{V}t)+ik_2\xi_2+ik_3\xi_3\right] dZ_{v_i}(k_i) \tag{6.35}$$

$$\omega'(\xi_i,t) = \int_{-\infty}^{\infty} exp\left[ik_1(\xi_1+\bar{V}t)+ik_2\xi_2+ik_3\xi_3\right] dZ_{\omega}(k_i) \tag{6.36}$$

Then, the perturbation equations (6.30-6.31) in the spectral domain read as:

$$\phi\frac{\partial(dZ_Y)}{\partial t} - \phi\bar{V}ik_1dZ_Y + ik_1vdZ_Y - G_idZ_{v_i} = -D_{ij}k_ik_jdZ_Y - \alpha(rdZ_\omega + r_Y\bar{\omega}dZ_Y + r_\eta\bar{\omega}dZ_\eta) \tag{6.37}$$

$$\frac{\partial(dZ_\eta)}{\partial t} - \bar{V}ik_1dZ_\eta = rdZ_\omega + r_Y\bar{\omega}dZ_Y + r_\eta\bar{\omega}dZ_\eta \tag{6.38}$$

where the mean concentration gradient in equation (6.37) is defined as $G_i = -\partial\bar{Y}/\partial\xi_i$ Since tracer and mineral undergo a reaction process, however, the concentration perturbations change in time and therefore the transient terms as well as the mean concentration gradients cannot be neglected. The approach employed here introduces a frame of reference that follows the reaction zone not only in space but also in time, (Wilhelm *et al.*,1997). This frame of reference consists of a transformation of the time coordinate, in which, the time variations of the concentration perturbations become negligible at large times. Equations (6.37-6.38) can be solved by considering reaction to be the only cause of concentration perturbation variations in time. This is achieved by solving the following simplified set of equations as an intermediate step:

$$\phi\frac{\partial(dZ_Y)}{\partial t} = -\alpha(r_Y\omega_YdZ_Y + r_\eta\omega_\eta dZ_\eta) \tag{6.39}$$

$$\frac{\partial(dZ_\eta)}{\partial t} = r_Y\omega_YdZ_Y + r_\eta\omega_\eta dZ_\eta \tag{6.40}$$

Hence, effective reaction coefficients ω_Y and ω_η are introduced for the species concentrations, which allow for the fact that ω at which concentration perturbations attenuate at the field

scale may be different from the mean reaction coefficient $\bar{\omega}$ due to medium heterogeneity. The solution of this system of equations provides the following time-scaling expressions:

$$\frac{\phi}{\alpha} dZ_Y = d\hat{Z}_Y exp\left(-\int_0^t r_Y \omega_Y dt'\right) - \int_0^t r_\eta \omega_\eta dZ_\eta exp\left(-\int_0^t r_Y \omega_Y dt''\right) dt' \tag{6.41}$$

$$dZ_\eta = d\hat{Z}_\eta exp\left(-\int_0^t r_\eta \omega_\eta dt'\right) - \int_0^t r_Y \omega_Y dZ_Y exp\left(-\int_0^t r_\eta \omega_\eta dt''\right) dt' \tag{6.42}$$

Physically we can interpret the time-scaling as traveling along with the tracer amplitude as it is decreased by reaction. The result of the scaling introduces the spatial amplitudes for conservative quantities $dZ_{\hat{Y}}$ and $dZ_{\hat{\eta}}$. Following this, the equations are substituted into the perturbation equations in spectral domain. At large times, $dZ_{\hat{Y}}$ and $dZ_{\hat{\eta}}$ can be neglected. This produces two linear algebraic equations expressed in the original time coordinate for the spectral amplitudes dZ_Y and dZ_η:

$$\left[ik_1(\upsilon - \phi\bar{V}) + \alpha r_Y(\bar{\omega} - \omega_Y)\right] dZ_Y - G_i dZ_{\upsilon_i} + \alpha r dZ_\omega + \alpha r_\eta(\bar{\omega} - \omega_\eta) dZ_\eta = 0 \tag{6.43}$$

$$-\left[i\bar{V}k_1 + r_\eta(\bar{\omega} - \omega_\eta)\right] dZ_\eta - r dZ_\omega - r_Y(\bar{\omega} - \omega_Y) dZ_Y = 0 \tag{6.44}$$

The local dispersion has previously been found to have negligible influence during the evaluation of integrals of the form encountered here; therefore, it is neglected (Gelhar and Axness 1983). The expression for dZ_Y and dZ_η are then found as:

$$\Delta dZ_Y = G_i\left[i\bar{V}k_1 + r_\eta(\bar{\omega} - \omega_\eta)\right] dZ_{\upsilon_i} - i\bar{V}k_1 \alpha r dZ_\omega \tag{6.45}$$

$$\Delta dZ_\eta = G_i r_Y(\bar{\omega} - \omega_Y) dZ_{\upsilon_i} - ik_1 r(\upsilon - \phi\bar{V}) dZ_\omega \tag{6.46}$$

with a Δ defined as

$$\Delta = (\phi\bar{V} - \upsilon)k_1^2\bar{V} + ik_1\left[\bar{V}\alpha r_Y(\bar{\omega} - \omega_Y) + (\upsilon - \phi\bar{V}) r_\eta(\bar{\omega} - \omega_\eta)\right] \tag{6.47}$$

Next, the cross correlations appearing in the mean equations need to be determined using the spectral representation theorem

$$\overline{a'b'} = \int_{-\infty}^{\infty} S_{ab} d\vec{k} = \int_{-\infty}^{\infty} E[dZ_a * dZ_b^*] \tag{6.48}$$

where a and b are arbitrary random fields and $'*'$ correspond to complex conjugate of quantity b. These definitions yield the cross correlations appear in our reactive flow problem as follows:

$$\overline{\upsilon_i' Y'} = G_i I_1(\upsilon_i, \upsilon_j) + G_i r_\eta(\bar{\omega} - \omega_\eta) I_0(\upsilon_1, \upsilon_j) - \alpha r I_1(\omega, \upsilon_i) \tag{6.49}$$

$$\overline{\omega' Y'} = G_i I_1(\upsilon_i, \omega) + G_i r_\eta(\bar{\omega} - \omega_\eta) I_0(\upsilon_1, \omega) - \alpha r I_1(\omega, \omega) \tag{6.50}$$

$$\overline{\omega' \eta'} = -G_i r_Y(\bar{\omega} - \omega_Y) I_0(\upsilon_i, \omega) - \upsilon r I_4(\omega, \omega) + \phi r I_1(\omega, \omega) \tag{6.51}$$

$$\overline{Y'^2} = 0 \tag{6.52}$$

$$\overline{\eta'^2} = 0 \tag{6.53}$$

$$\begin{aligned} \overline{Y' \eta'} = &-G_i \alpha r r_Y(\bar{\omega} - \omega_Y) I_3(\upsilon_i, \omega) - G_i \upsilon r I_5(\upsilon_i, \omega) + G_i r \upsilon r_\eta(\bar{\omega} - \omega_\eta) I_6(\upsilon_i, \omega) \\ &+\phi G_i r I_2(\upsilon_i, \omega) - \phi r r_\eta(\bar{\omega} - \omega_\eta) G_i I_3(\upsilon_i, \omega) + r^2 \upsilon \alpha I_5(\omega, \omega) - \phi \alpha r^2 I_2(\omega, \omega) \end{aligned} \tag{6.54}$$

During the derivation of cross-correlations given in equations (6.49-6.54), the higher order non-linear terms involving the product $G_i G_j$ is neglected. I_i terms are integrals described in Appendix I.

6.3 Results: Field Scale Coefficients

The upscaled fluid flow, tracer mass transport and reaction coefficients can now be obtained explicitly from the mean equations (6.28-6.29) for which the cross correlation terms are found and given in equations (6.49-6.54). More specifically, the mean equations now consist of fluctuation-induced reactive terms (zero-order derivatives of the reactant concentrations), convective terms (first-order derivatives of the mean tracer concentration) and dispersive terms (second-order derivatives of the mean tracer concentration). Grouping terms consisting of zeroth-order derivatives of the species concentrations appearing in the mean equations results in the following expression representing an effective reaction coefficient

$$\omega_e = \bar{\omega} - \frac{\lambda_1 \sigma_\omega^2 \left[\beta^2(\bar{\omega}-\omega_e) - \alpha\bar{V}(\upsilon-\phi\bar{V})\bar{\omega}\bar{Y}(1-\bar{\eta})\right]}{(\bar{\omega}-\omega_e)\Gamma} \tag{6.55}$$

where, $\bar{\omega}$ and ω_e=ω_Y=ω_η are the mean and the effective reaction rate coefficients, respectively. In addition, σ_ω^2 along with parameters β and Γ are introduced

$$\sigma_\omega^2 = b^2\sigma_f^2 + \sigma_\delta^2; \quad \beta = \alpha\bar{V}(1-\bar{\eta}) - (\upsilon-\phi\bar{V})\bar{Y}; \quad \Gamma = \beta\left[\lambda_1(\bar{\omega}-\omega_e)\beta - \bar{V}(\upsilon-\phi\bar{V})\right]$$

These parameters, as will be seen, play important role on the reactive flow dynamics. Similarly, the effective fluid flow velocity is determined by simply recognizing that all the advective terms (first order derivatives) in right hand side of the mean equation minus those in the left hand side is equal to $(\upsilon_e - \phi\bar{V})$. This produces the following equation for effective velocity:

$$\upsilon_e = \upsilon - \alpha\bar{V}\left[\frac{A'_{11} b\gamma(1-\bar{\eta})\beta}{\Gamma}\right]\left\{1 + \frac{\bar{\omega}\bar{Y}(\upsilon-\phi\bar{V})}{(\bar{\omega}-\omega_e)\beta} + \frac{\beta}{\Gamma}\left[\lambda_1\alpha\bar{V}(\bar{\omega}-\omega_e)(1-\bar{\eta}) - \bar{V}(\upsilon-\phi\bar{V})\right]\right\} \tag{6.56}$$

where $A'_{11} = \sigma_f^2\lambda_1/\gamma^2$ corresponds to the longitudinal dispersivity in the absence of reaction. γ is the flow factor defined in Appendix I. and taken to be equal to $\gamma = exp(\sigma_f^2/6)$. Finally, the longitudinal dispersion coefficient $\upsilon A'_{11}$ could easily be obtained by grouping together the dispersive terms in the mean tracer mass balance into the $\partial\left(\upsilon A_{11}\partial\bar{Y}/\partial\xi_1\right)/\partial\xi_1$ form. Hence, the longitudinal effective dispersivity is obtained:

$$A_{11} = A'_{11}\left[\frac{\upsilon\alpha\bar{V}^2(1-\bar{\eta})}{\Gamma}\right] \tag{6.57}$$

Consequently, the field-scale partial differential equations for the tracer and mineral mass are written as

$$\phi\frac{\partial\bar{Y}}{\partial t}+\upsilon_e\frac{\partial\bar{Y}}{\partial x_1}=\frac{\partial}{\partial x_1}\left(\upsilon A_{11}\frac{\partial\bar{Y}}{\partial x_1}\right)-\alpha\omega_e\bar{Y}(1-\bar{\eta})+... \tag{6.58}$$

$$\frac{\partial\bar{\eta}}{\partial t}=\omega_e\bar{Y}(1-\bar{\eta})+... \tag{6.59}$$

Here, it is important to note that product represents the upscaled dispersive mixing due to non-uniform advection only, since the local dispersion has been neglected during the application of spectral theory.

6.4 Discussion: Upscaled Reactive Flow System Dynamics

Next, a sensitivity analysis is presented for the reactive flow problem described by the nonlinear equations(6.58-6.59). Numerical calculations are less instructive and, as it will be shown, expected to be tedious; therefore, focus of the investigation is on a length scale-invariant behavior of the derived upscaled coefficients given by the algebraic equations (6.55-6.57). Three particular locations are chosen along the propagating reaction wave where the species concentrations are independent of the spatial coordinate. These locations are (i) the trailing edge, with the conditions $\bar{Y} = \bar{\eta} = 1.0$; (ii) the center, where $\bar{Y} = 1 - \bar{\eta} = C$ and (iii) the leading edge, with $\bar{Y} = \bar{\eta} = 0$. Table 6.1 lists the parameters and their base values used during the analysis. The investigation starts with the effective reaction rate coefficient, which is also necessary to evaluate the other field-scale coefficients.

Table 6.1: Problem parameters for the heterogeneous gas/matrix system

Parameter	Unit	Value
ϕ	fraction	0.25
σ_f	-	0.4
υ	m/d	1
α	-	1.0
$\bar{\omega}$	fraction	10.0
λ_1	m	0.8
b	-	± 8.0

6.4.1 Effective Reaction Coefficient

Since the mineral at the trailing and the tracer at the leading edges are consumed completely, the two reactive species do not co-exist at the edges of the reaction wave; therefore, the reaction does not take place at these limits. However, the effective reaction rate coefficient ω_e can be estimated therein and analyzed. At the trailing edge, equation (6.55) simplifies to the following cubic form:

$$\lambda_1 \chi^3 + \bar{V}\chi^2 - \lambda_1 \sigma_\omega^2 \chi = 0 \tag{6.60}$$

where $\chi = \bar{\omega} - \omega_e$ indicates deviation from the mean value of the reaction rate coefficient due to the presence of heterogeneities. The estimated roots of equation (6.60) are sketched in Figure 6.1 (top, left column) with variance σ_ω^2 for constant values of the medium correlation length and reaction propagation velocity, equation (6.27). There exist three branches of reactive states at the trailing edge; one with a fixed value equal to zero, for which the reaction coefficient takes its mean value, i.e., $\omega_e = \bar{\omega}$, and a pair of asymmetrically diverging branches. For a fixed value of the variance and taking the model equation below

$$\frac{d\chi}{dt} = \lambda_1 \chi^3 + \bar{V}\chi^2 - \lambda_1 \sigma_\omega^2 \chi \tag{6.61}$$

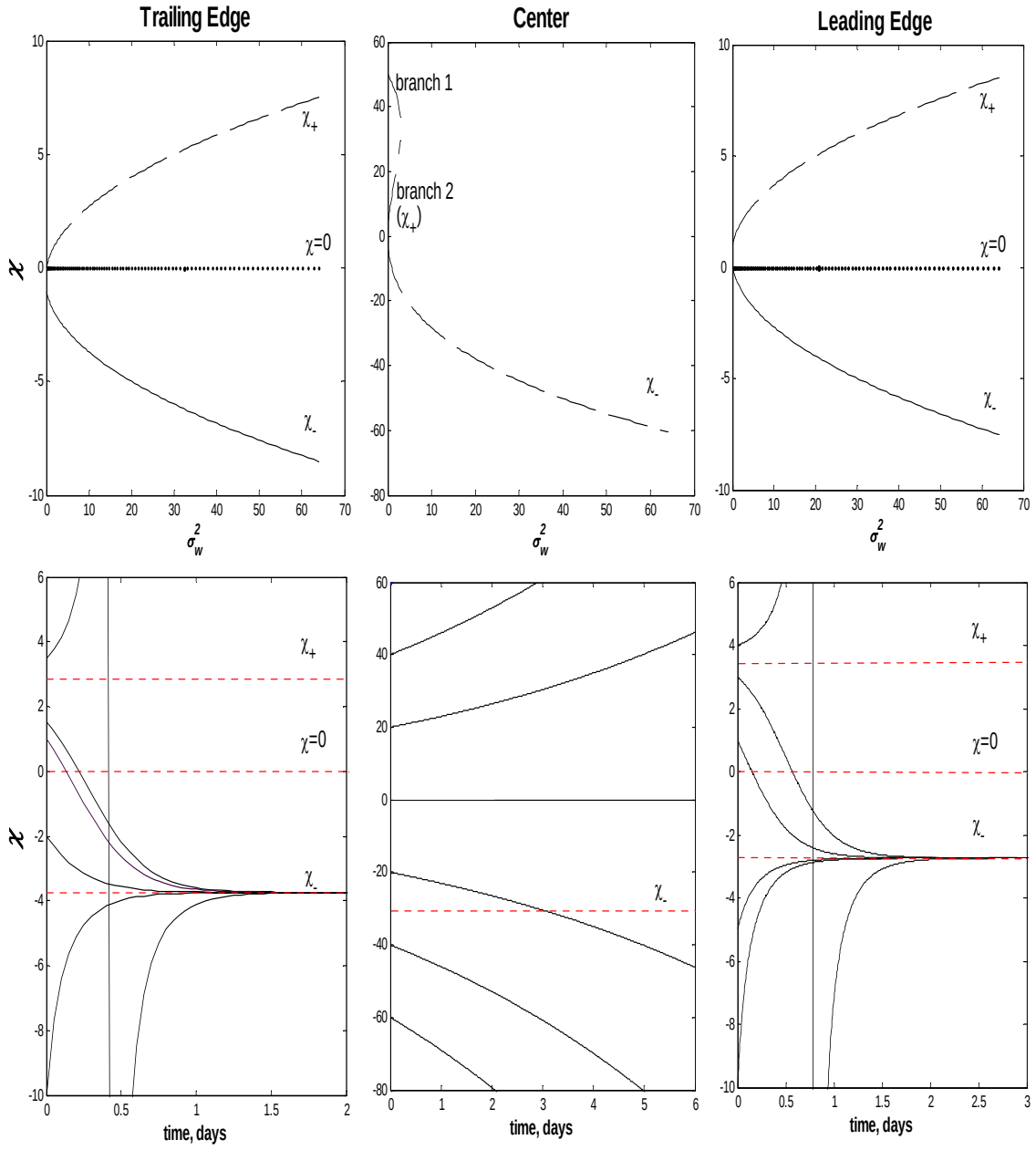

Figure 6.1: Stability analysis of χ at the trailing edge (left column), center (middle) and leading edge (right column) of the reaction wave. At the trailing edge $\chi_{\pm} = \left(-\bar{V} \pm \sqrt{\bar{V}^2 4\lambda_1^2\sigma_\omega^2}\right)/2\lambda_1$; at the leading edge $\chi_{\pm} = \left[\bar{V}(\upsilon - \phi\bar{V}) \pm \sqrt{\bar{V}^2(\upsilon - \phi\bar{V})^2 4\lambda_1^2\sigma_\omega^2\alpha^2\bar{V}^2}\right]/2\lambda_1\alpha\bar{V}$; ε=1.0E-2 and C=0.5 for calculations at the center

it can be shown that initial χ disturbances decay as $t \to \infty$ and that the equation (6.60) has only one accessible branch at the trailing edge of the reaction wave. Some typical solutions for σ_ω^2=10.0 are given in Figure 6.1 (bottom, left column) showing that all the chosen initial values converge to χ_- branch within less than 2 days. For the initial values larger than root χ_+, however, acute oscillations are observed prior to their eventual decay. Nonetheless the system is capable of damping those and, consequently, no bifurcations appear. It is thus conclusive that χ_- is the stable reaction branch and that the effective reaction rate coefficient is always larger than its mean value at the trailing edge. Figure 6.2 (top) shows that the coefficient increases moderately with the permeability variance and decreases with the permeability correlation length scale. At the leading edge of the reaction zone, equation (6.55) reduces to

$$\lambda_1 \alpha \bar{V} \chi^3 - \bar{V}(\upsilon - \phi \bar{V}) \chi^2 - \lambda_1 \sigma_\omega^2 \alpha \bar{V} \chi = 0 \tag{6.62}$$

which has three roots and, as in the trailing case, initial disturbance trajectories are drawn to one stable branch, i.e., χ_-. Using equation (21), $\upsilon - \phi \bar{V} = \alpha \bar{V}$, it can be shown that the equation (6.62) reduces to a form similar to the equation (6.60):

$$\lambda_1 \chi^3 - \bar{V} \chi^2 - \lambda_1 \sigma_\omega^2 \chi = 0 \tag{6.63}$$

Hence, the observed branches in Figure 6.1 (right column) have similar characteristics as in the trailing case. As shown in Figure 6.2, however, the heterogeneity effect on the coefficient is negligibly small at the leading edge. Center of the reaction wave has previously been described as the place where the reactive species concentrations are equal. Setting $\bar{Y} = 1 - \bar{\eta} = C$, however, gives β=0 in equation (6.55), which, interestingly, leads to infinitely large effective reaction coefficient values. This singular behavior points to a dramatically changing reactive flow dynamics inside the reaction wave. Difficulty in analysis can, however, be partially overcome by observing the behavior of χ in the neighborhood of the centerline $x = x_0$ of equal concentrations. For the purpose, we introduce the following linearization on the concentration profiles:

$$\bar{Y} = \bar{Y}|_{x=x_0} + \left(\frac{d\bar{Y}}{dx}|_{x=x_0} \right) (x - x_0) + ... \cong C + \varepsilon \tag{6.64}$$

$$1 - \bar{\eta} = 1 - \bar{\eta}|_{x=x_0} + \left(\frac{d\bar{\eta}}{dx}|_{x=x_0} \right) (x - x_0) - ... \cong C - \varepsilon \tag{6.65}$$

Hence, the first terms (C) on the right hand side of equations (6.64) give value of the equal species concentration at the centerline, whereas the first two terms ($C\varepsilon$) give straight-line fits of the concentration profiles at the centerline. Substituting equations (6.64-6.65) into equation (6.55), re-organizing and using equation (6.27), the following expression is obtained.

$$\chi = \frac{4\lambda_1 \sigma_\omega^2 \varepsilon^2 \chi - \lambda_1 \sigma_\omega^2 \bar{\omega}(C^2 - \varepsilon^2)}{4\lambda_1 \varepsilon^2 \chi^2 + 2\bar{V}\varepsilon\chi} \tag{6.66}$$

This algebraic equation gives three branches of solutions for fixed values of C and ε , see Figure 6.1 (top, middle column). Branches 1 and 2 take real and positive ($\omega_e < \bar{\omega}$) values albeit when the medium variance is relatively small. The reaction rate is negative for the first branch; therefore, these solutions do not correspond to any physically meaningful state of the reactive flow system. The reaction is positive for the second branch (χ_+) only in the homogeneous limit, $\sigma_\omega^2 \to 0$, however. The third branch (χ_-), on the other hand, shows trends similar to those stable branches observed at the leading and trailing edges of the reaction wave.

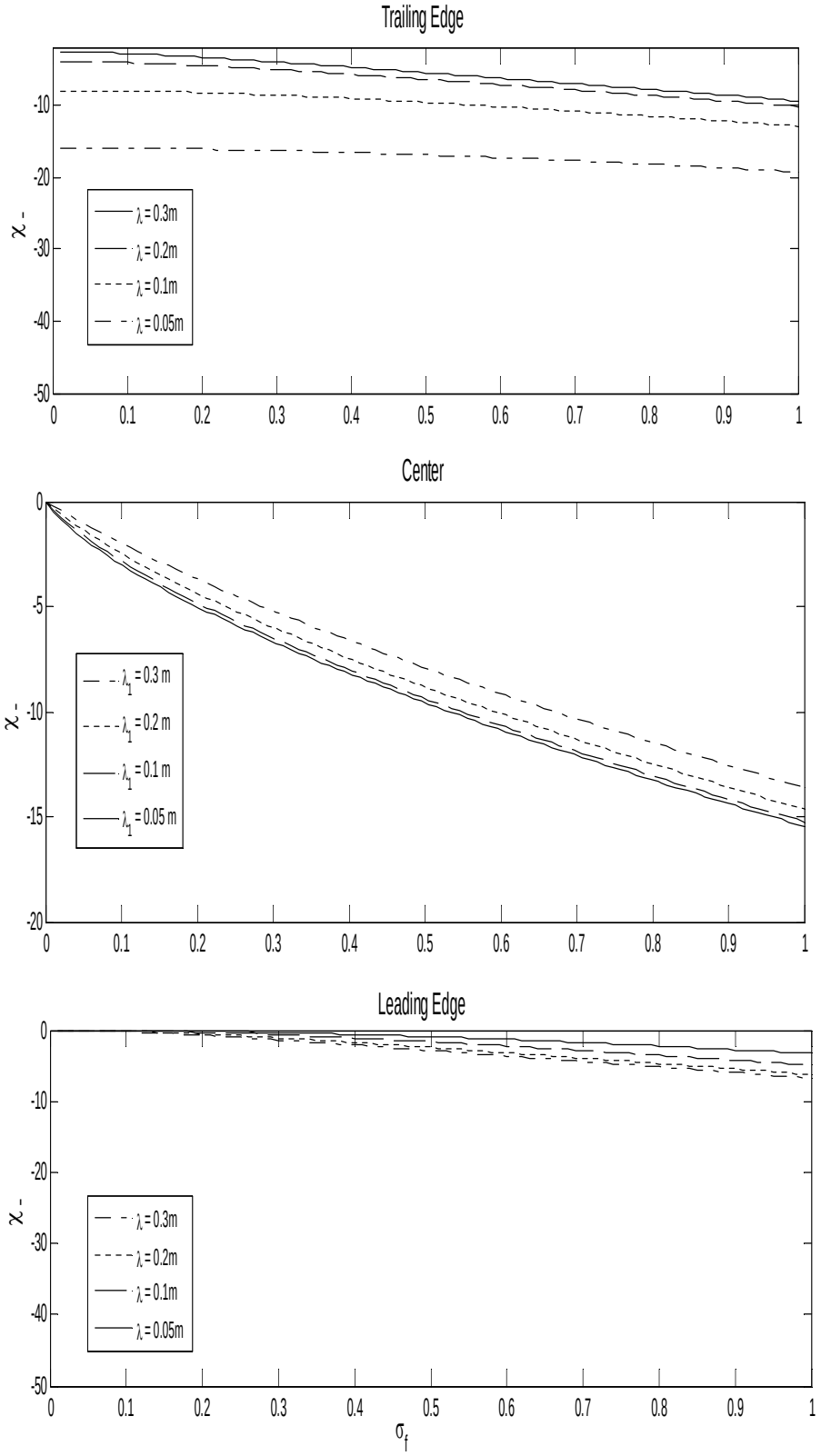

Figure 6.2: Effects of permeability variance and correlation length on the effective reaction rate coefficient. ε=1.0E-2 and C=0.5 for calculations at the center

At this stage, magnitude of the effective reaction coefficient at the center of the reaction wave needs to be further discussed based on the $\chi_{\pm}$branches. For typical values of C (which appears to play a secondary role), Figure 6.3 shows the estimated values varying with ε. It is clear that the effective reaction coefficient diverges and takes infinitely large values as the centerline of the wave is approached, i.e., $\varepsilon \to 0$. Hence, also branch 2 is not a physically meaningful state, yielding negative reaction rates at the center. This leaves the branch χ_- as the only possible solution corresponding to the reactive flow system. However, Figure 6.1 (bottom, right) shows that the reactive flow system is not capable of damping the initial disturbances. Curiously, only χ=0, which was not a branch but a particular solution in the homogeneous limit, appears as the stable one for the trajectory originating at χ=0. We note, however, that trajectories of the initial disturbances near zero tend to grow (with relatively much lower rates) and the later is not an asymptotically stable point.

The observed uncertainty concerning properties of the effective reaction rate coefficient inside the reaction wave could be lessened following a different approach using signs of first and second order derivatives of the coefficient at the edges of the reaction wave with respect to a mean species concentration. The effective coefficient takes:

Trailing edge: $\left(\partial\chi_-/\partial\bar{Y}\right)_{\bar{\eta}} > 0$ and $\left(\partial^2\chi_-/\partial\bar{Y}^2\right)_{\bar{\eta}} > 0$

Leading edge: $\left(\partial\chi_-/\partial\bar{Y}\right)_{\bar{\eta}} < 0$ and $\left(\partial^2\chi_-/\partial\bar{Y}^2\right)_{\bar{\eta}} < 0$

which, as shown in Figure 6.4, yields concave down trends originating at the edges of the reaction wave. Accordingly, it can be argued that the branch is suitable to complete the χ_- coefficient profile along the wave and that the effective reaction coefficient inside the reaction zone takes values significantly larger than its mean and those at the edges, see Figure 6.2. In the following, we continue the analysis taking this branch as the valid one for the center of the reaction wave.

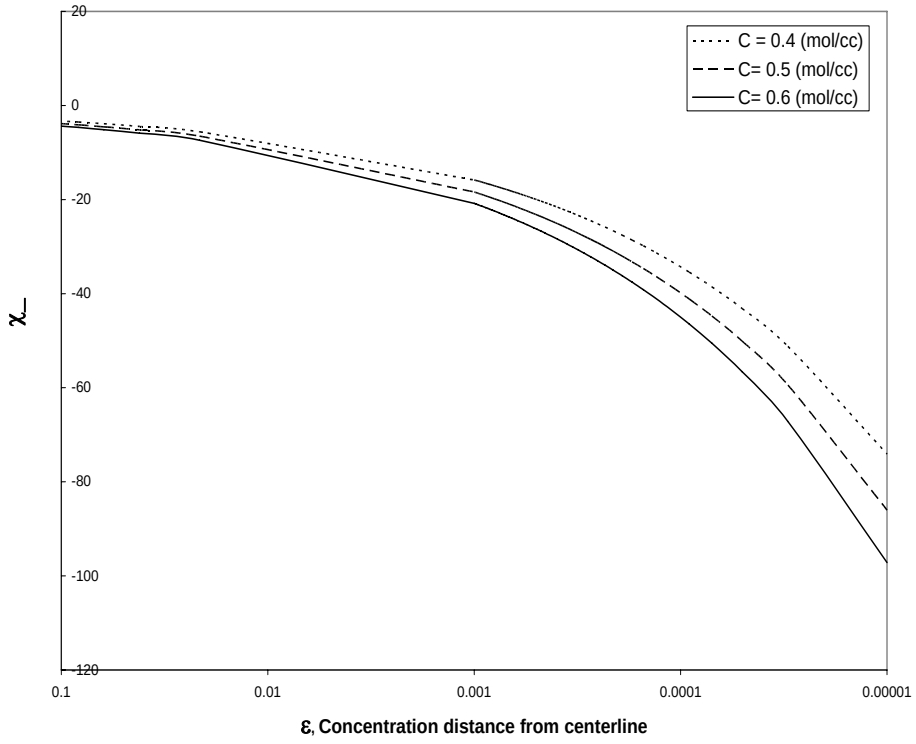

Figure 6.3: Reaction coefficient in vicinity of the centerline for varying ε and C

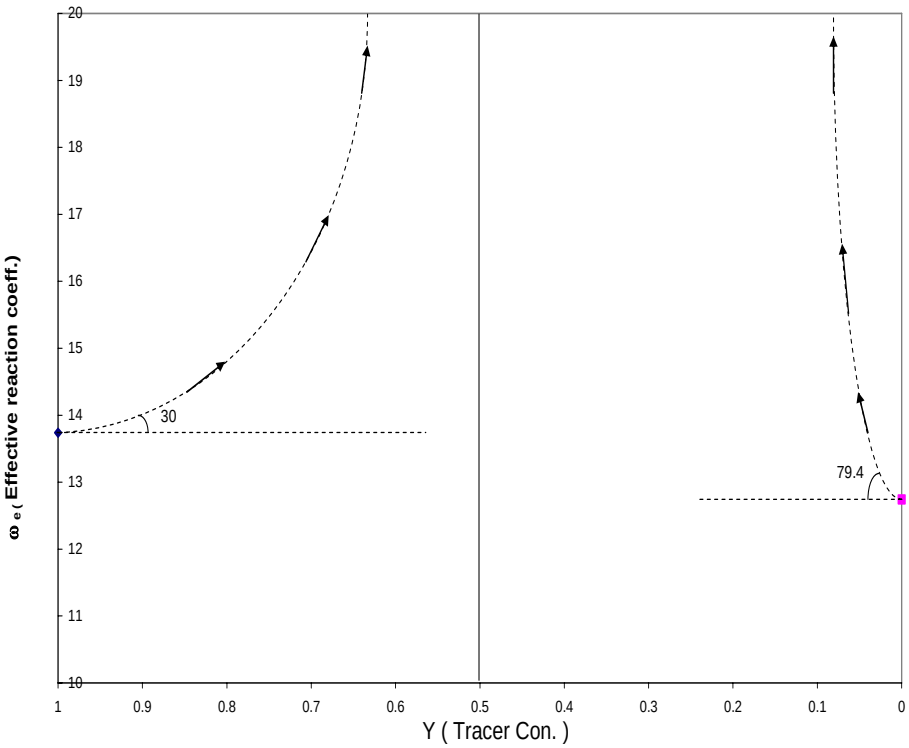

Figure 6.4: Trends in reaction coefficient in vicinity of the trailing and leading edges

6.4.2 Effective Fluid Flow Velocity and Longitudinal Macrodispersivity

At the trailing and leading edges of the reaction wave, equation (6.56) reduces to

$$\begin{aligned} &Trailing\ \ edge : v_e = v \\ &Leading\ \ edge : v_e = v - \frac{2\alpha A'_{11} b\gamma}{\alpha\lambda_1\chi - (v - \phi\bar{V})} \end{aligned} \tag{6.67}$$

Thus, the medium heterogeneities have no effect on the effective fluid flow velocity as the fluid enters the reaction wave. However, the velocity is under their influence at the leading edge: equation (6.67) clearly shows that the effective reaction rate coefficient and longitudinal dispersivity leads to variations in fluid velocity. In addition, there exist two possible routes for the fluid depending on the nature of the prescribed linear relationship between the reaction coefficient (i.e., mineral surface area) and permeability, i.e., sign of b. We note that the later was not influential during the analysis of reaction rate coefficient. Figure 6.5 (bottom) shows the estimated fluid velocity changes at the leading edge of the reaction wave with the medium heterogeneity. The condition $b < 0$ clearly leads to a retardation. The effect is negligible in the homogeneous limit although it is a dominant one and becomes more pronounced with the increasing intensity of medium heterogeneity. $b > 0$ case, on the other hand, yields increasingly large values of fluid velocity with the intensity of heterogeneity. In ε=1.0E-2 neighborhood of the reaction wave centerline, the effective fluid velocity is given by equation (6.68).

$$v_e = v - \left[\frac{-A'_{11} b\gamma(C-\varepsilon)}{\bar{V} + 2\lambda_1\varepsilon\chi}\right]\left[1 - \frac{\bar{\omega}(C+\varepsilon)}{2\varepsilon\chi} + \frac{\bar{V} - \lambda_1(C-\varepsilon)\chi}{\bar{V} + 2\lambda_1\varepsilon\chi}\right] \tag{6.68}$$

Figure 6.5 (top) shows the estimated velocity in heterogeneous media for fixed C and ε. The trends are similar to those at the leading edge, although the influence of heterogeneity is significantly amplified at this location. Equation (6.57) reduces to the following expressions for the effective macrodispersion coefficient at the leading and trailing edges of the reaction

wave.

$$
\begin{aligned}
&Trailing\ \ edge : A_{11} = 0 \\
&Leading\ \ edge : A_{11} = \frac{2\upsilon A'_{11}}{(\upsilon - \phi\bar{V})\left[1 + \sqrt{1 + \left(\frac{2\lambda_1\sigma_\omega}{\bar{V}}\right)^2}\right]}
\end{aligned}
\tag{6.69}
$$

Mineral is completely consumed at the trailing edge, i.e.,$1 - \bar{\eta}$=0, consequently it appears that the effective coefficient is zero. At the center of the reaction wave, no simple analytical expression for the coefficient can be obtained. Nonetheless, the numerically estimated macrodispersion is larger than that in the absence of reaction, Figure 6 (top). Thus, the presence of a reaction mechanism enhances the tracer mixing process inside the reaction wave as the later propagates in heterogeneous porous media. Although it is significant, macrodispersion at the leading edge pales in comparison to its values at the centerline. Furthermore, there exists a damping affect of the permeability correlation length, increasing values of which cause the macrodispersion to decrease and become less than its conservative value, Figure 6.6 (bottom).

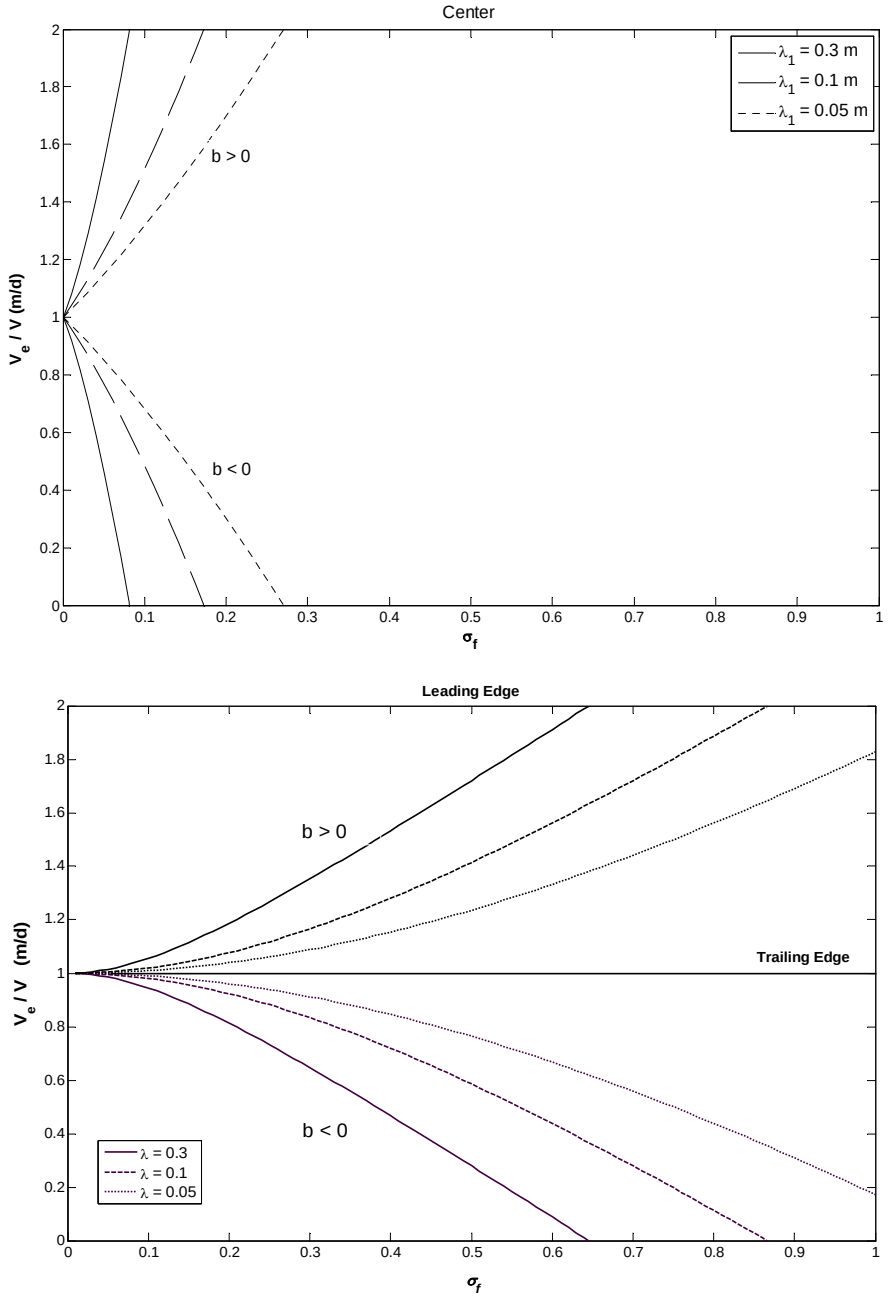

Figure 6.5: Effects of permeability variance and correlation length on effective fluid velocity, where $b = \pm 8$

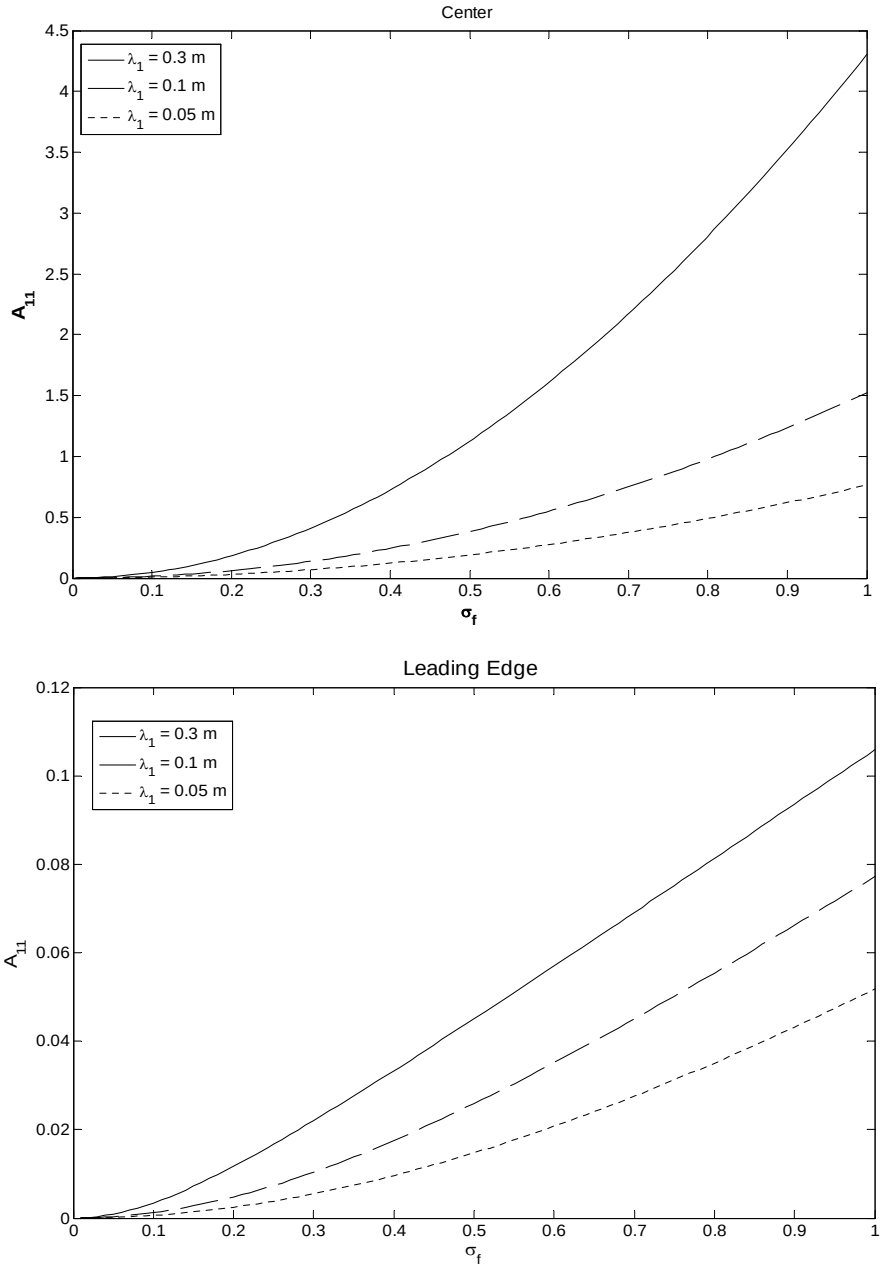

Figure 6.6: Effects of permeability variance and correlation length on the effective longitudinal macrodispersivity

6.5 Summary

In this study the heterogeneity effect of porous medium permeability on fluid flow, transport and dissolution reaction is analytically shown using a stochastic Eulerian approach. The results equations (6.55-6.59) show rich nonlinear interplay between the existing mechanisms. It is found that the conversion efficiency and medium heterogeneity intensity have a balancing role on the upscaled reaction rate coefficient and macrodispersion. The heterogeneity effect becomes more pronounced only when the conversion efficiency is low. The effect of heterogeneity on steady planar reaction wave is investigated. It is revealed that the planar reaction wave is intrinsically unstable. The later is anticipated to expand due to development of non-uniform velocity field along the reaction wave. The upscaling approach has previously been developed under an assumption of somewhat small permeability variance. Thus, an uncertainty on the adequacy of first-order approximations equations (6.62-6.65) as the governing perturbation equations still exists for large values of the variance. Further, in order to apply the results of this kind of stochastic analysis to a field situation, the hypothesis of ergodicity must be invoked. The later requires that the ensemble average is equivalent to a spatial average over some volume of the porous medium. In addition, upscaling of the governing equations was performed based on the assumption of an ideal liquid solution the fluid properties of which is not significantly influenced by the dissolution reaction.

CHAPTER VII

CONCLUSIONS

In this dissertation, first we investigated the effects of matrix pore structure and mineral content variations in gas transport and storage in tight formations like coal and shale environments. We used the proven technique widely used in water resources and chemical engineering disciplines, small perturbation theory, to quantify these effects and then to upscale (or homogenize) the transport and storage processes over the matrix body. The cross-correlations between porosity and the rest of dependent variables, appeared in the mean equations, are defined assuming Gaussian statistics for porosity characterized by gaussian correlation function. The beauty of using this method is the ability to find the explicit expressions for the perturbed quantities in the upscaled equations. Applying the method for the case where only the transport of free gas in the matrix considered in the presence of linear sorption kinetics, the macro-transport and -kinetics effects of heterogeneity recognized. Macro-transport shows the dependency to P*é*clet number and persist at the diffusive ultra-low permeability limit, and Macro-kinetics is directly related to Thiele modulus. Macro-transport and -kinetics effect leads to trapping of the gas in the matrix due to presence of heterogeneity during the gas release processes and to an adsorption threshold during the gas uptake by the matrix. Theses effects are proportional to initially adsorbed gas amount, i.e., Loading effect, and becoming more pronounced by increasing the variance of porosity introducing higher level of heterogeneity. In conclusion, upscaled deterministic governing equation is derived that describes the gas matrix system behavior and includes the effects of matrix heterogeneity. We found that equilibrium sorption conditions are not satisfied for low to ultra-low permeability samples like coal and shale and nature of transport in theses formations are mainly diffusive.

The assumption of having only free gas transport was a good approach to perform a fundamental studies, however, there are a vast literature exist on transport of adsorbed

gas. Several experiments by different researchers have been performed using different gases to investigate the magnitude of gas transport mechanism in micro-porous materials such as carbon and coal. They showed that there must be an additional transport of adsorbed phase beside free gas transport. In several experiments it has been found that although a slow mechanism of transport surface diffusion is quantified as dominant one, in some cases with significantly larger contribution than viscose flow. We incorporated the sorption non-linearity and adsorbed phase transport, surface diffusion, into the formulations and applied the same upscaling approach to investigate the effects of heterogeneity in the presence of new mechanisms. It is found that the nonlinearity participates into both macro-transport and -kinetics, promoting the surface diffusion effects. Whereas, surface diffusion increases the ultimate gas recovery through macro-transport effect and decreases the time needed to reach the ultimate recovery significantly through macro-kinetics. As the consequence of these effects, it is shown that the gas-matrix system never reaches the equilibrium adsorption limit due to nonlinear gas dynamics. Therefore, one needs to be more cautious using Langmuir isotherms to investigate the gas sorption capacity of the coal and shale matrices.

Next gas transport and storage in coalbed methane environment is investigated, where multi-continuum approach is used, to release the matrix averaging and multi-component transport limitations presented in conventional methods. It is numerically observed that the stronger affinity of CO_2 to the coal material initiates a mechanism of displacement of originally in place CH_4 when CO_2 is introduced to the coalbed environment. Furthermore, it is found that the small scale lateral molecular interaction between CO_2 and CH_4 molecules, α, plays a significant role enhancing methane production. It is cleared that CO_2 injection is beneficial for methane recovery at every stage of methane production due to positive counter diffusion and competitive adsorption effects.

In last chapter, the application of the small perturbation theory to quantify the effects of heterogeneity, introduced by random permeability field, is investigated in an isothermal advection-reaction problem, e.g., acidizing, where a one-step nonlinear dissolution reaction takes place between injected tracer and a stationary mineral residing in the pore space. The upscaling of the governing equations performed assuming an ideal liquid solution where it's

density remains the same, even though we have mineral dissolution. As a result upscaled governing equations obtained with explicit macro-scale expressions for the coefficients of reaction, fluid flow and tracer macro-dispersion. The effects of heterogeneity on steady planar reaction wave are investigated and it is revealed that the reaction wave is intrinsically unstable. This is anticipated to expand due to development of non-uniform velocity field along the reaction wave.

Nomenclature

B_0=Absolute permeability[cm^2]

C = free gas concentration [mol/cc pore]

C_μ = adsorbed gas concentration [mol/cc solid]

$C_{\mu s}$ = Maximum adsorbed gas concentration [mol/cc solid]

D = molecular diffusion coefficient [cm^2/s]

$\mathcal{D}$ = apparent diffusion coefficient [cm^2/s]

D_s=Surface diffusion coefficient [cm^2/s]

E=adsorbate adsorbent interaction energy[J/mol]

g=average free gas concentration [mol/cc]

K = partition (distribution) coefficient [fraction]

k_f = gas adsorption rate coefficient [1/s]

k_r = gas desorption rate coefficient [1/s]

$k_{r\infty}$ = gas desorption rate constant at zero energy level [1/s]

R=universal gas constant[$JK^{-1}mol^{-1}$]

r=pore half width [cm]

t = time coordinate[s]

T=temperature[K]

x = space coordinate [cm]

z=Gas compressibility factor Greek Letters

α = effective drift velocity [m/s]

ϕ = porosity [fraction]

Φ = solid-to-bulk volume ratio [fraction]

σ_f^2 = variance of porosity fluctuations

μ=gas viscosity[Kg/cm.s]

λ=porosity correlation length [cm]

ν=vibration frequency factor [1/s]

Subscripts

m= matrix

f= fracture

References

1. Ambrose, R.J., Hartman R. C., Campos, M. D., Akkutlu, I. Y., Sondergeld, C. H.:New Pore-scale Considerations for Shale Gas in Place Calculations. SPE 131772. 2010.

2. Alvarado, V., Scriven, L.E. and Davis, H.T.: Stochastic-Perturbation Analysis of a One-Dimensional Dispersion-Reaction Equation: Effects of Spatially-Varying Reaction Rates. *Transport in Porous Media* 32:139-161. 1998.

3. Ash, R., Barrer, R.M. Pope, F.R.S. and C.G.: Flow of adsorbable gases and vapours in a microporous medium Proc. Roy. Soc, A271. 1963.

4. Aylmore, L.A.G. and Barrer, R.M.: Surface and volume flow of single gases and of binary gas mixtures in a microporous carbon membrane, Proc. Roy. Soc. A290 (1966), p. 477

5. Bhatia SK.: Modeling the pore structure of coal. AIChE J. 1987;33:17071718.

6. Barenblatt, G.I., Zheltov, I.P., and Kochina, I.N.: Basic Concepts in the Theory of Seepage of Homogeneous Liquids in Fissured Rocks. J. Appl. Math., 24, 1286-1303. 1960.

7. Bond R.L, Holland R, Smith G.W, Thurlow G.G.: Coal Extracts as Promoters of Dropwise Condensation of Steam: Nature 1956; Vol.178; 4530 p.431-431

8. Brusseau, M.L., Jessup, R.E. and Rao, P.S.C.: Nonequilibrium Sorption of Organic Chemicals: Elucidation of Rate Limiting Processes. *Environ.Sci.Tech.*, 25,134-142. 1991.

9. Bustin R.M., Bustin A.M.M., Cui X., Ross D.J.K., Murthy Pathi V.S.,Impact of Shale Properties on Pore Structure and Storage Characteristics, SPE 119892-MS, 2008.

10. Bustin R.M.: Gas shale tapped for big play. American Association of Petroleum Geologists, Explorer, February 2005, available online at http://www.aapg.org/explorer/divisions/2005/02emd.cfm.

11. Carman, P.C. and Raal, F.A.: Diffusion and flow of gases and vapours through micropores III. Surface diffusion coefficients and activation energies Proc. Roy. Soc. London, A209 (1951) 38.

12. Clarkson C.R. and Bustin R.M.: The Effect of Pore Structure and Gas Pressure upon the Transport Properties of coal: a Laboratory and Modeling Study", Fuel 78, 1333-1344. 1999.

13. Closmann P.J.: An Aquifer Model for Fissured Reservoirs," SPE 4434, Soc. of Pet. Eng., Dallas, Texas. 1975.

14. Crosdale, P.J., Basil B.B. and Valix M.: Coalbed Methane Sorption Related to Coal Composition. Int. Journal of Coal Geology, 38, 3-26. 1998.

15. Do, D.D. and Wang, K.: A New Model for the Description of Adsorption Kinetics in Heterogeneous Activated Carbon. *Carbon* 36:10, 1539-1554. 1998.

16. Do, D.D.: Adsorption analysis: Equilibria and kinetics, Imperial college press. 1998.

17. Dubinin, M.M.:*Chemistry and Physics of Carbon.* Marcel Dekker, New York.1966.

18. Durlofsky, L.J., Jones, R.C. and Milliken, W.J.: A Nonuniform Coarsening Approach for the Scale-up of displacement Processes in Heterogeneous Porous Media; Adv. Water Resources Vol. 20:5-6 pp. 335-347, 1997.

19. Ebrhard, J.: Upscaling For Stationary Transport In Hetereogeneous Porous Media. MULTISCALE MODEL. SIMUL. Vol. 3, No. 4, pp. 957976

20. Ertekin, T., King, R.G., Schwerer, C.F.: Dynamic Gas Slippage: A Unique Dual-Mechanism Approach to the Flow of Gas in Tight Formations. SPE Formation Evaluation, February 1986.

21. Fan, Y.,Wang, Y., and Bryant, R.S., A Comprehensive Model of Matrix Acidization; Paper presented at the SPE European Formation Damage Conference held in The Hague, The Netherlands, 1997.

22. Farooq, S. Ruthven, D.M.: Numerical simulation of a kinetically controlled pressure swing adsorption bulk separation process based on a diffusion model Chem. Eng. Sci, 46 (1991) 2213

23. Fathi, E., and Akkutlu, I.Y.: Matrix heterogeneity effects on gas transport and adsorption in coalbedand shale gas reservoirs. Journal of Transport in Porous Media (2009) 80:281-3044.

24. Fathi, E., Akkutlu I.Y. and Cunha L.B., Effects of Porosity and Material Fluctuations on Gas Transport and Sorption Kinetics in Coalbeds; CIPC Paper 2007-179 presented at the Canadian Petroleum Society's 58th Annual Tech. Meeting in Calgary, Alberta, Canada, June 12-14, 2007.

25. Forster, D.: Hydrodynamics Fluctuations, Broken Symmetry and Correlation Functions. Benjamin-Cummings, Reading, MA (1977).

26. Fogler, H.S., Lund, K., and McCune, C.C., Predicting the Flow and Reaction of HCL/HF Acid Mixtures in Porous Sandstone Cores; SPEJ, pp. 248-260, 1976.

27. Gan, H. Nandi, S.P., Walker P.L., Nature of porosity in American Coals: (1972) Fuel, Vol.51, p.272-277.

28. Gelhar, L.W. 1993. *Stochastic Subsurface Hydrology.* Prentice Hall, Englewood Cliffs.

29. Gelhar, L.W., and Axness, C.L., Three-dimensional Stochastic Analysis of Macrodispersion in Aquifers; Water Resour. Res., Vol. 19, No. 1, pp. 161-180, 1983.

30. Gilliland, E.R. Baddour, R.F. and Russell, J.L.: Rates of Flow Through Microporous Solids, AIChE Journal, 4 (1958) 90.

31. Gwo J., O'Brien R., and Jardin P.1998. Mass Transfer in Structured Porous Media: Embedding Meso-scale Structure and Microscale Hydrodynamics in a Two-region Model" Journal of hydrology, 208, 204-222.

32. Harris, L.A., Yust, C.S. (1976). Fuel, 55, 233-236.

33. Hewitt J.L., " Geological Overview, Coal, and Coalbed Methane Resources of the Warrior Basin-Alabama and Mississippi," American Association of Petroleum Geologists Studies in Geology 17 (984)73-104.

34. Hinch, E.J., and Bhatt, B.S., Stability of an Acid Moving Through Porous Rock; J. Fluid Mech., Vol. 212, pp. 279-288, 1990.

35. Hu, B.X., Deng, F. and Cushman, J.H. 1995. Non-local Reactive Transport with Physical and Chemical Heterogeneity: Linear Non-equilibrium Sorption with Random K_d. *Water Resources Research*, 31:9, 2239-2252.

36. Jagiello, J., Bandosz, T.J., Putyera, K. and Schwarz, J.A. 1995. Micropore Structure of Template-derived Carbons Studied using Adsorption of Gases with Different molecular Diameters. *J. Chem. Soc., Faraday Trans.*, 91, 2929-2933.

37. Jenkins, C.D. and Boyer C.M.II 2008. Coalbed- and Shale-gas Reservoirs; *Journal of Petroleum Tech.*, 92-99.

38. Kang, S. M. , Fathi, E. Akkutlu, I. Y. and Sigal, R. F.: CO2 Storage Capacity of Organic-richShales. SPEJ a special issue on CO2 sequestration (2010)

39. Karacan, O.C. 2003. An Effective Method for Resolving Spatial Distribution of Adsorption Kinetics in Heterogeneous Porous Media: Applied for Carbon Dioxide Sequestration in Coal; *Chemical Engineering Science, 58, 4681-4693.*

40. King, G.R. 1990. Material Balance Techniques for Coal Seam and Devonian Shale. *SPE 20730.*

41. Koss, V.A. Wickens ,D. Cucka, P. La Cava, A.I. Proc Carbon 86 (4 internationale Kohlensttofftagung), Deutsche Keramische Gesellschaft, Baden-Baden Germany, 1986, p. 388.

42. Lamberson M.N., Bustin R.M., Coalbed methane characteristics of Gates formation coals, Northeastern British colombia: Effect of Maceral Composition 1993.

43. Larsen, J.W. and P. Wernett, Pore Structure of Illinois No. 6 Coal,Energy Fuels,2, 719720 (1988).

44. L'Heureux, I. 2004. Stochastic Reaction-Diffusion Phenomena in Porous Media with Nonlinear Kinetics: Effects of Quenched Porosity Fluctuations. *Physical Review Letters*, 93:18, 180602.

45. Lu M. and Connell L.D. 2007. A Dual Porosity Model for Gas Reservoir Flow Incorporating Adsorption Behaviour- Part 1. Theoretical Development and Asymptotic Analyses," Transport in Porous Media, 68, 153-173.

46. Loucks, R.G., Reed, R.M., Ruppel, S.C., and Jarvie, D.M. 2009. Morphology, Genesis, and Distribution of Nanometer-Scale Pores in Siliceous Mudstones of the Mississippian Barnett Shale. Journal of Sedimentary Research, v. 79, pp. 848-861.

47. McCabe, L.W., Smith, J.C., and Harriott, P.: Unit Operations of Chemical Engineering. Chemical Engineering Series. McCraw-Hill Inc., (1993).

48. Miralles-Wilhelm, F., Gelhar, L.W., and Kapoor, V., Stochastic Analysis of Oxygen-limited Biodegradation in Three-dimensionally Heterogeneous Aquifers; Water Resour. Res., Vol. 33, pp. 1251-1263, 1997.

49. Nuttall, B.C. 2005. Analysis of Devonian Black Shales in Kentucky for Potential Carbon Dioxide Sequestration and Enhanced Natural Gas Production. *Kentucky Geological Survey Report* DE-FC26-02NT41442.

50. Pruess K.P. and Wu Y.S. 1989. A new semi analytical method for numerical simulation of fluid and heat flow in fractured reservoirs. SPE 18426, Soc. of Pet. Eng., Dallas, Texas.

51. Ruckenstein, E., Vaidyanathan, A.S. and Youngquist, G.R. 1971. Sorption by Solids with Bidisperse Pore Structures. *Chemical Engineering Science*, 26, 1305-1318.

52. Sarma P., and Aziz K. 2006. New Transfer Functions for Simulation of Naturally Fractured Reservoirs with Dual Porosity Models", SPE 90231, Soc. of Pet. Eng.,

Dallas, Texas.

53. Saghafi A.; "Coal Seam Gas Reservoir Characterization", Gas from Coal Symposium, 27 March 2001, Brisbane.

54. Satriana, ed, Unconventional Natural Gas, Noyes Data Corp.: Park Ridge, N.J. (1980) 150.

55. Schlebaum W. Scharaa G. Vanriemsdijk W. H.: Influence of Nonlinear Sorption Kinetics on the Slow-Desorbing Organic Contaminant Fraction in Soil. Environ. Sci. Technol. 1999, 33, 1413-1417

56. Sevenster, P.G.: Diffusion of Gas through Coal. Fuel(1959) 38, pp. 403-415.

57. Shi, J.Q. and Durucan S. 2008. Modeling of Mixed-Gas Adsorption and Diffusion in Coalbed Reservoirs," SPE 114197 Soc. of Pet. Eng., Dallas, Texas.

58. Shi, J.Q. and Durucan S. 2005. Gas Storage and Flow in Coalbed Reservoirs: Implementation of a Bidisperse Pore Model for Gas Diffusion in a Coal Matrix. SPERE&E.

59. Siemons, N., Wolf Karl-Heinz A.A., Bruining J.:Interpretation of carbon dioxide diffusion behavior in coals. International Journal of Coal Geology 72 (2007)315-324

60. Sherwood, J.D., Stability of a Plane Reaction Front in a Porous Medium; Chem. Eng. Sci., Vol. 42, pp. 1823-1829, 1987.

61. Smith, D.M., Williams, F.L. 1984. Diffusional Effects in the Recovery of Methane from Coalbeds. *Society of Petroleum Engineers Journal*, 529-535.

62. Sondergeld, C.H., Ambrose, R.J., Rai, C.S. and Moncrieff, J. 2009. Micro-Structural Studies of Gas Shales, SPE 131771-PP, SPE Unconventional Gas Conference, Pittsburg, PA 23-25 February 2010.

63. Srinivasan R. Auvil S.R. Schork J.M.:Mass transfer in carbon molecular sieves- an interpretation of langmuir kinetics. The chemical Eng. Journal 57 (1995) 137-144.

64. Thimons, E. P., Kissell, F. N.:Diffusion of Methane through Coal. Fuel (1973) 52,pp.274-280.

65. Tiselius, A. (1935) Sorption und Diffusion von Ammoniak in Analcim. Z. Phys. Chem. A174, 401.

66. Tiselius, A. (1934) Die Diffusion von Wasser in einem Zeolith-Kristall. Ein Beitrag zur Frage der Beweglichkeit adsorbierter Moleku le. Z. Phys. Chem. A169, 425.

67. Wang, F. P., Reed, R. M. 2009. Pore Networks and Fluid Flow in Gas Shales. SPE-124253, paper presented at the Annual Technical Conference and Exhibition, SPE, New Orleans, LA, October 4-7.

68. Warren J.E., and Root P.J. 1963. The Behaviour of Naturally Fractured Reservoirs. SPEJ, 3(11), 245- 255.

69. Walker, P.L. and O.P. Mahajan, Pore Structure in Coals,Energy Fuels,7, 559560 (1993).

70. Weida S.D., Lambert S.W. and Boyer, C.M.II 2005. Challenging the Traditional Coalbed Methane Exploration and Evaluation. *SPE 98069*.

71. Welty, C., and Gelhar, L.W., Stochastic Analysis of the Effects of Fluid Density and Viscosity Variability on Macrodispersion in Heterogeneous Porous Media; Water Resour. Res., Vol. 27, pp. 2061-2075, 1991.

72. White C.M., Smith D.H., Jones K.L., Goodman A.L., Jikich S.A. LaCount R.B., DuBose S.B., Ozdemir E., Morsi B.I., Schroeder K.T., Sequestration of Carbon Dioxide in Coal with Enhanced Coalbed Methane Recovery-A Review. Energy Fuels, 2005, 19 (3), pp 659724.

73. Yang R.T., Chen Y.D. and Yeh Y.T. 1991. Prediction of Cross-Term Coefficients in Binary Diffusion: Diffusion in Zeolite. Chemical Engineering Science, 46:12, 3089-3099.

74. Yang R.T. 1997. Gas Separation by Adsorption Processes. Imperial College Press, London.

75. Yi, J., Akkutlu, I.Y., and Deutsch C.V.: Gas Transport in Bidisperse Coal Particles: Investigation for an Effective Diffusion Coefficient in Coalbeds. Journal of Canadian Petroleum Technology, Volume 47 No 10, 20-26, October 2008.

Appendices

Appendix A- Convolution Integrals

Table 1.

$$P_{ks} = \sum_{m=1,2} \int \frac{1}{2\pi} G^{-1}_{k-Q\,s} \overline{\xi_{Qm} \tilde{\Phi}_{-Q}} \left[i(k-Q) \right]^m dQ$$

$$Q_{ks} = \sum_{m,n=1,2} \int \frac{1}{2\pi} G^{-1}_{k-Q\,s} \overline{\xi_{Qm} \xi_{-Qn}} \left[i(k-Q) \right]^m (ik)^n dQ$$

$$S_{ks} = \sum_{m=1,2} \int \frac{1}{2\pi} G^{-1}_{k-Q\,s} \beta \overline{\xi_{Qm} \tilde{\alpha'}_{-Q}} \left[i(k-Q) \right]^m (ik) dQ$$

$$T_{ks} = \sum_{m=1,2} \int \frac{1}{2\pi} L_{k-Q\,s} \overline{\xi_{Qm} \tilde{K}_{-Q}} \left[i(k-Q) \right]^m dQ$$

$$U_{ks} = \int \frac{1}{2\pi} G^{-1}_{k-Q\,s} \beta \overline{\tilde{\alpha}'_Q \tilde{\Phi}_{-Q}} \left[i(k-Q) \right] dQ$$

$$V_{ks} = \sum_{m=1,2} \int \frac{1}{2\pi} G^{-1}_{k-Q\,s} \beta \overline{\xi_{Qm} \tilde{\alpha'}_{-Q}} \left[i(k-Q) \right] (ik)^m dQ$$

$$W_{ks} = \int \frac{1}{2\pi} G^{-1}_{k-Q\,s} \beta^2 \overline{\tilde{\alpha}'_Q \tilde{\alpha}'_Q} \left[i(k-Q) \right] (ik) dQ$$

$$Y_{ks} = \int \frac{1}{2\pi} L_{k-Q\,s} \overline{\tilde{\alpha}'_Q \tilde{K}_{-Q}} \left[i(k-Q) \right] dQ$$

$$Z_{ks} = \int \frac{1}{2\pi} \breve{G}^{-1}_{k-Q\,t=0} \overline{\tilde{\Phi}_Q \tilde{\Phi}_{-Q}} dQ$$

$$M_{ks} = \sum_{m=1,2} \int \frac{1}{2\pi} \breve{G}^{-1}_{k-Q\,t=0} \overline{\tilde{\Phi}_Q \xi_{Qm}} (ik)^m dQ$$

$$N_{ks} = \int \frac{1}{2\pi} \breve{G}^{-1}_{k-Q\,t=0} \beta \overline{\tilde{\alpha'}_Q \tilde{\Phi}_{-Q}} (ik) dQ$$

$$O_{ks} = \int \frac{1}{2\pi} \breve{L}_{k-Q\,t=0} \overline{\tilde{K}_Q \tilde{\Phi}_{-Q}} dQ$$

Table 2.

$$I_{ks} = \int \frac{1}{2\pi} G^{-1}_{k-Q\,s} \overline{\tilde{K}_Q \tilde{\Phi}_{-Q}} dQ$$

$$E_{ks} = \int \frac{1}{2\pi} G^{-1}_{k-Q\,s} \overline{\tilde{K}_Q \tilde{\alpha}_{-Q}}\ ik dQ$$

$$F_{ks} = \int \frac{1}{2\pi} G^{-1}_{k-Q\,s} \overline{\tilde{K}_Q \tilde{D}_{-Q}} (ik)^2 dQ$$

$$J_{ks} = \int \frac{1}{2\pi} L_{k-Q\,s} \overline{\tilde{K}_Q \tilde{K}_{-Q}}\, dQ$$

Appendix B- Auto and Cross Correlations

Table 3.

$$\overline{\tilde{\Phi}_{-Q}\tilde{\alpha}_{Q}} = i\left(D' + \bar{D}/\bar{\phi}\right)\sigma_{\phi}^{2}Q\sqrt{2\pi}\lambda\exp\left(-Q^{2}\lambda^{2}/2\right)$$

$$\overline{\tilde{\Phi}_{-Q}\tilde{D}_{Q}} = D'\sigma_{\phi}^{2}\sqrt{2\pi}\lambda\exp\left(-Q^{2}\lambda^{2}/2\right)$$

$$\overline{\tilde{\alpha}_{Q}\tilde{\alpha}_{-Q}} = \left(D' + \bar{D}/\bar{\phi}\right)^{2}\sigma_{\phi}^{2}Q^{2}\sqrt{2\pi}\lambda\exp\left(-Q^{2}\lambda^{2}/2\right)$$

$$\overline{\tilde{D}_{-Q}\tilde{\alpha}_{Q}} = \overline{\tilde{\alpha}_{Q}\tilde{D}_{-Q}} = iD'\left(D' + \bar{D}/\bar{\phi}\right)\sigma_{\phi}^{2}Q\sqrt{2\pi}\lambda\exp\left(-Q^{2}\lambda^{2}/2\right)$$

$$\overline{\tilde{D}_{-Q}\tilde{D}_{Q}} = D'^{2}\sigma_{\phi}^{2}\sqrt{2\pi}\lambda\exp\left(-Q^{2}\lambda^{2}/2\right)$$

$$\overline{\tilde{\Phi}_{-Q}\tilde{\alpha}'_{Q}} = i\left(C' + \bar{C}/\bar{\phi}\right)\sigma_{\phi}^{2}Q\sqrt{2\pi}\lambda\exp\left(-Q^{2}\lambda^{2}/2\right)$$

$$\overline{\tilde{\Phi}_{-Q}\tilde{\Phi}_{Q}} = \sigma_{\phi}^{2}\sqrt{2\pi}\lambda\exp\left(-Q^{2}\lambda^{2}/2\right)$$

$$\overline{\tilde{\Phi}_{-Q}\tilde{K}_{Q}} = K'\sigma_{\phi}^{2}\sqrt{2\pi}\lambda\exp\left(-Q^{2}\lambda^{2}/2\right)$$

$$\overline{\tilde{K}_{-Q}\tilde{\alpha}'_{Q}} = iK'\left(C' + \bar{C}/\bar{\phi}\right)\sigma_{\phi}^{2}Q\sqrt{2\pi}\lambda\exp\left(-Q^{2}\lambda^{2}/2\right)$$

$$\overline{\tilde{\alpha}'_{Q}\tilde{\alpha}'_{-Q}} = \left(C' + \bar{C}/\bar{\phi}\right)^{2}\sigma_{\phi}^{2}Q^{2}\sqrt{2\pi}\lambda\exp\left(-Q^{2}\lambda^{2}/2\right)$$

$$\overline{\tilde{\alpha}_{Q}\tilde{\alpha}'_{-Q}} = \left(C' + \bar{C}/\bar{\phi}\right)\left(D' + \bar{D}/\bar{\phi}\right)\sigma_{\phi}^{2}Q^{2}\sqrt{2\pi}\lambda\exp\left(-Q^{2}\lambda^{2}/2\right)$$

$$\overline{\tilde{D}_{Q}\tilde{\alpha}'_{-Q}} = iD'\left(C' + \bar{C}/\bar{\phi}\right)\sigma_{\phi}^{2}Q\sqrt{2\pi}\lambda\exp\left(-Q^{2}\lambda^{2}/2\right)$$

$$\overline{\tilde{K}_{-Q}\tilde{\alpha}_{Q}} = iK'\left(D' + \bar{D}/\bar{\phi}\right)\sigma_{\phi}^{2}Q\sqrt{2\pi}\lambda\exp\left(-Q^{2}\lambda^{2}/2\right)$$

$$\overline{\tilde{K}_{-Q}\tilde{D}_{Q}} = K'D'\sigma_{\phi}^{2}\sqrt{2\pi}\lambda\exp\left(-Q^{2}\lambda^{2}/2\right)$$

Appendix C- Upscaling approach

Space-Fourier and time-Laplace transform of the mean equations (4.7-4.8) are taken. This process gives the following algebraic equations for the mean free gas and the adsorbed phase in the Fourier–Laplace domain:

$$(s\ +\ k^2\bar{D})\,\bar{C}_{ks} - \bar{C}_{k,t=0} + (s\,\bar{\Phi} + k^2\bar{\Phi}\bar{D}_s)\,(\bar{C}_\mu)_{ks} - \bar{\Phi}\,(\bar{C}_\mu)_{k,t=0} = \bar{R}_{ks} \tag{7.1}$$

$$(\bar{C}_\mu)_{ks} = \frac{(\bar{C}_\mu)_{k,t=0} + k_r\left[\bar{K}\bar{C}(C_{\mu s}) - \bar{C}_\mu + (C_{\mu s} - \bar{C}_\mu)\overline{\tilde{K}\tilde{C}} - \bar{C}\overline{\tilde{K}\tilde{C}_\mu} - \bar{K}\overline{\tilde{C}_\mu\tilde{C}}\right]_{ks}}{s\ +\ k_r} \tag{7.2}$$

where k is the wave number, s the Laplace transform variable, $\bar{C}_{k,t=0}$ and $(\bar{C}_\mu)_{k,t=0}$ are the Fourier transform of the initial amounts of free and adsorbed gas respectively. Substituting equation (7.2) into the equation (7.1) leads to the formal solution of the free gas mass in Fourier–Laplace domain as follow:

$$\bar{C}_{ks} = \hat{G}_{ks}^{-1}\bar{R}_{ks} + \hat{G}_{ks}^{-1}\mathrm{X_{ks}} \tag{7.3}$$

where $\hat{G}_{ks}$ and $\mathrm{X_{ks}}$ are defined as

$$\hat{G}_{ks} = \left[s + k^2D + \frac{\bar{\Phi}k_r\bar{K}(s + k^2\bar{D}_s)C_{\mu s}}{s + k_r}\right]_{ks} \tag{7.4}$$

$$\begin{aligned}\mathrm{X_{ks}} =& \bar{C}_{k,t=0} + \left(\bar{\Phi} - \frac{\bar{\Phi}(s + k^2\bar{D}_s)}{s + k_r}\right)\bar{C}_{\mu(k,t=0)} \\ &- \frac{\bar{\Phi}k_r(s + k^2\bar{D}_s)}{s + k_r}\left[\overline{\tilde{K}\tilde{C}}(C_{\mu s} - C_\mu) - \bar{K}\bar{C}\bar{C}_\mu - \bar{K}\overline{\tilde{C}_\mu\tilde{C}} - \bar{C}\overline{\tilde{K}\tilde{C}_\mu}\right]_{ks}\end{aligned} \tag{7.5}$$

In order to find the equivalent expression for free gas fluctuation $\tilde{C}$ in Fourier–Laplace domain, we use the mean-field approximation for the terms $\beta\bar{C}\partial^2\tilde{C}/\partial x^2$ and $\beta\tilde{C}\partial^2\bar{C}/\partial x^2$. Assuming the average gas amount is replaced by its value averaged over a large space domain L and time interval τ: $\bar{\bar{C}} = \int_0^\tau\int_0^L C(x,t)dxdt/L\tau \equiv g$ and $\partial\bar{\bar{C}}/\partial\bar{\phi} = g'$. Equivalently, we take $\bar{C}_{ks} = g$ in Fourier–Laplace domain. In homogeneous porous media, $\bar{\alpha_1}$, $\bar{\alpha_2}$ and $\bar{\alpha'}$ are defined as (L'Heureux, 2004)

$$\begin{aligned}\bar{\alpha_1} &\cong \overline{\tilde{D}\frac{\partial\tilde{\phi}}{\partial x}} - \left(\frac{\bar{D}}{\bar{\phi}}\right)\overline{\tilde{\phi}\frac{\partial\tilde{\phi}}{\partial x}} \\ \bar{\alpha_2} &\cong \overline{\Phi\tilde{D}_s\frac{\partial\tilde{\phi}}{\partial x}} - \left(\frac{\bar{D}_s}{\bar{\phi}}\right)\overline{(1-\tilde{\phi})\frac{\partial\tilde{\phi}}{\partial x}} \\ \bar{\alpha'} &\cong \overline{\tilde{C}\frac{\partial\tilde{\phi}}{\partial x}} - \left(\frac{\bar{C}}{\bar{\phi}}\right)\overline{\tilde{\phi}\frac{\partial\tilde{\phi}}{\partial x}}\end{aligned}$$

These are already second order in porosity fluctuations; therefore, $\bar{\alpha_1}\partial\tilde{C}/\partial x \cong 0$, $\bar{\alpha_2}\partial\tilde{C}_\mu/\partial x \cong 0$ and $\bar{\alpha'}\partial\tilde{C}/\partial x \cong 0$ are taken. Next, we apply Fourier–Laplace transform to the perturbation equations (4.10-4.11):

$$\left(s + k^2\bar{D} + 2\beta g k^2\right)\tilde{C}_{ks} + \left(\bar{\Phi}s + \bar{\Phi}D_s k^2\right)\tilde{C}_{\mu ks} = \tilde{R}_{ks} \tag{7.6}$$

$$\tilde{C}_{\mu,ks} = \frac{k_r\bar{K}\left(C_{\mu s} - \bar{C}_{\mu ks}\right)\tilde{C}_{ks}}{\left(s + k_r + k_r\bar{K}\bar{C}_{ks}\right)} + \frac{k_r M_{ks}}{\left(s + k_r + k_r\bar{K}\bar{C}_{ks}\right)} \tag{7.7}$$

Substituting equation (7.7) into equation (7.6) leads to the formal solution for $\tilde{C}_{ks}$ in Fourier-Laplace domain as

$$\tilde{C}_{ks} = G_{ks}^{-1}\tilde{R}_{ks} - L_{ks}M_{ks} \tag{7.8}$$

where $G_{ks},$ and L_{ks} is defined as follow

$$G_{ks} = \left[s + (\bar{D} + 2\beta g)k^2 + \frac{\bar{\Phi}k_r\bar{K}(s + \bar{D}_s k^2)(C_{\mu s} - \bar{C}_\mu)_{ks}}{s + k_r + k_r\bar{K}\bar{C}_{ks}}\right] \tag{7.9}$$

$$L_{ks} = \left[\frac{\bar{\Phi}k_r(s + \bar{D}_s k^2)}{s + k_r + k_r\bar{K}\bar{C}_{ks}}\right] G_{ks}^{-1} \tag{7.10}$$

In the space–time domain, the fluctuating free gas mass is given by the convolution integral

$$\begin{aligned}\tilde{C}(x,t) &= \int_0^t \int G^{-1}(x - x', t - t')\,\tilde{R}(x', t')\,dx'dt' - \int_0^t \int L(x - x', t - t')\,M(x', t')\,dx'dt' \\ &\equiv G^{-1}_{x-x',t-t'} * \tilde{R}_{x',t'} - L_{x-x',t-t'} * M_{x',t'}\end{aligned} \tag{7.11}$$

Next we substitute equation (7.8) into (7.7). Now $\tilde{C}_\mu$ can be expressed in space–time domain as follows

$$\begin{aligned}\tilde{C}_\mu(x,t) &= \int_0^t \int \breve{G}^{-1}(x - x', t - t')\,\tilde{R}(x', t')\,dx'dt' - \int_0^t \int \breve{L}(x - x', t - t')\,M(x', t')\,dx'dt' \\ &\equiv \breve{G}^{-1}_{x-x',t-t'} * \tilde{R}_{x',t'} - \breve{L}_{x-x',t-t'} * M_{x',t'}\end{aligned} \tag{7.12}$$

Here we introduced

$$\breve{G}_{ks}^{-1} = \left[\frac{\bar{K}k_r(C_{\mu s} - \bar{C}_\mu)_{ks}}{s + k_r + k_r\bar{K}\bar{C}_{ks}}\right] G_{ks}^{-1} \quad \text{and} \quad \breve{L}_{ks} = \left(\frac{-\bar{K}k_r(C_{\mu s} - \bar{C}_\mu)_{ks}}{s + k_r + k_r\bar{K}\bar{C}_{ks}} L_{ks} - \frac{k_r}{s + k_r + k_r\bar{K}\bar{C}_{ks}}\right)$$

Having an analytical expressions for $\tilde{C}$ and $\tilde{C}_\mu$ the cross-correlation terms in mean equations (4.7-4.8) are obtained solving a series of convolution integrals. The summation term in equation (4.7) can be obtained by multiplying the proper spatial derivative of the molar density fluctuation $\tilde{C}$ with the fluctuating transport term $\xi_m(x)$ neglecting the third order porosity fluctuation terms and taking the expectation.

$$\sum_{m=1,2} \overline{\frac{\xi_m \partial^m \tilde{C}}{\partial x^m}} = \sum_{m=1,2} \frac{\partial^m G^{-1}_{x-x',t-t'}}{\partial x^m} * \overline{\xi_m \tilde{R}_{x',t'}} - \sum_{m=1,2} \frac{\partial^m L_{x-x',t-t'}}{\partial x^m} * \overline{\xi_m M_{x',t'}} \tag{7.13}$$

The rest of the cross correlation terms in equation (4.7) are obtained similarly using the definitions of $\tilde{C}$ and $\tilde{C}_\mu$:

$$\beta \overline{\frac{\tilde{\alpha}' \partial \tilde{C}}{\partial x}} = \frac{\partial G^{-1}_{x-x',t-t'}}{\partial t} * \beta \overline{\tilde{\alpha}' \tilde{R}} - \frac{\partial L_{x-x',t-t'}}{\partial t} * \beta \overline{\tilde{\alpha}' M} \tag{7.14}$$

$$\overline{\tilde{\alpha}_2 \frac{\partial \tilde{C}_\mu}{\partial x}} = \frac{\partial \breve{G}^{-1}_{x-x',t-t'}}{\partial x} * \overline{\tilde{\alpha}_2 \tilde{R}} + \frac{\partial \breve{L}_{x-x',t-t'}}{\partial x} * \overline{\tilde{\alpha}_2 M} \tag{7.15}$$

$$\overline{\frac{\tilde{\Phi} \partial \tilde{C}_\mu}{\partial t}} = \frac{\partial \breve{G}^{-1}_{x-x',t-t'}}{\partial t} * \overline{\tilde{\Phi} \tilde{R}} + \frac{\partial \breve{L}_{x-x',t-t'}}{\partial t} * \overline{\tilde{\Phi} M} \tag{7.16}$$

$$\bar{D}_s \overline{\tilde{\Phi} \frac{\partial^2 \tilde{C}_\mu}{\partial x^2}} = \frac{\partial^2 \breve{G}^{-1}_{x-x',t-t'}}{\partial x^2} * \bar{D}_s \overline{\tilde{\Phi} \tilde{R}} + \frac{\partial^2 \breve{L}_{x-x',t-t'}}{\partial x^2} * \bar{D}_s \overline{\tilde{\Phi} M} \tag{7.17}$$

$$\bar{\Phi} \overline{\tilde{D}_s \frac{\partial^2 \tilde{C}_\mu}{\partial x^2}} = \frac{\partial^2 \breve{G}^{-1}_{x-x',t-t'}}{\partial x^2} * \bar{\Phi} \overline{\tilde{D}_s \tilde{R}} + \frac{\partial^2 \breve{L}_{x-x',t-t'}}{\partial x^2} * \bar{\Phi} \overline{\tilde{D}_s M} \tag{7.18}$$

The solution of the equations (7.13)-(7.18) are found, taking the space-Fourier and time-Laplace transformation of them and dropping the third order terms in the porosity fluctuations:

$$\begin{aligned} \left(\sum_{m=1,2} \overline{\frac{\xi_m \partial^m \tilde{C}}{\partial x^m}} \right)_{ks} =& P_{1,ks} \bar{C}_{\mu\, k,t=0} + P_{2,ks} \bar{C}_{ks} + P_{3,ks} \bar{C}_{ks} + P_{4,ks} \bar{C}_{\mu ks} + P_{5,ks} \bar{C}_{\mu ks} \\ &+ P_{6,ks} \bar{C}_{\mu ks} - P_{7,ks} \bar{C}_{ks} + P_{8,ks} \bar{C}_{ks} \bar{C}_{\mu ks} \end{aligned} \tag{7.19}$$

$$\begin{aligned} \left(\beta \overline{\frac{\tilde{\alpha}' \partial \tilde{C}}{\partial x}} \right)_{ks} =& Q_{1,ks} \bar{C}_{\mu\, k,t=0} + Q_{2,ks} \bar{C}_{ks} + Q_{3,ks} \bar{C}_{ks} + Q_{4,ks} \bar{C}_{\mu ks} + Q_{5,ks} \bar{C}_{\mu ks} \\ &+ Q_{6,ks} \bar{C}_{\mu ks} - Q_{7,ks} \bar{C}_{ks} + Q_{8,ks} \bar{C}_{ks} \bar{C}_{\mu ks} \end{aligned} \tag{7.20}$$

$$\left(\overline{\tilde{\alpha}_2\frac{\partial\tilde{C}_\mu}{\partial x}}\right)_{ks} = T_{1,ks}\bar{C}_{\mu\,k,t=0} + T_{2,ks}\bar{C}_{ks} + T_{3,ks}\bar{C}_{ks} + T_{4,ks}\bar{C}_{\mu ks} + T_{5,ks}\bar{C}_{\mu ks} + T_{6,ks}\bar{C}_{\mu ks} - T_{7,ks}\bar{C}_{ks} + T_{8,ks}\bar{C}_{ks}\bar{C}_{\mu ks} \tag{7.21}$$

$$\left(\overline{\frac{\tilde{\Phi}\partial\tilde{C}_\mu}{\partial t}}\right)_{ks} = U_{1,ks}\bar{C}_{\mu\,k,t=0} + U_{2,ks}\bar{C}_{ks} + U_{3,ks}\bar{C}_{ks} + U_{4,ks}\bar{C}_{\mu ks} + U_{5,ks}\bar{C}_{\mu ks} + U_{6,ks}\bar{C}_{\mu ks} - U_{7,ks}\bar{C}_{ks} + U_{8,ks}\bar{C}_{ks}\bar{C}_{\mu ks} \tag{7.22}$$

$$\left(\bar{D}_s\overline{\tilde{\Phi}\frac{\partial^2\tilde{C}_\mu}{\partial x^2}}\right)_{ks} = V_{1,ks}\bar{C}_{\mu\,k,t=0} + V_{2,ks}\bar{C}_{ks} + V_{3,ks}\bar{C}_{ks} + V_{4,ks}\bar{C}_{\mu ks} + V_{5,ks}\bar{C}_{\mu ks} + V_{6,ks}\bar{C}_{\mu ks} - V_{7,ks}\bar{C}_{ks} + V_{8,ks}\bar{C}_{ks}\bar{C}_{\mu ks} \tag{7.23}$$

$$\left(\bar{\Phi}\overline{\tilde{D}_s\frac{\partial^2\tilde{C}_\mu}{\partial x^2}}\right)_{ks} = W_{1,ks}\bar{C}_{\mu\,k,t=0} + W_{2,ks}\bar{C}_{ks} + W_{3,ks}\bar{C}_{ks} + W_{4,ks}\bar{C}_{\mu ks} + W_{5,ks}\bar{C}_{\mu ks} + W_{6,ks}\bar{C}_{\mu ks} - W_{7,ks}\bar{C}_{ks} + W_{8,ks}\bar{C}_{ks}\bar{C}_{\mu ks} \tag{7.24}$$

In order to evaluate these integrals, the porosity fluctuations $\tilde{\phi}$ around the mean porosity $\bar{\phi}$ assumed to be Gaussian random variable with zero mean and variance σ_ϕ^2, and the spatial correlation function defined as $\overline{\tilde{\phi}(x)\tilde{\phi}(y)} = \sigma_\phi^2 f(|x-y|)$. Then auto– and cross–covariances appearing in the integrals can be defined using Gaussian correlation function, $f(x)$ and f_Q in space-time and spectral domain respectively. For instance one can write the auto correlation of the drift velocity $\alpha_1$as follows

$$\overline{\tilde{\alpha}_{1x}\tilde{\alpha}_{1x'}} = \left(D' + \bar{D}/\bar{\phi}\right)^2 \overline{\partial_x\tilde{\phi}(x)\partial_{x'}\tilde{\phi}(x')} = -\left(D' + \bar{D}/\bar{\phi}\right)^2 \sigma_\phi^2 d^2 f(x)/dx^2 \tag{7.25}$$

in space and time domain, that is $\overline{\xi_{Q1}\xi_{-Q1}} = \overline{\tilde{\alpha}_Q\tilde{\alpha}_{-Q}} = \left(D' + \bar{D}/\bar{\phi}\right)^2 \sigma_\phi^2 Q^2 f_Q$ in Fourier space domain. Here, σ_ϕ^2 is the variance of porosity and $f_Q = \sqrt{2\pi}\lambda \exp\left(-Q^2\lambda^2/2\right)$ is the Fourier transform of the porosity correlation function $f(x) = \exp\left(-x^2/2\lambda^2\right)$. We also defined $D' = d\bar{D}/d\bar{\phi} > 0$, $D'_s = d\bar{D}_s/d\bar{\phi} > 0$ and $K' = d\bar{K}/d\bar{\phi} < 0$. Using defined auto- and cross-covariances presented in Appendix D, Table 4, equations (7.19-7.24) are obtained solving a series of convolution integrals introduced in Appendix D, Table 5. In the table, Q is dummy wave number label. Similar procedure is applied to obtain the explicit analytical solutions for the cross-correlations in Eq. 4.8. We can express the cross-correlation terms

$\overline{\tilde{K}\tilde{C}}$, $\overline{\tilde{K}\tilde{C}_\mu}$ and $\overline{\tilde{C}\tilde{C}_\mu}$ in equation (4.8) using the definitions of $\tilde{C}$ and $\tilde{C}_\mu$(Eq. 7.11-7.12) in the following form

$$\overline{\tilde{K}\tilde{C}} = G^{-1} * \overline{\tilde{K}\tilde{R}} - L * \overline{\tilde{K}M} \tag{7.26}$$

$$\overline{\tilde{K}\tilde{C}_\mu} = \breve{G}^{-1} * \overline{\tilde{K}\tilde{R}} - \breve{L} * \overline{\tilde{K}M} \tag{7.27}$$

$$\overline{\tilde{C}\tilde{C}_\mu} = \breve{G}^{-1} * G^{-1} * \overline{\tilde{R}\tilde{R}} - \breve{G}^{-1} * L * \overline{\tilde{R}M} - \breve{L} * G^{-1} * \overline{\tilde{R}M} + \breve{L} * L * \overline{MM} \tag{7.28}$$

Taking space–Fourier and time–Laplace transform of equation (7.26-7.28) leads to

$$\begin{aligned}\left(\overline{\tilde{K}\tilde{C}}\right)_{ks} =& S1_{ks}\bar{C}_{\mu\,k,t=0} + S2_{ks}\bar{C}_{ks} + S3_{ks}\bar{C}_{ks} + S4_{ks}\bar{C}_{\mu ks} + S5_{ks}\bar{C}_{\mu ks} \\ &+ S6_{ks}\bar{C}_{\mu ks} - S7_{ks}\bar{C}_{ks} + S8_{ks}\bar{C}_{ks}\bar{C}_{\mu ks}\end{aligned} \tag{7.29}$$

$$\begin{aligned}\left(\overline{\tilde{K}\tilde{C}_\mu}\right)_{ks} =& I1_{ks}\bar{C}_{\mu\,k,t=0} + I2_{ks}\bar{C}_{ks} + I3_{ks}\bar{C}_{ks} + I4_{ks}\bar{C}_{\mu ks} + I5_{ks}\bar{C}_{\mu ks} \\ &+ I6_{ks}\bar{C}_{\mu ks} - I7_{ks}\bar{C}_{ks} + I8_{ks}\bar{C}_{ks}\bar{C}_{\mu ks}\end{aligned} \tag{7.30}$$

$$\left(\overline{\tilde{C}\tilde{C}_\mu}\right)_{ks} = F1_{ks}\bar{C}_{\mu\,k,t=0}\bar{C}_{ks} \tag{7.31}$$

which, also includes a set of integral terms given in Appendix D, Table 4. . Using conventional approximations s=k=0 in Q–dependent terms of the integrands, the following solutions are obtained for the integrals defined in Tables 3 and 4 and inserted in equations (7.19-7.24) and (7.29-7.31):

$$\begin{aligned}\left(\sum_{m=1,2}\frac{\overline{\xi_m\partial^m\tilde{C}}}{\partial x^m}\right)_{ks} =& \frac{(1+\bar{K}\bar{C}_{ks})\sigma_\phi^2\dfrac{\bar{D}}{\bar{\phi}}\ \bar{C}_{\mu\,k,t=0}}{(1+\bar{K}\bar{C}_{ks})(\bar{D}+2\beta g)+\bar{\Phi}\bar{D}_s\bar{K}(C_{\mu s}-\bar{C}_{\mu ks})} \\ &- \frac{(1+\bar{K}\bar{C}_{ks})\sigma_\phi^2 D'\left(2D'+\dfrac{\bar{D}}{\bar{\phi}}\right)\ (ik)^2\bar{C}_{ks}}{(1+\bar{K}\bar{C}_{ks})(\bar{D}+2\beta g)+\bar{\Phi}\bar{D}_s\bar{K}(C_{\mu s}-\bar{C}_{\mu ks})} \\ &- \frac{(1+\bar{K}\bar{C}_{ks})\sigma_\phi^2 D'_s\bar{\Phi}\left(2D'+\dfrac{\bar{D}}{\bar{\phi}}\right)\ (ik)^2\bar{C}_{\mu ks}}{(1+\bar{K}\bar{C}_{ks})(\bar{D}+2\beta g)+\bar{\Phi}\bar{D}_s\bar{K}(C_{\mu s}-\bar{C}_{\mu ks})} \\ &+ \frac{(1+\bar{K}\bar{C}_{ks})\sigma_\phi^2\bar{D}_s\dfrac{\bar{D}}{\bar{\phi}}\ (ik)^2\bar{C}_{\mu ks}}{(1+\bar{K}\bar{C}_{ks})(\bar{D}+2\beta g)+\bar{\Phi}\bar{D}_s\bar{K}(C_{\mu s}-\bar{C}_{\mu ks})} \\ &- \frac{\sigma_\phi^2\bar{\Phi}K'\bar{D}_s\dfrac{\bar{D}}{\bar{\phi}}(C_{\mu s}-\bar{C}_{\mu ks})\ \bar{C}_{ks}}{\lambda^2\left[(1+\bar{K}\bar{C}_{ks})(\bar{D}+2\beta g)+\bar{\Phi}\bar{D}_s\bar{K}(C_{\mu s}-\bar{C}_{\mu ks})\right]}\end{aligned} \tag{7.32}$$

$$
\begin{aligned}
\left(\beta\overline{\tilde{\alpha}'\frac{\partial\tilde{C}}{\partial x}}\right)_{ks} =& \frac{(1+\bar{K}\bar{C}_{ks})\sigma_\phi^2\beta(C'+\frac{\bar{C}}{\bar{\phi}})_{ks}\ \ \bar{C}_{\mu\,k,t=0}}{(1+\bar{K}\bar{C}_{ks})(\bar{D}+2\beta g)+\bar{\Phi}\bar{D}_s\bar{K}(C_{\mu s}-\bar{C}_{\mu ks})} \\
&- \frac{(1+\bar{K}\bar{C}_{ks})\sigma_\phi^2\beta D'(C'+\frac{\bar{C}}{\bar{\phi}})_{ks}\ \ (ik)^2\bar{C}_{ks}}{(1+\bar{K}\bar{C}_{ks})(\bar{D}+2\beta g)+\bar{\Phi}\bar{D}_s\bar{K}(C_{\mu s}-\bar{C}_{\mu ks})} \\
&- \frac{(1+\bar{K}\bar{C}_{ks})\sigma_\phi^2\beta(C'+\frac{\bar{C}}{\bar{\phi}})_{ks}(\bar{\Phi}D'_s-\bar{D}_s)\ \ (ik)^2\bar{C}_{\mu ks}}{(1+\bar{K}\bar{C}_{ks})(\bar{D}+2\beta g)+\bar{\Phi}\bar{D}_s\bar{K}(C_{\mu s}-\bar{C}_{\mu ks})} \\
&- \frac{\sigma_\phi^2\bar{\Phi}K'\bar{D}_s\beta(C'+\frac{\bar{C}}{\bar{\phi}})_{ks}(C_{\mu s}-\bar{C}_{\mu ks})\ \ \bar{C}_{ks}}{\lambda^2\left[(1+\bar{K}\bar{C}_{ks})(\bar{D}+2\beta g)+\bar{\Phi}\bar{D}_s\bar{K}(C_{\mu s}-\bar{C}_{\mu ks})\right]}
\end{aligned} \tag{7.33}
$$

$$
\begin{aligned}
\left(\overline{\tilde{\alpha}_2\frac{\partial\tilde{C}_\mu}{\partial x}}\right)_{ks} =& \frac{\bar{K}\sigma_\phi^2(C_{\mu s}-\bar{C}_{\mu ks})(D'_s+\frac{\bar{D}_s}{\bar{\phi}})\ \ \bar{C}_{\mu\,k,t=0}}{(1+\bar{K}\bar{C}_{ks})(\bar{D}+2\beta g)+\bar{\Phi}\bar{D}_s\bar{K}(C_{\mu s}-\bar{C}_{\mu ks})} \\
&- \frac{\bar{K}\sigma_\phi^2(C_{\mu s}-\bar{C}_{\mu ks})D'(D'_s+\frac{\bar{D}_s}{\bar{\phi}})\ \ (ik)^2\bar{C}_{ks}}{(1+\bar{K}\bar{C}_{ks})(\bar{D}+2\beta g)+\bar{\Phi}\bar{D}_s\bar{K}(C_{\mu s}-\bar{C}_{\mu ks})} \\
&- \frac{\bar{K}\sigma_\phi^2(C_{\mu s}-\bar{C}_{\mu ks})(\bar{\Phi}D'_s-\bar{D}_s)(D'_s+\frac{\bar{D}_s}{\bar{\phi}})\ \ (ik)^2\bar{C}_{\mu ks}}{(1+\bar{K}\bar{C}_{ks})(\bar{D}+2\beta g)+\bar{\Phi}\bar{D}_s\bar{K}(C_{\mu s}-\bar{C}_{\mu ks})} \\
&- \frac{\bar{K}K'\bar{\Phi}\bar{D}_s\sigma_\phi^2(C_{\mu s}-\bar{C}_{\mu ks})^2(D'_s+\frac{\bar{D}_s}{\bar{\phi}})\ \ \bar{C}_{ks}}{\lambda^2\left[(1+\bar{K}\bar{C}_{ks})(\bar{D}+2\beta g)+\bar{\Phi}\bar{D}_s\bar{K}(C_{\mu s}-\bar{C}_{\mu ks})\right]} \\
&+ \frac{K'\sigma_\phi^2(D'_s+\frac{\bar{D}_s}{\bar{\phi}})(C_{\mu s}-\bar{C}_{\mu ks})\ \ \bar{C}_{ks}}{\lambda^2\left(1+\bar{K}\bar{C}_{ks}\right)}
\end{aligned} \tag{7.34}
$$

$$
\begin{aligned}
\left(\bar{D}_s\overline{\tilde{\Phi}\frac{\partial^2\tilde{C}_\mu}{\partial x^2}}\right)_{ks} =& -\frac{\bar{K}\sigma_\phi^2(C_{\mu s}-\bar{C}_{\mu ks})\bar{D}_s\ \ \bar{C}_{\mu\,k,t=0}}{(1+\bar{K}\bar{C}_{ks})(\bar{D}+2\beta g)+\bar{\Phi}\bar{D}_s\bar{K}(C_{\mu s}-\bar{C}_{\mu ks})} \\
&- \frac{\bar{K}\sigma_\phi^2(C_{\mu s}-\bar{C}_{\mu ks})D'\bar{D}_s\ \ (ik)^2\bar{C}_{ks}}{(1+\bar{K}\bar{C}_{ks})(\bar{D}+2\beta g)+\bar{\Phi}\bar{D}_s\bar{K}(C_{\mu s}-\bar{C}_{\mu ks})} \\
&- \frac{\bar{K}\sigma_\phi^2(C_{\mu s}-\bar{C}_{\mu ks})(\bar{\Phi}D'_s-\bar{D}_s)\bar{D}_s\ \ (ik)^2\bar{C}_{\mu ks}}{(1+\bar{K}\bar{C}_{ks})(\bar{D}+2\beta g)+\bar{\Phi}\bar{D}_s\bar{K}(C_{\mu s}-\bar{C}_{\mu ks})} \\
&- \frac{\bar{K}K'\bar{\Phi}\bar{D}_s^2\sigma_\phi^2(C_{\mu s}-\bar{C}_{\mu ks})^2\ \ \bar{C}_{ks}}{\lambda^2(1+\bar{K}\bar{C}_{ks})\left[(1+\bar{K}\bar{C}_{ks})(\bar{D}+2\beta g)+\bar{\Phi}\bar{D}_s\bar{K}(C_{\mu s}-\bar{C}_{\mu ks})\right]} \\
&+ \frac{K'\sigma_\phi^2\bar{D}_s(C_{\mu s}-\bar{C}_{\mu ks})\ \ \bar{C}_{ks}}{\lambda^2\left(1+\bar{K}\bar{C}_{ks}\right)}
\end{aligned} \tag{7.35}
$$

$$
\begin{aligned}
\left(\overline{\bar{\Phi}\tilde{D}_s\frac{\partial^2\tilde{C}_\mu}{\partial x^2}}\right)_{ks} =& -\frac{\bar{K}\sigma_\phi^2(C_{\mu s}-\bar{C}_{\mu ks})\bar{\Phi}D'_s\ \ \bar{C}_{\mu\, k,t=0}}{(1+\bar{K}\bar{C}_{ks})(\bar{D}+2\beta g)+\bar{\Phi}\bar{D}_s\bar{K}(C_{\mu s}-\bar{C}_{\mu ks})}\\
&-\frac{\bar{K}\sigma_\phi^2(C_{\mu s}-\bar{C}_{\mu ks})D'\bar{\Phi}D'_s\ \ (ik)^2\bar{C}_{ks}}{(1+\bar{K}\bar{C}_{ks})(\bar{D}+2\beta g)+\bar{\Phi}\bar{D}_s\bar{K}(C_{\mu s}-\bar{C}_{\mu ks})}\\
&-\frac{\bar{K}\sigma_\phi^2(C_{\mu s}-\bar{C}_{\mu ks})(\bar{\Phi}D'_s+\bar{D}_s)\bar{\Phi}D'_s\ \ (ik)^2\bar{C}_{\mu ks}}{(1+\bar{K}\bar{C}_{ks})(\bar{D}+2\beta g)+\bar{\Phi}\bar{D}_s\bar{K}(C_{\mu s}-\bar{C}_{\mu ks})}\\
&+\frac{\bar{K}K'\bar{\Phi}^2\bar{D}_sD'_s\sigma_\phi^2(C_{\mu s}-\bar{C}_{\mu ks})^2\ \ \bar{C}_{ks}}{\lambda^2(1+\bar{K}\bar{C}_{ks})\left[(1+\bar{K}\bar{C}_{ks})(\bar{D}+2\beta g)+\bar{\Phi}\bar{D}_s\bar{K}(C_{\mu s}-\bar{C}_{\mu ks})\right]}\\
&-\frac{\bar{\Phi}K'\sigma_\phi^2D'_s(C_{\mu s}-\bar{C}_{\mu ks})\ \ \bar{C}_{ks}}{\lambda^2\left(1+\bar{K}\bar{C}_{ks}\right)}
\end{aligned}
\tag{7.36}
$$

$$
\begin{aligned}
\left(\overline{\tilde{K}\tilde{C}}\right)_{ks} =& -\frac{K'\sigma_\phi^2\lambda^2(1+\bar{K}\bar{C}_{ks})\ \ \bar{C}_{\mu\, k,t=0}}{(1+\bar{K}\bar{C}_{ks})(\bar{D}+2\beta g)+\bar{\Phi}\bar{D}_s\bar{K}(C_{\mu s}-\bar{C}_{\mu ks})}\\
&-\frac{K'\sigma_\phi^2\lambda^2(1+\bar{K}\bar{C}_{ks})D'\ \ (ik)^2\bar{C}_{ks}}{(1+\bar{K}\bar{C}_{ks})(\bar{D}+2\beta g)+\bar{\Phi}\bar{D}_s\bar{K}(C_{\mu s}-\bar{C}_{\mu ks})}\\
&-\frac{K'\sigma_\phi^2\lambda^2(\bar{\Phi}D'_s-\bar{D}_s)(1+\bar{K}\bar{C}_{ks})\ \ (ik)^2\bar{C}_{\mu ks}}{(1+\bar{K}\bar{C}_{ks})(\bar{D}+2\beta g)+\bar{\Phi}\bar{D}_s\bar{K}(C_{\mu s}-\bar{C}_{\mu ks})}\\
&-\frac{\bar{\Phi}\bar{D}_sK'^2\sigma_\phi^2(C_{\mu s}-\bar{C}_{\mu ks})\ \ \bar{C}_{ks}}{(1+\bar{K}\bar{C}_{ks})(\bar{D}+2\beta g)+\bar{\Phi}\bar{D}_s\bar{K}(C_{\mu s}-\bar{C}_{\mu ks})}
\end{aligned}
\tag{7.37}
$$

$$
\begin{aligned}
\left(\overline{\tilde{K}\tilde{C}_\mu}\right)_{ks} =& -\frac{\bar{K}\sigma_\phi^2(C_{\mu s}-\bar{C}_{\mu ks})K'\lambda^2\ \ \bar{C}_{\mu\, k,t=0}}{(1+\bar{K}\bar{C}_{ks})(\bar{D}+2\beta g)+\bar{\Phi}\bar{D}_s\bar{K}(C_{\mu s}-\bar{C}_{\mu ks})}\\
&-\frac{\bar{K}\sigma_\phi^2(C_{\mu s}-\bar{C}_{\mu ks})D'K'\lambda^2\ \ (ik)^2\bar{C}_{ks}}{(1+\bar{K}\bar{C}_{ks})(\bar{D}+2\beta g)+\bar{\Phi}\bar{D}_s\bar{K}(C_{\mu s}-\bar{C}_{\mu ks})}\\
&-\frac{\bar{K}\sigma_\phi^2(C_{\mu s}-\bar{C}_{\mu ks})K'\lambda^2(\bar{\Phi}D'_s-\bar{D}_s)\ \ (ik)^2\bar{C}_{\mu ks}}{(1+\bar{K}\bar{C}_{ks})(\bar{D}+2\beta g)+\bar{\Phi}\bar{D}_s\bar{K}(C_{\mu s}-\bar{C}_{\mu ks})}\\
&-\frac{\bar{K}K'^2\bar{\Phi}\bar{D}_s\sigma_\phi^2(C_{\mu s}-\bar{C}_{\mu ks})^2\ \ \bar{C}_{ks}}{(1+\bar{K}\bar{C}_{ks})\left[(1+\bar{K}\bar{C}_{ks})(\bar{D}+2\beta g)+\bar{\Phi}\bar{D}_s\bar{K}(C_{\mu s}-\bar{C}_{\mu ks})\right]}
\end{aligned}
\tag{7.38}
$$

$$
\left(\overline{\tilde{C}\tilde{C}_\mu}\right)_{ks} =\frac{2\bar{K}^2\bar{\Phi}\bar{D}_s\sigma_\phi^2(C_{\mu s}-\bar{C}_{\mu ks})K'\lambda^2\ \ \bar{C}_{\mu\, k,t=0}\bar{C}_{ks}}{\left[(1+\bar{K}\bar{C}_{ks})(\bar{D}+2\beta g)+\bar{\Phi}\bar{D}_s\bar{K}(C_{\mu s}-\bar{C}_{\mu ks})\right]^2}
\tag{7.39}
$$

Taking the inverse Laplace-Fourier transform of Eq. (7.32-7.39)and substituting to the governing mean equations (4.7-4.8)after rearranging and simplifying the new governing equations can be written as follow:

$$\begin{aligned}
\frac{\partial \bar{C}}{\partial t} =& -\bar{\Phi}\frac{\partial \bar{C}_\mu}{\partial t} + \bar{D}\frac{\partial^2 \bar{C}}{\partial x^2} + \bar{\Phi}\bar{D}_s\frac{\partial^2 \bar{C}_\mu}{\partial x^2}\bar{\alpha_1}\frac{\partial \bar{C}}{\partial x} + \beta\bar{\alpha}'\frac{\partial \bar{C}}{\partial x} + \bar{\alpha_2}\frac{\partial \bar{C}_\mu}{\partial x} + \beta\bar{C}\frac{\partial^2 \bar{C}}{\partial x^2} \\
&+ \left(\frac{(1+\bar{K}\bar{C})\left[\frac{\bar{D}}{\bar{\phi}} + \beta(C' + \frac{\bar{C}}{\bar{\phi}})\right] + \bar{K}(C_{\mu s} - \bar{C}_\mu)[(1+\bar{\Phi})D'_s + \bar{\Phi}\bar{D}_s]}{(1+\bar{K}\bar{C})(\bar{D} + 2\beta g) + \bar{\Phi}\bar{D}_s\bar{K}(C_{\mu s} - \bar{C}_\mu)} \right) \sigma_\phi^2 \bar{C}_{\mu 0} \\
&- \left(\frac{(1+\bar{K}\bar{C})\left[2D' + \frac{\bar{D}}{\bar{\phi}} + \beta(C' + \frac{\bar{C}}{\bar{\phi}})\right] + \bar{K}(C_{\mu s} - \bar{C}_\mu)[(1+\bar{\Phi})D'_s + \frac{1+\bar{\phi}}{\bar{\phi}}\bar{D}_s]}{(1+\bar{K}\bar{C})(\bar{D} + 2\beta g) + \bar{\Phi}\bar{D}_s\bar{K}(C_{\mu s} - \bar{C}_\mu)} \right) D'\sigma_\phi^2 \frac{\partial^2 \bar{C}}{\partial x^2} \\
&- \left(\frac{(1+\bar{K}\bar{C})\left[2D'D'_s\bar{\Phi} + (\bar{\Phi}D'_s - \bar{D}_s)\left(\frac{\bar{D}}{\bar{\phi}} + \beta(C' + \frac{\bar{C}}{\bar{\phi}})\right)\right]}{(1+\bar{K}\bar{C})(\bar{D} + 2\beta g) + \bar{\Phi}\bar{D}_s\bar{K}(C_{\mu s} - \bar{C}_\mu)} \right. \\
&\left. + \frac{\bar{K}(C_{\mu s} - \bar{C}_\mu)\left[(D'_s + \frac{\bar{D}_s}{\bar{\Phi}})(\bar{\Phi}D'_s - \bar{D}_s) + (\bar{\Phi}D'_s + \bar{D}_s)^2\right]}{(1+\bar{K}\bar{C})(\bar{D} + 2\beta g) + \bar{\Phi}\bar{D}_s\bar{K}(C_{\mu s} - \bar{C}_\mu)} \right) \sigma_\phi^2 \frac{\partial^2 \bar{C}_\mu}{\partial x^2} \\
&- \left(\frac{(1+\bar{K}\bar{C})\bar{\Phi}\bar{D}_s K'(C_{\mu s} - C_\mu)\left[\frac{\bar{D}}{\bar{\phi}} + \beta(C' + \frac{\bar{C}}{\bar{\phi}})\right] + \bar{K}(C_{\mu s} - \bar{C}_\mu)^2\bar{\Phi}\bar{D}_s K' C_{\mu s}[(1-\bar{\Phi})D'_s + \bar{\Phi}\bar{D}_s]}{\lambda^2(1+\bar{K}\bar{C})\left[(1+\bar{K}\bar{C})(\bar{D} + 2\beta g) + \bar{\Phi}\bar{D}_s\bar{K}(C_{\mu s} - \bar{C}_\mu)\right]} \right. \\
&\left. + \frac{K'(C_{\mu s} - C_\mu)(D'_s + \frac{\bar{D}_s}{\bar{\Phi}} - \bar{\Phi}D'_s + \bar{D}_s)}{\lambda^2(1+\bar{K}\bar{C})} \right) \sigma_\phi^2 \bar{C}
\end{aligned} \tag{7.40}$$

$$\begin{aligned}
\frac{\partial \bar{C}_\mu}{\partial t} =& k_r\left[\bar{K}\bar{C}(C_{\mu s} - \bar{C}_\mu) - \bar{C}_\mu\right] \\
&- \frac{k_r(C_{\mu s} - \bar{C}_\mu)K'\sigma_\phi^2\lambda^2\bar{C}_{\mu 0}}{(1+\bar{K}\bar{C})(\bar{D} + 2\beta g) + \bar{\Phi}\bar{D}_s\bar{K}(C_{\mu s} - \bar{C}_\mu)}\left[1 + \frac{\bar{\Phi}\bar{D}_s K'(C_{\mu s} - \bar{C}_\mu)\bar{C}}{(1+\bar{K}\bar{C})C_{\mu 0}\lambda^2}\right. \\
&\left. + \frac{2\bar{\Phi}\bar{D}_s\bar{K}^2(C_{\mu s} - \bar{C}_\mu)\bar{C}}{(1+\bar{K}\bar{C})(\bar{D} + 2\beta g) + \bar{\Phi}\bar{D}_s\bar{K}(C_{\mu s} - \bar{C}_\mu)}\right]
\end{aligned} \tag{7.41}$$

Appendix D- Auto and Cross Correlations

Table 4. Auto- and Cross-Correlations

$$\overline{\tilde{\Phi}_{-Q}\tilde{\alpha}_{Q}} = i\left(D' + \bar{D}/\bar{\phi}\right)\sigma_{\phi}^{2}Q\sqrt{2\pi}\lambda\exp\left(-Q^{2}\lambda^{2}/2\right)$$

$$\overline{\tilde{\Phi}_{-Q}\tilde{\alpha}_{2Q}} = i\left(D'_{s} + \bar{D}_{s}/\bar{\phi}\right)\sigma_{\phi}^{2}Q\sqrt{2\pi}\lambda\exp\left(-Q^{2}\lambda^{2}/2\right)$$

$$\overline{\tilde{\Phi}_{-Q}\tilde{D}_{sQ}} = D'_{s}\sigma_{\phi}^{2}\sqrt{2\pi}\lambda\exp\left(-Q^{2}\lambda^{2}/2\right)$$

$$\overline{\tilde{\Phi}_{-Q}\tilde{D}_{Q}} = D'\sigma_{\phi}^{2}\sqrt{2\pi}\lambda\exp\left(-Q^{2}\lambda^{2}/2\right)$$

$$\overline{\tilde{\alpha}_{Q}\tilde{\alpha}_{-Q}} = \left(D' + \bar{D}/\bar{\phi}\right)^{2}\sigma_{\phi}^{2}Q^{2}\sqrt{2\pi}\lambda\exp\left(-Q^{2}\lambda^{2}/2\right)$$

$$\overline{\tilde{\alpha}_{2Q}\tilde{\alpha}_{2-Q}} = \left(D'_{s} + \bar{D}_{s}/\bar{\phi}\right)^{2}\sigma_{\phi}^{2}Q^{2}\sqrt{2\pi}\lambda\exp\left(-Q^{2}\lambda^{2}/2\right)$$

$$\overline{\tilde{D}_{-Q}\tilde{\alpha}_{Q}} = -iD'\left(D' + \bar{D}/\bar{\phi}\right)\sigma_{\phi}^{2}Q\sqrt{2\pi}\lambda\exp\left(-Q^{2}\lambda^{2}/2\right)$$

$$\overline{\tilde{D}_{s-Q}\tilde{\alpha}_{Q}} = -iD'_{s}\left(D'_{s} + \bar{D}/\bar{\phi}\right)\sigma_{\phi}^{2}Q\sqrt{2\pi}\lambda\exp\left(-Q^{2}\lambda^{2}/2\right)$$

$$\overline{\tilde{D}_{s-Q}\tilde{\alpha}_{2Q}} = -iD'_{s}\left(D'_{s} + \bar{D}_{s}/\bar{\phi}\right)\sigma_{\phi}^{2}Q\sqrt{2\pi}\lambda\exp\left(-Q^{2}\lambda^{2}/2\right)$$

$$\overline{\tilde{D}_{-Q}\tilde{D}_{Q}} = D'^{2}\sigma_{\phi}^{2}\sqrt{2\pi}\lambda\exp\left(-Q^{2}\lambda^{2}/2\right)$$

$$\overline{\tilde{D}_{s-Q}\tilde{D}_{sQ}} = D'^{2}_{s}\sigma_{\phi}^{2}\sqrt{2\pi}\lambda\exp\left(-Q^{2}\lambda^{2}/2\right)$$

$$\overline{\tilde{D}_{-Q}\tilde{D}_{sQ}} = D'D'_{s}\sigma_{\phi}^{2}\sqrt{2\pi}\lambda\exp\left(-Q^{2}\lambda^{2}/2\right)$$

$$\overline{\tilde{\Phi}_{-Q}\tilde{\alpha}'_{Q}} = i\left(C' + \bar{C}/\bar{\phi}\right)\sigma_{\phi}^{2}Q\sqrt{2\pi}\lambda\exp\left(-Q^{2}\lambda^{2}/2\right)$$

$$\overline{\tilde{\Phi}_{-Q}\tilde{\Phi}_{Q}} = \sigma_{\phi}^{2}\sqrt{2\pi}\lambda\exp\left(-Q^{2}\lambda^{2}/2\right)$$

$$\overline{\tilde{\Phi}_{-Q}\tilde{K}_{Q}} = K'\sigma_{\phi}^{2}\sqrt{2\pi}\lambda\exp\left(-Q^{2}\lambda^{2}/2\right)$$

$$\overline{\tilde{K}_{-Q}\tilde{\alpha}'_{Q}} = iK'\left(C' + \bar{C}/\bar{\phi}\right)\sigma_{\phi}^{2}Q\sqrt{2\pi}\lambda\exp\left(-Q^{2}\lambda^{2}/2\right)$$

$$\overline{\tilde{\alpha}'_{Q}\tilde{\alpha}'_{-Q}} = \left(C' + \bar{C}/\bar{\phi}\right)^{2}\sigma_{\phi}^{2}Q^{2}\sqrt{2\pi}\lambda\exp\left(-Q^{2}\lambda^{2}/2\right)$$

$$\overline{\tilde{\alpha}_{Q}\tilde{\alpha}'_{-Q}} = -\left(C' + \bar{C}/\bar{\phi}\right)\left(D' + \bar{D}/\bar{\phi}\right)\sigma_{\phi}^{2}Q^{2}\sqrt{2\pi}\lambda\exp\left(-Q^{2}\lambda^{2}/2\right)$$

$$\overline{\tilde{\alpha}_{2Q}\tilde{\alpha}'_{-Q}} = -\left(C' + \bar{C}/\bar{\phi}\right)\left(D'_{s} + \bar{D}_{s}/\bar{\phi}\right)\sigma_{\phi}^{2}Q^{2}\sqrt{2\pi}\lambda\exp\left(-Q^{2}\lambda^{2}/2\right)$$

$$\overline{\tilde{D}_{Q}\tilde{\alpha}'_{-Q}} = -iD'\left(C' + \bar{C}/\bar{\phi}\right)\sigma_{\phi}^{2}Q\sqrt{2\pi}\lambda\exp\left(-Q^{2}\lambda^{2}/2\right)$$

$$\overline{\tilde{D}_{sQ}\tilde{\alpha}'_{-Q}} = -iD'_{s}\left(C' + \bar{C}/\bar{\phi}\right)\sigma_{\phi}^{2}Q\sqrt{2\pi}\lambda\exp\left(-Q^{2}\lambda^{2}/2\right)$$

$$\overline{\tilde{K}_{-Q}\tilde{\alpha}_{Q}} = iK'\left(D' + \bar{D}/\bar{\phi}\right)\sigma_{\phi}^{2}Q\sqrt{2\pi}\lambda\exp\left(-Q^{2}\lambda^{2}/2\right)$$

$$\overline{\tilde{K}_{-Q}\tilde{\alpha}_{2Q}} = iK'\left(D'_{s} + \bar{D}_{s}/\bar{\phi}\right)\sigma_{\phi}^{2}Q\sqrt{2\pi}\lambda\exp\left(-Q^{2}\lambda^{2}/2\right)$$

$$\overline{\tilde{K}_{-Q}\tilde{\alpha}_{Q}} = iK'\left(D' + \bar{D}/\bar{\phi}\right)\sigma_{\phi}^{2}Q\sqrt{2\pi}\lambda\exp\left(-Q^{2}\lambda^{2}/2\right)$$

$$\overline{\tilde{K}_{-Q}\tilde{D}_{sQ}} = K'D'_{s}\sigma_{\phi}^{2}\sqrt{2\pi}\lambda\exp\left(-Q^{2}\lambda^{2}/2\right)$$

Table 5. Examples of Convolution Integrals (reset of the integrals are defined similarly)

$$P_{1,ks} = \sum_{m=1,2} \int \frac{1}{2\pi} G^{-1}_{k-Q\,s} \overline{\xi_{Qm} \tilde{\Phi}_{-Q}} \left[i(k-Q) \right]^m dQ$$

$$P_{2,ks} = \sum_{m,n=1,2} \int \frac{1}{2\pi} G^{-1}_{k-Q\,s} \overline{\xi_{Qm} \xi_{-Qn}} \left[i(k-Q) \right]^m (ik)^n dQ$$

$$P_{3,ks} = \sum_{m=1,2} \int \frac{1}{2\pi} G^{-1}_{k-Q\,s} \beta \overline{\xi_{Qm} \tilde{\alpha}'_{-Q}} \left[i(k-Q) \right]^m (ik) dQ$$

$$P_{4,ks} = \sum_{m=1,2} \int \frac{1}{2\pi} G^{-1}_{k-Q\,s} \overline{\xi_{Qm} \tilde{\alpha}_{2-Q}} \left[i(k-Q) \right]^m (ik) dQ$$

$$P_{5,ks} = \sum_{m=1,2} \int \frac{1}{2\pi} G^{-1}_{k-Q\,s} \bar{\Phi} \overline{\xi_{Qm} \tilde{D}_{s-Q}} \left[i(k-Q) \right]^m (ik)^2 dQ$$

$$P_{6,ks} = \sum_{m=1,2} \int \frac{1}{2\pi} G^{-1}_{k-Q\,s} \bar{D}_s \overline{\xi_{Qm} \tilde{\Phi}_{-Q}} \left[i(k-Q) \right]^m (ik)^2 dQ$$

$$P_{7,ks} = \int \frac{1}{2\pi} L_{k-Q\,s} C_{\mu s} \overline{\xi_{Qm} \tilde{K}_{-Q}} \left[i(k-Q) \right] dQ$$

$$P_{8,ks} = \int \frac{1}{2\pi} L_{k-Q\,s} \overline{\xi_{Qm} \tilde{K}_{-Q}} \left[i(k-Q) \right] dQ$$

$$Q_{1,ks} = \sum_{m=1,2} \int \frac{1}{2\pi} G^{-1}_{k-Q\,s} \beta \overline{\tilde{\alpha}'_{Qm} \tilde{\Phi}_{-Q}} \left[i(k-Q) \right]^m dQ$$

$$Q_{2,ks} = \sum_{m,n=1,2} \int \frac{1}{2\pi} G^{-1}_{k-Q\,s} \beta \overline{\xi_{Qm} \tilde{\alpha}'_{-Qn}} \left[i(k-Q) \right]^m (ik)^n dQ$$

$$Q_{3,ks} = \sum_{m=1,2} \int \frac{1}{2\pi} G^{-1}_{k-Q\,s} \beta^2 \overline{\tilde{\alpha}'_{Qm} \tilde{\alpha}'_{-Q}} \left[i(k-Q) \right]^m (ik) dQ$$

$$Q_{4,ks} = \sum_{m=1,2} \int \frac{1}{2\pi} G^{-1}_{k-Q\,s} \beta \overline{\tilde{\alpha}'_{Qm} \tilde{\alpha}_{2-Q}} \left[i(k-Q) \right]^m (ik) dQ$$

$$Q_{5,ks} = \sum_{m=1,2} \int \frac{1}{2\pi} G^{-1}_{k-Q\,s} \beta \bar{\Phi} \overline{\tilde{\alpha}'_{Qm} \tilde{D}_{s-Q}} \left[i(k-Q) \right]^m (ik)^2 dQ$$

$$Q_{6,ks} = \sum_{m=1,2} \int \frac{1}{2\pi} G^{-1}_{k-Q\,s} \beta \bar{D}_s \overline{\tilde{\alpha}'_{Qm} \tilde{\Phi}_{-Q}} \left[i(k-Q) \right]^m (ik)^2 dQ$$

$$Q_{7,ks} = \int \frac{1}{2\pi} L_{k-Q\,s} C_{\mu s} \beta \overline{\tilde{\alpha}'_{Qm} \tilde{K}_{-Q}} \left[i(k-Q) \right] dQ$$

$$Q_{8,ks} = \int \frac{1}{2\pi} L_{k-Q\,s} \beta \overline{\tilde{\alpha}'_{Qm} \tilde{K}_{-Q}} \left[i(k-Q) \right] dQ$$

$$T_{1,ks} = \sum_{m=1,2} \int \frac{1}{2\pi} \breve{G}^{-1}_{k-Q\,s} \overline{\tilde{\alpha}_{2Qm} \tilde{\Phi}_{-Q}} \left[i(k-Q) \right]^m dQ$$

$$T_{2,ks} = \sum_{m,n=1,2} \int \frac{1}{2\pi} \breve{G}^{-1}_{k-Q\,s} \overline{\xi_{Qm} \tilde{\alpha}_{2-Qn}} \left[i(k-Q) \right]^m (ik)^n dQ$$

$$T_{3,ks} = \sum_{m=1,2} \int \frac{1}{2\pi} \breve{G}^{-1}_{k-Q\,s} \beta \overline{\tilde{\alpha}_{2Qm} \tilde{\alpha}'_{-Q}} \left[i(k-Q) \right]^m (ik) dQ$$

$$T_{4,ks} = \sum_{m=1,2} \int \frac{1}{2\pi} \breve{G}^{-1}_{k-Q\,s} \overline{\tilde{\alpha}_{2Qm} \tilde{\alpha}_{2-Q}} \left[i(k-Q) \right]^m (ik) dQ$$

$$T_{5,ks} = \sum_{m=1,2} \int \frac{1}{2\pi} \breve{G}^{-1}_{k-Q\,s} \bar{\Phi} \overline{\tilde{\alpha}_{2Qm} \tilde{D}_{s-Q}} \left[i(k-Q) \right]^m (ik)^2 dQ$$

$$T_{6,ks} = \sum_{m=1,2} \int \frac{1}{2\pi} \breve{G}^{-1}_{k-Q\,s} \bar{D}_s \overline{\tilde{\alpha}_{2Qm} \tilde{\Phi}_{-Q}} \left[i(k-Q) \right]^m (ik)^2 dQ$$

$$T_{7,ks} = \int \frac{1}{2\pi} \breve{L}_{k-Q\,s} C_{\mu s} \overline{\tilde{\alpha}_{2Qm} \tilde{K}_{-Q}} \left[i(k-Q) \right] dQ$$

$$T_{8,ks} = \int \frac{1}{2\pi} \breve{L}_{k-Q\,s} \overline{\tilde{\alpha}_{2Qm} \tilde{K}_{-Q}} \left[i(k-Q) \right] dQ$$

Table 6.

$$S_{1,ks} = \int \frac{1}{2\pi} G^{-1}_{k-Q\,s} \overline{\tilde{K}_{Qm} \tilde{\Phi}_{-Q}} dQ$$

$$S_{2,ks} = \sum_{m=1,2} \int \frac{1}{2\pi} G^{-1}_{k-Q\,s} \overline{\xi_{Qm} \tilde{K}_{-Q}} (ik)^m dQ$$

$$S_{3,ks} = \int \frac{1}{2\pi} G^{-1}_{k-Q\,s} \beta \overline{\tilde{K}_{Qm} \tilde{\alpha'}_{-Q}} (ik) dQ$$

$$S_{4,ks} = \int \frac{1}{2\pi} G^{-1}_{k-Q\,s} \overline{\tilde{K}_{Qm} \tilde{\alpha}_{2-Q}} (ik) dQ$$

$$S_{5,ks} = \int \frac{1}{2\pi} G^{-1}_{k-Q\,s} \bar{\Phi} \overline{\tilde{K}_{Qm} \tilde{D}_{s-Q}} (ik)^2 dQ$$

$$S_{6,ks} = \int \frac{1}{2\pi} G^{-1}_{k-Q\,s} \bar{D}_s \overline{\tilde{K}_{Qm} \tilde{\Phi}_{-Q}} (ik)^2 dQ$$

$$S_{7,ks} = \int \frac{1}{2\pi} L_{k-Q\,s} C_{\mu s} \overline{\tilde{K}_{Qm} \tilde{K}_{-Q}} dQ$$

$$S_{8,ks} = \int \frac{1}{2\pi} L_{k-Q\,s} \overline{\tilde{K}_{Qm} \tilde{K}_{-Q}} dQ$$

$$I_{1,ks} = \int \frac{1}{2\pi} \breve{G}^{-1}_{k-Q\,s} \overline{\tilde{K}_{Qm} \tilde{\Phi}_{-Q}} dQ$$

$$I_{2,ks} = \sum_{m=1,2} \int \frac{1}{2\pi} \breve{G}^{-1}_{k-Q\,s} \overline{\xi_{Qm} \tilde{K}_{-Qn}} (ik)^m dQ$$

$$I_{3,ks} = \int \frac{1}{2\pi} \breve{G}^{-1}_{k-Q\,s} \beta \overline{\tilde{K}_{Qm} \tilde{\alpha'}_{-Q}} (ik) dQ$$

$$I_{4,ks} = \int \frac{1}{2\pi} \breve{G}^{-1}_{k-Q\,s} \overline{\tilde{K}_{Qm} \tilde{\alpha}_{2-Q}} (ik) dQ$$

$$I_{5,ks} = \int \frac{1}{2\pi} \breve{G}^{-1}_{k-Q\,s} \bar{\Phi} \overline{\tilde{K}_{Qm} \tilde{D}_{s-Q}} (ik)^2 dQ$$

$$I_{6,ks} = \int \frac{1}{2\pi} \breve{G}_{k-Q\,s} \bar{D}_s \overline{\tilde{K}_{Qm} \tilde{\Phi}_{-Q}} (ik)^2 dQ$$

$$I_{7,ks} = \int \frac{1}{2\pi} \breve{L}_{k-Q\,s} C_{\mu s} \overline{\tilde{K}_{Qm} \tilde{K}_{-Q}} (ik)^2 dQ$$

$$I_{8,ks} = \int \frac{1}{2\pi} \breve{L}_{k-Q\,s} \overline{\tilde{K}_{Qm} \tilde{K}_{-Q}} (ik)^2 dQ$$

Appendix E - Estimation of the Surface Diffusion Coefficients, D_{s1} and D_{s2}

$$\frac{\partial C_{\mu 1}}{\partial x} = \frac{\partial}{\partial x}\left(\frac{C_m b_1' C_1}{1 + b_1' C_1 + b_2' C_2}\right) = \left[\frac{C_m b_1' + C_m b_1' b_2' C_2}{(1 + b_1' C_1 + b_2' C_2)^2}\right]\frac{\partial C_1}{\partial x} - \left[\frac{C_m b_1' b_2' C_1}{(1 + b_1' C_1 + b_2' C_2)^2}\right]\frac{\partial C_2}{\partial x}$$

(7.42)

$$\frac{\partial C_{\mu 2}}{\partial x} = \frac{\partial}{\partial x}\left(\frac{C_m b_2' C_2}{1 + b_1' C_1 + b_2' C_2}\right) = \left[\frac{C_m b_2' + C_m b_1' b_2' C_1}{(1 + b_1' C_1 + b_2' C_2)^2}\right]\frac{\partial C_2}{\partial x} - \left[\frac{C_m b_1' b_2' C_2}{(1 + b_1' C_1 + b_2' C_2)^2}\right]\frac{\partial C_1}{\partial x}$$

(7.43)

$$\frac{\partial C_{\mu 1}/\partial x}{\partial C_{\mu 2}/\partial x} = \frac{(b_1' + b_1' b_2' C_2)\partial C_1/\partial x - (b_1' b_2' C_1)\partial C_2/\partial x}{(b_2' + b_1' b_2' C_1)\partial C_2/\partial x - (b_1' b_2' C_2)\partial C_1/\partial x} \tag{7.44}$$

$$D_{s1} = D_{11} + D_{12}\frac{(b_2' + b_1' b_2' C_1)\partial C_2/\partial x - (b_1' b_2' C_2)\partial C_1/\partial x}{(b_1' + b_1' b_2' C_2)\partial C_1/\partial x - (b_1' b_2' C_1)\partial C_2/\partial x} \tag{7.45}$$

$$D_{s2} = D_{22} + D_{21}\frac{(b_1' + b_1' b_2' C_2)\partial C_1/\partial x - (b_1' b_2' C_1)\partial C_2/\partial x}{(b_2' + b_1' b_2' C_1)\partial C_2/\partial x - (b_1' b_2' C_2)\partial C_1/\partial x} \tag{7.46}$$

Appendix F - Scaling and Nondimensionalization

$$c_1 = \frac{C_1}{C_{10}+C_{20}}; c_2 = \frac{C_2}{C_{10}+C_{20}}; c_{\mu 1} = \frac{C_{\mu 1}}{C_{\mu 10}+C_{\mu 20}}; c_{\mu 2} = \frac{C_{\mu 2}}{C_{\mu 10}+C_{\mu 20}}; r = \frac{x}{L} \tag{7.47}$$

$$c_m = \frac{C_m}{C_{\mu 10}+C_{\mu 20}}; c_{f1} = \frac{C_{f1}}{C_{10}+C_{20}}; c_{f2} = \frac{C_{f2}}{C_{10}+C_{20}}; \tau = \frac{\delta_1 D_{p1} t}{L^2} = \frac{\delta_1 D_{p2} t}{L^2} \tag{7.48}$$

$$\delta_1 = \frac{1}{1+\left(\frac{1-\phi-\phi_f}{\phi}\right)\left(\frac{C_{\mu 10}+C_{\mu 20}}{C_{10}+C_{20}}\right)}, \quad \delta_2 = 1-\delta_1 \tag{7.49}$$

$$\varepsilon_1 = \left(\frac{C_{\mu 10}+C_{\mu 20}}{C_{10}+C_{20}}\right)\left(\frac{1-\phi-\phi_f}{\phi}\right)\left(\frac{D_{s1}}{D_{s10}}\right)\left(\frac{D_{s10}}{D_{p1}}\right) \tag{7.50}$$

$$\varepsilon_2 = \left(\frac{C_{\mu 10}+C_{\mu 20}}{C_{10}+C_{20}}\right)\left(\frac{1-\phi-\phi_f}{\phi}\right)\left(\frac{D_{s2}}{D_{s20}}\right)\left(\frac{D_{s20}}{D_{p2}}\right) \tag{7.51}$$

$$\theta_1 = \left(\frac{C_{10}+C_{20}}{D_{p1}}\right)\left(\frac{R_g T k_p}{\mu}\right) \tag{7.52}$$

$$\theta_2 = \left(\frac{C_{10}+C_{20}}{D_{p2}}\right)\left(\frac{R_g T k_p}{\mu}\right) \tag{7.53}$$

$$\lambda_1 = b_1'\left(C_{10}+C_{20}\right); \qquad \lambda_2 = b_2'\left(C_{10}+C_{20}\right) \tag{7.54}$$

$$\delta_1\frac{\partial c_i}{\partial \tau} + \delta_2\frac{\partial c_{\mu i}}{\partial \tau} = \frac{\partial}{\partial r}\left(\frac{\partial c_i}{\partial r}\right) + \theta_i\frac{\partial}{\partial r}\left(c_i\frac{\partial c_i}{\partial r}\right) + \frac{\partial}{\partial r}\left(\varepsilon_i\frac{\partial c_{\mu i}}{\partial r}\right); \quad i = 1,2 \tag{7.55}$$

$$c_{\mu i} = \frac{c_m \lambda_i c_i}{1+\lambda_1 c_1 + \lambda_2 c_2}; \quad i = 1,2 \tag{7.56}$$

$$\frac{\partial c_{\mu 1}}{\partial \tau} = g_1\frac{\partial c_1}{\partial \tau} - g_1'\frac{\partial c_2}{\partial \tau} \tag{7.57}$$

$$\frac{\partial c_{\mu 2}}{\partial \tau} = g_2\frac{\partial c_2}{\partial \tau} - g_2'\frac{\partial c_1}{\partial \tau} \tag{7.58}$$

$$g_1(c_1,c_2) = \frac{c_m\lambda_1(1+\lambda_2 c_2)}{\left(1+\lambda_1 c_1+\lambda_2 c_2\right)^2} \tag{7.59}$$

$$g_2(c_1, c_2) = \frac{c_m \lambda_2 (1 + \lambda_1 c_1)}{(1 + \lambda_1 c_1 + \lambda_2 c_2)^2} \tag{7.60}$$

$$g_1'(c_1, c_2) = \frac{c_m \lambda_1 \lambda_2 c_1}{(1 + \lambda_1 c_1 + \lambda_2 c_2)^2} \tag{7.61}$$

$$g_2(c_1, c_2) = \frac{c_m \lambda_1 \lambda_2 c_2}{(1 + \lambda_1 c_1 + \lambda_2 c_2)^2} \tag{7.62}$$

$$\frac{\partial}{\partial r}\left(\varepsilon_1 \frac{\partial c_{\mu 1}}{\partial r}\right) = \frac{\partial}{\partial r}\left(\varepsilon_1 g_1 \frac{\partial c_1}{\partial r}\right) - \frac{\partial}{\partial r}\left(\varepsilon_1 g_1' \frac{\partial c_2}{\partial r}\right) \tag{7.63}$$

$$\frac{\partial}{\partial r}\left(\varepsilon_2 \frac{\partial c_{\mu 2}}{\partial r}\right) = \frac{\partial}{\partial r}\left(\varepsilon_2 g_2 \frac{\partial c_2}{\partial r}\right) - \frac{\partial}{\partial r}\left(\varepsilon_2 g_2' \frac{\partial c_1}{\partial r}\right) \tag{7.64}$$

$$(\delta_1 + \delta_2 g_1)\frac{\partial c_1}{\partial \tau} - \delta_2 g_1' \frac{\partial c_2}{\partial \tau} = \frac{\partial}{\partial r}\left[(1 + \theta_1 c_1 + \varepsilon_1 g_1)\frac{\partial c_1}{\partial r}\right] - \frac{\partial}{\partial r}\left(\varepsilon_1 g_1' \frac{\partial c_2}{\partial r}\right) \tag{7.65}$$

$$(\delta_1 + \delta_2 g_2)\frac{\partial c_2}{\partial \tau} - \delta_2 g_2' \frac{\partial c_1}{\partial \tau} = \frac{\partial}{\partial r}\left[(1 + \theta_2 c_2 + \varepsilon_2 g_2)\frac{\partial c_2}{\partial r}\right] - \frac{\partial}{\partial r}\left(\varepsilon_2 g_2' \frac{\partial c_1}{\partial r}\right) \tag{7.66}$$

which could be further simplified in to

$$(\delta_1 + \delta_2 g_1 - \delta_2 g_1' \frac{\partial c_2}{\partial c_1})\frac{\partial c_1}{\partial \tau} = \frac{\partial}{\partial r}\left[\left(1 + \theta_1 c_1 + \varepsilon_1 g_1 - \varepsilon_1 g_1' \frac{\partial c_2}{\partial c_1}\right)\frac{\partial c_1}{\partial r}\right] \tag{7.67}$$

$$(\delta_1 + \delta_2 g_2 - \delta_2 g_2' \frac{\partial c_1}{\partial c_2})\frac{\partial c_2}{\partial \tau} = \frac{\partial}{\partial r}\left[\left(1 + \theta_2 c_2 + \varepsilon_2 g_2 - \varepsilon_2 g_2' \frac{\partial c_1}{\partial c_2}\right)\frac{\partial c_2}{\partial r}\right] \tag{7.68}$$

$$\frac{D_{s1}}{D_{s10}} = \frac{D_{11}}{D_{s10}} + \frac{D_{12}}{D_{s10}}\left[\frac{\lambda_2(1 + \lambda_1 c_1)\partial c_2/\partial r - \lambda_1 \lambda_2 c_2 \partial c_1/\partial r}{\lambda_1(1 + \lambda_2 c_2)\partial c_1/\partial r - \lambda_1 \lambda_2 c_1 \partial c_2/\partial r}\right] \tag{7.69}$$

$$\frac{D_{s2}}{D_{s20}} = \frac{D_{22}}{D_{s20}} + \frac{D_{21}}{D_{s20}}\left[\frac{\lambda_1(1 + \lambda_2 c_2)\partial c_1/\partial r - \lambda_1 \lambda_2 c_1 \partial c_2/\partial r}{\lambda_2(1 + \lambda_1 c_1)\partial c_2/\partial r - \lambda_1 \lambda_2 c_2 \partial c_1/\partial r}\right] \tag{7.70}$$

$$\frac{D_{11}}{D_{s10}} = (1 + \lambda_1 c_1) + \alpha\left(\frac{D_{s20}}{D_{s10}}\right)^{0.5}(\lambda_1 \lambda_2 c_1 c_2)^{0.5} \tag{7.71}$$

$$\frac{D_{22}}{D_{s20}} = (1 + \lambda_2 c_2) + \alpha\left(\frac{D_{s10}}{D_{s20}}\right)^{0.5}(\lambda_1 \lambda_2 c_1 c_2)^{0.5} \tag{7.72}$$

$$\frac{D_{12}}{D_{s10}} = (\lambda_1 c_1) + \alpha \left(\frac{D_{s20}}{D_{s10}}\right)^{0.5} \left(\frac{\lambda_1 c_1}{\lambda_2 c_2}\right)^{0.5} (1 + \lambda_2 c_2) \tag{7.73}$$

$$\frac{D_{21}}{D_{s20}} = (\lambda_2 c_2) + \alpha \left(\frac{D_{s10}}{D_{s20}}\right)^{0.5} \left(\frac{\lambda_2 c_2}{\lambda_1 c_1}\right)^{0.5} (1 + \lambda_1 c_1) \tag{7.74}$$

and in the fractures we have

$$\xi_1 = \frac{K_{L1}}{D_{p1}}; \qquad \gamma_1 = \frac{a_1 L^2}{D_{p1}};, \qquad \chi_1 = \left(\frac{C_{10} + C_{20}}{D_{p1}}\right)\left(\frac{R_g T k_f}{\mu}\right)$$

$$\xi_2 = \frac{K_{L2}}{D_{p2}}; \qquad \gamma_2 = \frac{a_2 L^2}{D_{p2}};, \qquad \chi_2 = \left(\frac{C_{10} + C_{20}}{D_{p2}}\right)\left(\frac{R_g T k_f}{\mu}\right)$$

$$\delta_1 \frac{\partial c_{fi}}{\partial \tau} = \frac{\partial}{\partial r}\left[(\xi_i + \chi_i c_{fi})\frac{\partial c_{fi}}{\partial r}\right] - \gamma_i (c_{fi} - c_i) \qquad i = 1, 2 \tag{7.75}$$

Appendix G- Auto and Cross Correlations

Table 7.

$$\overline{\tilde{\Phi}_{-Q}\tilde{\alpha}_{Q}} = i\left(D' + \bar{D}/\bar{\phi}\right)\sigma_{\phi}^{2}Q\sqrt{2\pi}\lambda\exp\left(-Q^{2}\lambda^{2}/2\right)$$

$$\overline{\tilde{\Phi}_{-Q}\tilde{\alpha}_{2Q}} = i\left(D'_{s} + \bar{D}_{s}/\bar{\phi}\right)\sigma_{\phi}^{2}Q\sqrt{2\pi}\lambda\exp\left(-Q^{2}\lambda^{2}/2\right)$$

$$\overline{\tilde{\Phi}_{-Q}\tilde{D}_{sQ}} = D'_{s}\sigma_{\phi}^{2}\sqrt{2\pi}\lambda\exp\left(-Q^{2}\lambda^{2}/2\right)$$

$$\overline{\tilde{\Phi}_{-Q}\tilde{D}_{Q}} = D'\sigma_{\phi}^{2}\sqrt{2\pi}\lambda\exp\left(-Q^{2}\lambda^{2}/2\right)$$

$$\overline{\tilde{\alpha}_{Q}\tilde{\alpha}_{-Q}} = \left(D' + \bar{D}/\bar{\phi}\right)^{2}\sigma_{\phi}^{2}Q^{2}\sqrt{2\pi}\lambda\exp\left(-Q^{2}\lambda^{2}/2\right)$$

$$\overline{\tilde{\alpha}_{2Q}\tilde{\alpha}_{2-Q}} = \left(D'_{s} + \bar{D}_{s}/\bar{\phi}\right)^{2}\sigma_{\phi}^{2}Q^{2}\sqrt{2\pi}\lambda\exp\left(-Q^{2}\lambda^{2}/2\right)$$

$$\overline{\tilde{D}_{-Q}\tilde{\alpha}_{Q}} = -iD'\left(D' + \bar{D}/\bar{\phi}\right)\sigma_{\phi}^{2}Q\sqrt{2\pi}\lambda\exp\left(-Q^{2}\lambda^{2}/2\right)$$

$$\overline{\tilde{D}_{s-Q}\tilde{\alpha}_{Q}} = -iD'_{s}\left(D'_{s} + \bar{D}/\bar{\phi}\right)\sigma_{\phi}^{2}Q\sqrt{2\pi}\lambda\exp\left(-Q^{2}\lambda^{2}/2\right)$$

$$\overline{\tilde{D}_{s-Q}\tilde{\alpha}_{2Q}} = -iD'_{s}\left(D'_{s} + \bar{D}_{s}/\bar{\phi}\right)\sigma_{\phi}^{2}Q\sqrt{2\pi}\lambda\exp\left(-Q^{2}\lambda^{2}/2\right)$$

$$\overline{\tilde{D}_{-Q}\tilde{D}_{Q}} = D'^{2}\sigma_{\phi}^{2}\sqrt{2\pi}\lambda\exp\left(-Q^{2}\lambda^{2}/2\right)$$

$$\overline{\tilde{D}_{s-Q}\tilde{D}_{sQ}} = D'^{2}_{s}\sigma_{\phi}^{2}\sqrt{2\pi}\lambda\exp\left(-Q^{2}\lambda^{2}/2\right)$$

$$\overline{\tilde{D}_{-Q}\tilde{D}_{sQ}} = D'D'_{s}\sigma_{\phi}^{2}\sqrt{2\pi}\lambda\exp\left(-Q^{2}\lambda^{2}/2\right)$$

$$\overline{\tilde{\Phi}_{-Q}\tilde{\alpha}'_{Q}} = i\left(C' + \bar{C}/\bar{\phi}\right)\sigma_{\phi}^{2}Q\sqrt{2\pi}\lambda\exp\left(-Q^{2}\lambda^{2}/2\right)$$

$$\overline{\tilde{\Phi}_{-Q}\tilde{\Phi}_{Q}} = \sigma_{\phi}^{2}\sqrt{2\pi}\lambda\exp\left(-Q^{2}\lambda^{2}/2\right)$$

$$\overline{\tilde{\Phi}_{-Q}\tilde{K}_{Q}} = K'\sigma_{\phi}^{2}\sqrt{2\pi}\lambda\exp\left(-Q^{2}\lambda^{2}/2\right)$$

$$\overline{\tilde{K}_{-Q}\tilde{\alpha}'_{Q}} = iK'\left(C' + \bar{C}/\bar{\phi}\right)\sigma_{\phi}^{2}Q\sqrt{2\pi}\lambda\exp\left(-Q^{2}\lambda^{2}/2\right)$$

$$\overline{\tilde{\alpha}'_{Q}\tilde{\alpha}'_{-Q}} = \left(C' + \bar{C}/\bar{\phi}\right)^{2}\sigma_{\phi}^{2}Q^{2}\sqrt{2\pi}\lambda\exp\left(-Q^{2}\lambda^{2}/2\right)$$

$$\overline{\tilde{\alpha}_{Q}\tilde{\alpha}'_{-Q}} = -\left(C' + \bar{C}/\bar{\phi}\right)\left(D' + \bar{D}/\bar{\phi}\right)\sigma_{\phi}^{2}Q^{2}\sqrt{2\pi}\lambda\exp\left(-Q^{2}\lambda^{2}/2\right)$$

$$\overline{\tilde{\alpha}_{2Q}\tilde{\alpha}'_{-Q}} = -\left(C' + \bar{C}/\bar{\phi}\right)\left(D'_{s} + \bar{D}_{s}/\bar{\phi}\right)\sigma_{\phi}^{2}Q^{2}\sqrt{2\pi}\lambda\exp\left(-Q^{2}\lambda^{2}/2\right)$$

$$\overline{\tilde{D}_{Q}\tilde{\alpha}'_{-Q}} = -iD'\left(C' + \bar{C}/\bar{\phi}\right)\sigma_{\phi}^{2}Q\sqrt{2\pi}\lambda\exp\left(-Q^{2}\lambda^{2}/2\right)$$

$$\overline{\tilde{D}_{sQ}\tilde{\alpha}'_{-Q}} = -iD'_{s}\left(C' + \bar{C}/\bar{\phi}\right)\sigma_{\phi}^{2}Q\sqrt{2\pi}\lambda\exp\left(-Q^{2}\lambda^{2}/2\right)$$

$$\overline{\tilde{K}_{-Q}\tilde{\alpha}_{Q}} = iK'\left(D' + \bar{D}/\bar{\phi}\right)\sigma_{\phi}^{2}Q\sqrt{2\pi}\lambda\exp\left(-Q^{2}\lambda^{2}/2\right)$$

$$\overline{\tilde{K}_{-Q}\tilde{\alpha}_{2Q}} = iK'\left(D'_{s} + \bar{D}_{s}/\bar{\phi}\right)\sigma_{\phi}^{2}Q\sqrt{2\pi}\lambda\exp\left(-Q^{2}\lambda^{2}/2\right)$$

$$\overline{\tilde{K}_{-Q}\tilde{\alpha}_{Q}} = iK'\left(D' + \bar{D}/\bar{\phi}\right)\sigma_{\phi}^{2}Q\sqrt{2\pi}\lambda\exp\left(-Q^{2}\lambda^{2}/2\right)$$

$$\overline{\tilde{K}_{-Q}\tilde{D}_{sQ}} = K'D'_{s}\sigma_{\phi}^{2}\sqrt{2\pi}\lambda\exp\left(-Q^{2}\lambda^{2}/2\right)$$

Appendix H- Estimation of the Reaction Wave Propagation Velocity

Here, a solution for the steadily moving reaction wave is considered using the reaction wave approach. As the fluid flows along the ξ_1 direction at a speed υ, propagation speed of the reaction front is V. We seek a solution of the form

$$Y = Y_0(\xi_1 - Vt) \tag{7.76}$$

$$\eta = \eta_0(\xi_1 - Vt) \tag{7.77}$$

In the absence of transient effects and local diffusion, the governing equations then become

$$-\phi V \frac{\partial Y}{\partial \xi_1} + \upsilon \frac{\partial Y}{\partial \xi_1} = -\alpha \tilde{r} = -\alpha V \frac{\partial \eta}{\partial \xi_1} \tag{7.78}$$

Far upstream, the tracer concentration is constant and equal to inlet concentration, the mineral is completely dissolved; whereas far downstream, all the tracer is spent and none of the mineral is reacted:

$$Y \to 1; \qquad \eta \to 1; \qquad \xi_1 \to -\infty$$

$$Y \to 0; \qquad \eta \to 0; \qquad \xi_1 \to +\infty$$

Integrating equation (B.2) once and using the upstream condition, we obtain

$$(\upsilon - \phi V)(Y - 1) = -\alpha V(\eta - 1) \tag{7.79}$$

Applying downstream condition, we find

$$(\upsilon - \phi V) = -\alpha V \tag{7.80}$$

which finally gives the reaction front velocity as

$$\bar{V} = \frac{\upsilon}{\varphi + \alpha} \tag{7.81}$$

Appendix I - Evaluation of the Cross- correlation Integrals

Expressions for the cross correlations include integrals I_0 to I_6, which are evaluated assuming the stratified medium approximation of (Gelhar and Axness 1983), where $(\lambda_1/\lambda_3)^2 << 1$ is taken. This simplification will help us express the spectra for cross correlations in terms of the spectral density function of permeability given in equation 6.12. The expression for I_0 is:

$$I_0(f,f) = \int_{-\infty}^{+\infty} \frac{S_{ff}}{\Delta} d\vec{k} \tag{7.82}$$

Multiplying the integral argument with complex conjugate of Δ we obtain

$$I_0(f,f) = \int_{-\infty}^{+\infty} \frac{\Delta^* S_{ff}}{\Delta\Delta^*} d\vec{k} = \frac{1}{\bar{V}(\phi\bar{V} - \upsilon)} \int_{-\infty}^{+\infty} \frac{S_{ff}}{k_1^2 (E/\bar{V})^2} d\vec{k} \tag{7.83}$$

where

$$E = \frac{\bar{\omega}\bar{V}\alpha r_Y + (\upsilon - \phi\bar{V})}{(\phi\bar{V} - \upsilon)} \tag{7.84}$$

Since the denominator of the integral in equation 7.83 is an even function of k_1, the imaginary term in the nominator produce a zero result upon integration, and multiplying both numerator and denominator with λ_1 we obtain

$$I_0(f,f) = \frac{\lambda_1^2}{\bar{V}(\phi\bar{V} - \upsilon)} \int_{-\infty}^{+\infty} \frac{S_{ff}}{\lambda_1^2 k_1^2 (\lambda_1 E/\bar{V})^2} d\vec{k} \tag{7.85}$$

where

$$S_{ff} d\vec{k} = \frac{\sigma_f^2 \lambda_1 \lambda_2 \lambda_3 d\vec{k_1} d\vec{k_2} d\vec{k_3}}{\pi^2 \left[1 + (k_1\lambda_1)^2 + (k_2\lambda_2)^2 + (k_3\lambda_3)^2\right]^2} \tag{7.86}$$

Introducing variables $u_i = \lambda_i k_i$ i=1,2,3 and defining $\kappa = \lambda_1 E/\bar{V}$

$$I_0(f,f) = \frac{\lambda_1^2 \sigma_f^2}{\bar{V}\pi^2(\phi\bar{V} - \upsilon)} \int_{-\infty}^{+\infty} \frac{d\vec{u}}{(u_1^2 + \kappa^2) + (1 + \vec{u}^2)} \tag{7.87}$$

The integral in this form can be evaluated in spherical coordinates to produce the following result

$$I_0(f,f) = \frac{\lambda_1 \sigma_f^2}{(\phi\bar{V} - \upsilon)} \left(\frac{1}{\kappa} - \frac{1}{1+\kappa}\right) \tag{7.88}$$

The integrals I_1 to I_6 are also evaluated using the same approach. The results are below

$$I_1(f,f) = \frac{\lambda_1 \sigma_f^2}{(\phi \bar{V} - \upsilon)} \left(\frac{1}{1+\kappa} \right) \tag{7.89}$$

$$I_2(f,f) = \frac{\lambda_1^2 \sigma_f^2}{(\phi \bar{V} - \upsilon)^2} \left(\frac{1}{\kappa} - \frac{1}{1+\kappa} \right) \tag{7.90}$$

$$I_3(f,f) = 0 \tag{7.91}$$

$$I_4(f,f) = \frac{\lambda_1 \sigma_f^2}{\bar{V}(\phi \bar{V} - \upsilon)} \left(\frac{1}{1+\kappa} \right) \tag{7.92}$$

$$I_5(f,f) = \frac{\lambda_1^2 \sigma_f^2}{\bar{V}(\phi \bar{V} - \upsilon)^2} \left(\frac{1}{\kappa} - \frac{1}{1+\kappa} \right) \tag{7.93}$$

$$I_6(f,f) = 0 \tag{7.94}$$

For the stratified medium approximation, the spectra for cross-correlations can be related to the spectrum of random permeability filed:

$$S_{\upsilon_1 \upsilon_1} = \frac{\upsilon^2}{\gamma^2} S_{ff}; \qquad S_{\upsilon_1 \omega} = \frac{b}{\gamma} S_{ff}; \qquad S_{\omega\omega} = b^2 S_{ff} + S_{\delta\delta}; \qquad \gamma = \frac{\mu \phi \upsilon}{k J_1}; \qquad J_1 = -\frac{\partial p}{\partial x_1}$$

Here, partial correlation residuals $\delta_i = 1, 2, 3$ are assumed to be statistically homogeneous random fields and described by three dimensional anisotropic auto-covariance with the following spectrum

$$S_{\delta\delta} = \frac{\sigma_f^2 \lambda_1 \lambda_2 \lambda_3}{\pi^2 \left[1 + (k_1 \lambda_1)^2 + (k_2 \lambda_2)^2 + (k_3 \lambda_3)^2 \right]^2} \tag{7.95}$$